Calculation of patient doses for diagnostic and interventional radiology procedures undertaken using cone beam computed tomography

A thesis submitted to The University of Manchester for the degree of

Doctor of Clinical Science

in the Faculty of Biology, Medicine and Health

2021

Peter G. McGookin

School of Medical Sciences

Division of Cancer Sciences

Contents

1. Abstract 10

2. Lay Abstract 11

3. Declaration 12

4. Copyright 13

5. Brief Statement for Examiners 14

6. Introduction 15

6.1. Cone Beam Computed Tomography Imaging Equipment 16

7. Literature Review 18

7.1. Eligibility Criteria 18

7.2. Literature Search 18

7.3. Patient Radiation Doses in Radiology 20

7.4. Anthropomorphic Phantoms and Dosmeters 23

7.5. Monte Carlo Simulation 29

7.6. Conversion Factors 33

7.7. Literature Review – Discussion 37

8. Aims and Objectives 38

9. Methodology 39

9.1. Choice of Dose Calculation Method 39

9.2. Monte Carlo Simulations 39

9.3. PCXMC Monte Carlo Set-up and Validation 41

9.3.1. PCXMC Geometry 45

9.3.2. PCXMC Set-up 46

9.4. Thermoluminescent Dosemeter Calibration 47

9.5. Rando Phantom Measurements 53

9.6. Monte Carlo Validation 56

10. Results 59

10.1. Introduction 59

10.2. Monte Carlo Error Analysis 61

10.3. Discussion of Dose Metrics Used 62

10.4. Effect of Number of Projections on Conversion Factor 62

10.5. Effect of Scan Orientation on Conversion Factor 64

10.6. Effect of Beam Half Value Layer on Dose Area Product to Effective Dose Conversion Factor 71

10.7. Effect of Field Size on Dose Area Product to Effective Dose Conversion Factor .. 74

10.8. Derivation of Conversion Factor for Dose Area Product to Effective Dose using Half Value Layer 80

10.9. Variation of Dose Area Product to Effective Dose Conversion Factor with kV and Additional Filtration 86

10.10. Effect of Half Value Layer and Field Size on Reference Air Kerma to Effective Dose Conversion Factor 91

10.11. Derivation of Conversion Factor for Reference Air Kerma to Effective Dose using Half Value Layer and Beam Area 96

10.12. Variation of Reference Air Kerma to Effective Dose Conversion Factor with kV and Additional Filtration 99

10.13. Impact of Arms on Conversion Factor 105

10.14. Impact of x-ray fields extending beyond the body 106

11. Discussion 110

11.1. Use of a Standard Size Mathematical Hermaphrodite Phantom 110

11.2. Comparison with Literature Review 112

11.2.1. Comparison with Wang et al. 114

11.3. Comparison with Rando Phantom Measurements 118

11.4. Use of Computed Tomography Dose Index and Dose Length Product as Dose Metrics for Cone Beam Computed Tomography 120

11.5. Errors and Uncertainties 121

12. Innovation 124

13. Conclusion 125

14. Future Work 127

15. References 128

16. Appendix 1 - List of Alliance Manchester Business School A Units and Medical Physics B Units Together with Assignments 137

17. Appendix 2 – Summary of Papers Included in the Literature Review 139

18. Appendix 3 – PCXMC Set-up 146

19. Appendix 4 – TLD Positions 148

Figures

Figure 1 Diagram showing how the Ziehm Vision RFD mobile C-Arm system performs a CBCT scan. Reproduced from (Ziehm Imaging, 2019, p. 6) 17
Figure 2 Results from Search Strategy 19
Figure 3 Results from Investigation into the Simulation Error and Time Taken for Different Numbers of Photons Simulated 44
Figure 4 Response of TLDs to X-ray Spectra Relative to Cs-137 Reproduced from (Aveyard & Katsidzira, 2016) 48
Figure 5 Comparison of X-ray Spectra for the Relevant ISON and Clinical Beams 51
Figure 6 Comparison between TLD Results (HP0.07) and Ionisation Chamber Measurements made using Clinical X-ray Acquisition Parameters. 52
Figure 7 Validation of PCXMC Simulations 56
Figure 8 Comparison of Simulated and Measured Organ Doses for Head Scan 57
Figure 9 Comparison of Simulated and Measured Organ Doses for Liver Scan 58
Figure 10 Comparison of Maximum Field Size for Head Examinations Showing Uncollimated Lateral (A) Uncollimated AP (B), Collimated Lateral (C) and Collimated AP (D) views 60
Figure 11 Influence of Number of Projections Simulated on Effective Dose Conversion Factor 64
Figure 12 Differences between Conversion Factors for CBCT Examinations Performed either the Primary Beam Through or not Through the Table for 120kV and 0.1mm Additional Copper Filtration with the Patient Positioned Supine 65
Figure 13 Variation of Conversion Factor with Varying HVL for AP and PA Examinations Using the Smallest Field Size 73
Figure 14 Variation of Conversion Factor with HVL for all Simulated X-ray Field Sizes 75
Figure 15 Impact of collimation on the conversion factors for head examinations showing a decrease in conversion factor when the X-ray field is greater than the phantom size. 80
Figure 16 Comparison of PCXMC Conversion Factor with Calculated Conversion Factor for Head, Heart, Kidney and Liver Examinations Performed both Through and Not Through the Table with an Ideal Fit and ± 20% Deviation 82

Figure 17 Comparison of PCXMC Conversion Factor with Calculated Conversion Factor for Prostate Examinations Performed both Through and Not Through the Table with an Ideal Fit and ± 20% Deviation 83
Figure 18 Comparison of PCXMC Conversion Factor with Updated Calculated Conversion Factors for Head, Heart, Kidney, Liver and Prostate Examinations both Through and Not Through the Table with an Ideal Fit and ± 20% Deviation 85
Figure 19 Results for Conversion Factors using the Reference Air Kerma as a Dose Metric 92
Figure 20 Conversion Factor for Reference Air Kerma Normalised to the X-ray Field Size . 94
Figure 21 Comparison of PCXMC Conversion Factor with Calculated Conversion Factors for Head, Heart, Kidney, Liver and Prostate Examinations with an Ideal Fit and ± 20% Deviation 97
Figure 22 Comparison of Conversion Factor for Examinations Undertaken With or Without the Arms in the Primary Beam 105
Figure 23 AKref to E conversion factors for head examinations using various x-ray areas 107
Figure 24 AKref to E conversion factors for head examinations using various X-ray widths while keeping the x-ray length the same..... 109
Figure 25 Lateral X-ray Views (produced from (Wang, et al., 2014, p. 1074)) for a) Uncollimated X-ray Beam, b) Collimated X-ray Beam, and PCXMC Simulation for c) Uncollimated X-ray Beam and d) Collimated X-ray Beam. Organs Shown for PCXMC are Brain (red), Salivary Glands (dark blue), Oral Mucosa (green) and Sinus (light blue). 117
Figure 26 Comparison of Effective Dose Calculations Performed using the 5 Methods Produced in this Work with the Rando Phantom Measurements 119

Tables

Table 1 Search Strategy used for Literature Review 19
Table 2 Weighting factors for various tissues in the body used to calculate E 21
Table 3 Summary of sensitivity, linearity and energy dependence for dosemeters encountered in the literature review 24
Table 4 Summary of the Range of Effective Doses for each Anatomical Region 26
Table 5 Specifications for the Various Anthropomorphic Phantoms Included in the Literature Review 28
Table 6 Summary of Papers using Monte Carlo Simulations for Effective Dose Calculations 31
Table 7 Summary of Papers using Conversion Factors to Determine Effective Dose 35
Table 8 Summary of Acquisition Parameters to be Investigated 42
Table 9 Results from measurements to determine the attenuation of the table using a Philips system 43
Table 10 Summary of the various input parameters required for the PCXMC simulations ... 46
Table 11 Clinical Acquisition Parameters used for Head and Liver CBCT Imaging using the Philips Allura Xper FD 20 Angiography System 49
Table 12 Beam Characteristics for ISON Narrow Beam and Broad Clinical Beam Conditions from (ISO 4037-3, 1999) and (Aveyard & Katsidzira, 2016) 50
Table 13 Ratios of absorbed dose in various media to absorbed dose in air from (Institute of Physical Sciences in Medicine, 1992, p. 23) 53
Table 14 Calculation of Effective Dose in Rando Phantom for Head CBCT scan 55
Table 15 Calculation of Effective Dose in Rando Phantom for Liver CBCT scan 55
Table 16 Summary of Acquisition Parameters Investigated 59
Table 17 Assessment of Total Number of Projections on Effective Dose Conversion Factor 63
Table 18 Comparison of Organ Dose Conversion Factor Differences for Examinations Performed with Primary Beam either Through or not Through the Table with the Patient Positioned Supine. 66

Table 19 Summary of the impact of the table and scan orientation on the E to DAP dose conversion factors. 68
Table 20 Variation of Conversion Factor with Varying kV for Examinations Performed Through or Not Through the Table for a Patient Positioned Supine. 70
Table 21 Impact of kV and Added Filtration on the HVL of an X-ray Beam 72
Table 22 Field sizes simulated as defined at the detector and calculated at the rotation distance 74
Table 23 Comparison of Mean and Range of Conversion Factors with Varying X-ray Field Size for Examinations Undertaken using 120kV with 0.9mmCu Filtration 77
Table 24 Organs with the Largest Differences in Radiation Dose as the X-ray Field Size is Varied 78
Table 25 Formulae for Dose Area Product to Effective Dose Conversion Factor using Beam HVL and Differences from PCXMC Results 81
Table 26 Updated Formulae for Dose Area Product to Effective Dose Conversion Factor using Beam HVL and X-ray Area at the Isocentre (A) and Differences from PCXMC Results. Results in Brackets are with the Beam HVL Less than 3mmAl Removed 84
Table 27 Conversion factors (DAP to Effective Dose) for varying kV and Additional Copper Filtration for Examinations Performed with Primary Beam Through the Table 87
Table 28 Conversion factors (DAP to Effective Dose) for varying kV and Additional Copper Filtration for Examinations Performed with Primary Beam not Through the Table 89
Table 29 Comparison of Mean and Range of Conversion Factors with Varying X-ray Field Size for the Different Examinations Simulated 95
Table 30 Formulae for Reference Air Kerma to Effective Dose Conversion Factor Using Beam HVL and X-ray Area at the Isocentre (A) and Differences from PCXMC Results. Results in Brackets are with the Beam HVL Less than 3mmAl Removed 96
Table 31 Normalised Conversion Factors (Reference Air Kerma to Effective Dose) for Varying kV and Additional Copper Filtration for Examinations Performed with the Primary Beam Through the Table 100

Table 32 Normalised Conversion factors (Reference Air Kerma to Effective Dose) for Varying kV and Additional Copper Filtration for Examinations Performed with the Primary Beam not Through the Table 103
Table 33 Comparison of Conversion Factors using the PCXMC Standard Sized Phantom with those Produced using Phantoms Corresponding to the Average UK Male and Female. All simulations use a hermaphrodite phantom. Figures in Brackets are Percentage Differences from the Standard Phantom). 111
Table 34 Comparison between Conversion Factors Reported in the Literature and Conversion Factors Produced in this Work..... 113
Table 35 Comparison Between Conversion Factors Produced by Wang et al. and this Work using Both ICRP60 and ICRP103 Weighting Factors..... 115
Table 36 Comparison of Organ Doses for Various Head Scans with Collimated and Uncollimated X-ray Beams..... 116
Table 37 Details of the Five Methods for Converting Dose Metric to Effective Dose 118
Table 38 Analysis of differences between the different methods and Rando measurements 120
Table 39 Summary of Methods used for Calculating Conversion Factors in other Applications of Diagnostic Radiology..... 122
Table 40 Sources of uncertainty in calculation and use of conversion factors 123
Table 41 Positioning of TLDs in various organs for Head Scans 148
Table 42 Positioning of TLDs in various organs for Liver Scans 149

Word Count: 25,407

1. Abstract

Cone Beam Computed Tomography (CBCT) is an established imaging technique for radiotherapy and dental applications that is increasingly finding applications in diagnostic radiology, interventional radiology and surgery. For these applications fluoroscopy equipment that is capable of producing CBCT images is used. These have different geometries and exposure parameters when compared to those for radiotherapy and dental applications and so the radiation doses to the patients need to be assessed. To ensure that the Ionising Radiation (Medical Exposure) Regulations 2017 (IR(ME)R, 2017) are adhered to knowledge of the patient doses and risks is required.

For this work Monte Carlo simulations have been performed to establish Effective Dose (E) conversion factors to allow the dose metric displayed on the system to be converted into a patient radiation dose. This information can then be used to estimate the risk from the exposure to ionising radiation and allow the technique to be compared to other imaging techniques. This will allow the IR(ME)R practitioner to justify the exposure as having a net benefit to the patient. Knowledge of the radiation doses also allows for imaging technique optimisation to be undertaken as required by IR(ME)R, 2017.

Conversion factors have been calculated depending on the anatomical site and the equipment exposure parameters. The conversion factors allow the dose metric to be converted to E using either the displayed Dose Area Product (DAP) or the reference Air Kerma (AK_{ref}) and X-ray beam area.

2. Lay Abstract

Cone Beam Computed Tomography (CBCT) is a relatively new imaging technique in diagnostic and interventional radiography that produces 3 dimensional (3D) images of the patient. CBCT imaging uses specialist equipment that is widely available in the hospital setting. These pieces of equipment are commonly used to produce live 2 dimensional (2D) X-ray images of the patient, allowing the clinical staff to observe processes (such as the heart beating), to provide treatments (removal of blockages in the arteries) or for surgery (inserting screws and plates). For CBCT imaging the X-ray source and imaging device are rotated around the patient while they lie still on the table. During the rotation the equipment takes several images (150 to 632 depending on the equipment and settings selected) which are then processed by a computer to produce 3D images of the patient.

A limitation with conventional 2D X-ray imaging is that there is no information regarding the depth of the area being imaged. Additionally any organs or objects above or below this may obscure it from view. There is therefore a benefit to having 3D images which allow the clinical staff to accurately locate the area of interest. The use of CBCT provides the clinical staff with this information during a procedure. Without CBCT imaging the patient would have to be transferred for 3D imaging.

In the UK it is a legal requirement that the radiation doses and risks from X-ray imaging are known. As this is a relatively new technique there are no established methods for determining the radiation doses from CBCT imaging. The equipment provides information about the amount of radiation it emits. This will be different to the amount of radiation that the patient absorbs which will also depend on what part of the body is being imaged. For this work, computer simulations of the CBCT examinations have been performed to allow the radiation information from the equipment to be used to calculate the radiation dose to the patient. This has been done for imaging of the head, chest, abdomen and pelvis regions. This allows the clinical staff to fulfil their legal obligations regarding the use of X-ray imaging.

3. Declaration

I declare that no portion of the work referred to in the thesis has been submitted in support of an application for another degree or qualification of this or any other university or other institute of learning.

4. Copyright

I. The author of this thesis (including any appendices and/or schedules to this thesis) owns certain copyright or related rights to it (the "Copyright") and he has given The University of Manchester certain rights to use such Copyright, including for administrative purposes.

II. Copies of the thesis, either in full or in extracts and whether in hard or electronic copy, may be made only in accordance with the Copyright, Designs and Patents Act 1988 (as amended) and regulations issued under it or, where appropriate, in accordance with licensing agreements which the University has from time to time. This page must form part of any such copies made.

III. The ownership of certain Copyright, patents, designs, trademarks and other intellectual property (the "Intellectual Property") and any reproductions of copyright works in the thesis, for example graphs and tables ("Reproductions"), which may be described in the thesis, may not be owned by the author and may be owned by third parties. Such Intellectual Property and Reproductions cannot and must not be made available for use without the prior written permission of the owner(s) of the relevant Intellectual Property and/or Reproductions.

IV. Further information on the conditions under which disclosure, publication and commercialisation of this thesis, the Copyright and any Intellectual Property and/or Reproductions described in it may take place is available in the University IP Policy (see http://documents.manchester.ac.uk/DocuInfo.aspx?DocID=24420), in any relevant Thesis restriction declarations deposited in the University Library, The University Library's regulations (see http://www.library.manchester.ac.uk/about/regulations/) and in The University's policy on Presentation of Theses.

5. Brief Statement for Examiners

This Research Project forms part of the Doctor of Clinical Science (DClinSci). In addition to the Research Project the course has taught components and an Innovation Project. The taught component consists of a Post Graduate Diploma in Healthcare Science Leadership delivered by the Alliance Manchester Business School and specialist Medical Physics units delivered by both the University of Manchester and University of Liverpool. An Innovation Project was undertaken as part of the course at the University of Manchester. A summary of the units undertaken and the associated assessments is provided in Appendix 1.

The Alliance Manchester Business School (A) units account for 120 of the course credits, specialist Medical Physics (B) units account for 150 credits and Innovation Project (C1) unit accounts for 70 credits. This Research Project accounts for the remaining 200 credits.

6. Introduction

X-rays are commonly used in healthcare for the diagnosis and treatment of a wide range of diseases. The most common use of these is the planar X-ray which produces a 2-dimensional (2D) projection through the patient. Fluoroscopy imaging produces a live X-ray image which allows for investigations of physical processes in the body (e.g. blood flow in cardiology examinations) or for monitoring during procedures (e.g. positioning of surgical tools). Computed Tomography (CT) imaging uses X-rays to produce images of slices through the patient allowing overlying anatomy to be visualised.

Cone beam computed tomography (CBCT) is another imaging technique that can be used to produce a series of images of slices through the patient to allow the 3-dimensional (3D) anatomy to be visualised in a similar way to CT. Images are acquired in CBCT using a large rectangular cone of X-rays while CT uses a narrow fan beam of X-rays. In CBCT a series of projection images are acquired as the X-ray source and detector rotate around the patient. CBCT has applications in various specialities including radiotherapy, dentistry, radiology and surgery.

In the UK the use of CBCT is governed by the Ionising Radiation (Medical Exposure) Regulations 2017 (IR(ME)R, 2017). Regulation 11 requires that every exposure to ionising radiation is justified as having a net benefit and that consideration is given to the use of alternative techniques which have the same objective but involve less or no radiation exposure. Regulation 12 requires that all exposures are optimised and that “doses arising from the exposure are kept as low as reasonably practicable consistent with the intended purpose” (IR(ME)R, 2017, p. 8). The IR(ME)R, 2017 regulations also impose duties on the employer to establish Diagnostic Reference Levels (DRLs) and to provide the patient with information regarding the benefits and risks prior to the exposure taking place. In order to comply with IR(ME)R, 2017 the radiation dose from a procedure would need to be evaluated to allow the practitioner to justify the exposure, the doses to be optimised, DRLs to be established and the risks provided to the patient.

While the principles of CBCT imaging are the same across the applications the equipment varies according to the application. This includes the physical geometry of the system, the size of the radiation beams and the X-ray exposure factors used. These factors need to be taken into account when assessing the radiation dose as imaging the same body part on different equipment or varying the exposure factors results in differences in radiation doses delivered.

For this work the radiation doses for CBCT for radiology (to include diagnostic and interventional radiology, and surgery) applications are to be investigated. In addition to these radiology applications CBCT also has applications in radiotherapy and dental imaging. Radiotherapy uses of CBCT have been excluded as they use different equipment and have a different intended purpose, i.e. to verify patient positioning and treatment volumes. Dental and extremity CBCT equipment have also been excluded as these are specialist pieces of equipment that have a different geometry to those used for radiology.

6.1. Cone Beam Computed Tomography Imaging Equipment

For this work fluoroscopy equipment capable of CBCT imaging has been investigated. Equipment is available from a range of manufacturers with different models available. The equipment consists of an X-ray tube, digital detector with fixed systems having a patient bed. There are mobile systems available which are positioned manually with the patient lying on a suitable bed.

CBCT imaging is desirable in the radiology setting due to the additional clinical information that can be provided through 3D imaging during procedures. Having 3D images allows the clinician to determine where in the patient the intervention needs to be undertaken while also providing information about the surrounding tissues. Without CBCT, images will only be visible in 2D and the patient would need to be imaged on a conventional CT scanner. Transferring a patient during a procedure is a time consuming process and if the patient is

ventilated can be associated with an increased risk of morbidity and mortality (Smith, et al., 1990).

For CBCT imaging the patient is positioned so that the anatomy of interest is at the isocentre (the point in space which the tube and detector rotate around). The position of the isocentre is dependent on the make and model of the equipment. The angular range that the tube and detector rotate through is also dependent on the equipment. In order to reconstruct a CBCT series of images, projection images from a minimum angular range of 180º is required. For the fixed equipment this is achieved through rotation of both the tube and detector. For mobile equipment such as the Ziehm Vision RFD it is not possible to perform a full 180º rotation. Therefore to ensure sufficient data is acquired for reconstruction the beam and detector are first translated, then rotated and finally translated as shown in Figure 1.

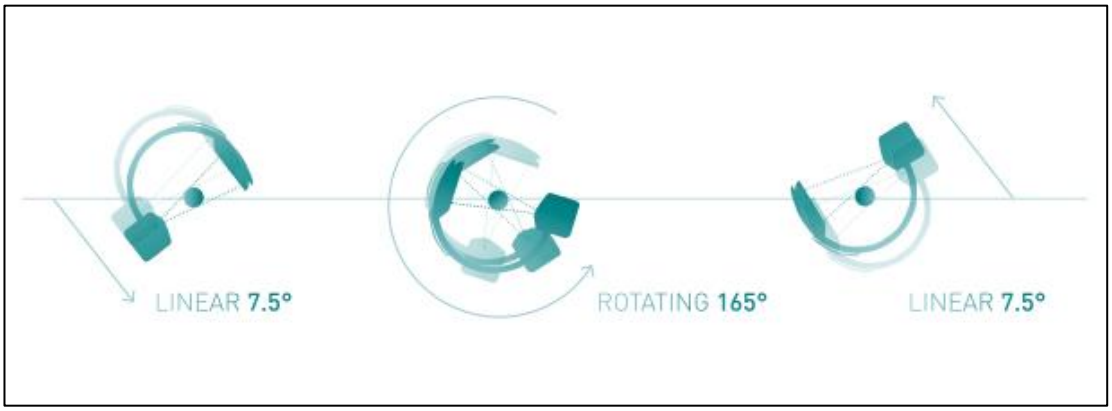

Figure 1 Diagram showing how the Ziehm Vision RFD mobile C-Arm system performs a CBCT scan. Reproduced from (Ziehm Imaging, 2019, p. 6)

In addition to the geometrical differences there are also different acquisition parameters available on the different models. Geometrical differences include the location of the isocentre and the rotation paths chosen. Acquisition parameters include the tube voltage, the tube current, the X-ray pulse duration and the filtration added to the X-ray beam. These differences in geometric and acquisition parameters mean that similar X-ray equipment may be giving different patient radiation doses. It is therefore not possible to give a single effective dose value for CBCT scans.

7. Literature Review

A literature review was undertaken on 17th December 2018 (and updated on 31st January 2019) to establish current knowledge regarding radiation doses from radiologic CBCT systems. The PubMed database was searched for keywords as detailed in Table 1. Initially the titles were reviewed against the established eligibility criteria and the abstracts were downloaded as appropriate. The abstracts were then assessed against the eligibility criteria and full papers of those that were eligible were downloaded. Those papers meeting the eligibility criteria were included in the review. Where applicable, references from the downloaded papers were also assessed and if they met the inclusion criteria added to the review. A summary of the papers included in the literature review is provided in Appendix 2.

7.1. Eligibility Criteria

Prior to conducting the literature review inclusion and exclusion criteria were established. The inclusion criteria were articles in peer reviewed journals providing details on patient effective dose from radiology CBCT systems. Only articles that were published in English were included. Articles that were related to radiotherapy, extremity or dental CBCT were excluded from the literature review. Additionally articles that did not assess patient radiation dose also were excluded.

7.2. Literature Search

The PubMed database was searched using the keywords and synonyms listed in Table 1. Synonyms were combined using the 'OR' function while the keywords were combined using the 'AND' function. The 'NOT' function was also used to exclude the terms dental and radiotherapy. The results of the search are summarised in Figure 2.

Table 1 Search Strategy used for Literature Review

Search Term	Number of results
“Radiation dose” AND “”CBCT” OR “Cone Beam CT” OR “Cone Beam Computed Tomography”” AND “Radiology” NOT “Dental” NOT “Radiotherapy”	318
“Effective dose” AND “Radiology” AND “CBCT” NOT “Dental” NOT “Radiotherapy”	153
“Cardiology” AND “Cone Beam Computed Tomography” AND “Effective Dose”	3
“Surgery” AND “Cone Beam Computed Tomography” AND “Effective Dose”	44

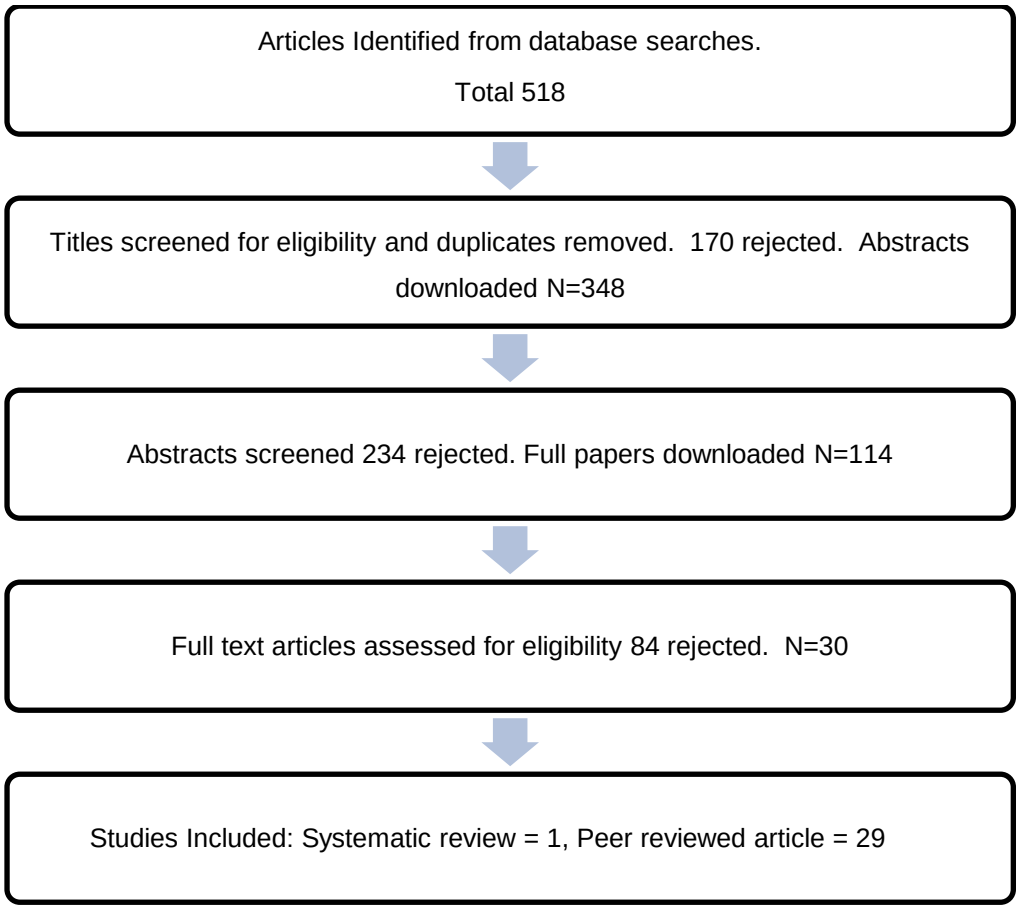

Figure 2 Results from Search Strategy

7.3. Patient Radiation Doses in Radiology

In the healthcare setting patients may be exposed to different types of ionising radiation as part of their diagnosis and treatment, including photons, electrons, protons or ions. For CBCT imaging X-ray photons are used to form images of the body and so this work will focus on their use. The International Commission on Radiological Protection (ICRP) recommend that the quantities Absorbed Dose (D), Equivalent Dose (H) and Effective Dose (E) are used for radiological protection (International Commission on Radiological Protection, 2007).

D is defined as the energy absorbed per unit mass of a particular organ or tissue, i.e. D=dε/dm where dε is the energy imparted from ionising radiation into matter of mass dm. The units of absorbed dose are joules per kilogram (J/kg) or gray (Gy).

H takes into account "the relative effectiveness of different radiation types…in causing stochastic effects at low doses" (Health Protection Agency, 2009, p. 13) and is defined as the sum of the Absorbed Dose multiplied by a radiation weighting factor (w_R). For a single type of radiation (R) (e.g. photons, electrons or neutrons) equivalent dose is defined as$H = w_R D$. For X-ray photons w_R is 1, making E and H numerically equal. The unit for H is the sievert (Sv).

For patient dose measurements E is the value of interest as this accounts for both the type of radiation and the different sensitivities of the various tissues (T) in the body to radiation. E is defined as the sum of the Equivalent Doses multiplied by a tissue weighting factor (w_T) for all tissues in the body, i.e. $E = \sum_T w_T H_T$. ICRP Report 103 (ICRP103) (International Commission on Radiological Protection, 2007) details the various tissue weighting factors which are given in Table 2. These have been updated from the previous tissue weighting factors published in ICRP Report 60 (ICRP60) (International Commission on Radiological Protection, 1991). The unit for E is also the sievert (Sv) and so care has to be given to ensuring that it is understood which dose (Equivalent or Effective) is being referred to.

Table 2 Weighting factors for various tissues in the body used to calculate E

	Tissue Weighting Factor (W_T)
Bone Marrow	0.12
Colon	0.12
Lung	0.12
Stomach	0.12
Breast	0.12
Remainder	0.12
Gonads	0.08
Bladder	0.04
Oesophagus	0.04
Liver	0.04
Thyroid	0.04
Bone Surface	0.01
Brain	0.01
Salivary Glands	0.01
Skin	0.01

A further quantity that is of interest is the Air Kerma AK. Kerma is an acronym for kinetic energy released per unit mass and can be defined for any material, in this case it is for air. For photons the AK is the energy transferred from the photons to the charged particles within the volume of interest. AK has the units of gray. AK differs from absorbed dose as it is the energy transferred to the material from the ionising radiation.

For patients D and thus H and E are not practical to measure in the various organs of the body as this would involve introducing dosemeters into the organs. An alternative method of assessing E in patients is therefore required. In addition to practical aspects of measuring the radiation dose, modern C-arm equipment used for CBCT imaging has a wide range of exposure parameters that influence the radiation dose absorbed in the patient. These parameters include the tube potential, the tube current, the number of projections, the angular range, irradiated area and the filtration of the X-ray beam. Patient specific factors such as the organs irradiated and the patient size will also have an effect on E.

IR(ME)R, 2017 and previously the Ionising Radiation Regulations 1999 have required that all equipment installed since 1st January 2000 must have suitable means (device or other feature) of informing the user of the equipment of the quantity of radiation produced during a radiological procedure. Equipment used in diagnostic radiology does not display E to the patient due to the limitations of calculating that have been discussed. Instead a dose metric is used which gives an indication of the quantity of radiation. Commonly used dose metrics include Dose Area Product (DAP), reference Air Kerma (AK_{ref}), Computed Tomography Dose Index (CTDI) and Dose Length Product (DLP).

DAP is defined as the integral of the absorbed dose (D) over the area of the x-ray beam $DAP = \int_A D(x,y)dxdy$. In the case where the dose doesn't vary across the area, DAP is the product of the absorbed dose and x-ray field area. The AK_{ref} is measured under specific conditions and represents a radiation dose in scatter free conditions at a fixed point 15cm from the isocentre in the direction of the X-ray source (ISO 60601-2-43, 2020).

The choice of dose metric is equipment specific with DAP being common for radiography and fluoroscopy, AK_{ref} for fluoroscopy and CTDI and DLP for CT. For radiography, fluoroscopy and CT these metrics can be used appropriately to estimate the effective dose received by the patient. For CBCT applications the dose metric used are either DAP and AK_{ref}, or CTDI and DLP, with different manufacturers using the different options. There are, however, no commonly used methods to convert these to E for CBCT.

To assess E for patients undergoing CBCT examinations the literature review has identified three methods that may be used; the use of an anthropomorphic phantom with suitable dosemeter, the use of Monte Carlo simulations or by applying a conversion factor to radiation measurements made either in air or a phantom.

7.4. Anthropomorphic Phantoms and Dosemeters

Nine of the papers reviewed used an anthropomorphic phantom with a detector to assess the radiation doses from CBCT to patients. Seven used the Rando Alderson phantom, one used CIRS model 701-D adult male phantom and one used the Kyoto Kagaku THRA1 phantom. For the dose measurements four of the studies used Thermoluminescent Dosimeters (TLDs), one used Metal Oxide Semiconductor Field-Effect Transistor (MOSFET), one used Hamamatsu silicon p-i-n-photodiodes, and one used EBT2 Gafchromic film.

All three of these phantoms contain tissue equivalent materials to represent soft tissue, lung and bone and have spaces to allow dosemeters to be placed inside the phantom. This way the doses in the locations corresponding to various organs or tissues can be measured then multiplied by the appropriate tissue weighting factor and E calculated.

In addition to the different phantoms used there are also differences in the choice of dosemeter that is used to measure the radiation dose within the phantom. From the literature review the most common was the TLD. TLDs are small chips that are individually positioned within the phantom and after exposure they need to be removed and the dose assessed. To ensure reliable results the TLDs need to be calibrated appropriately including testing to ensure individual chips produce comparable results. For multiple scans the TLDs have to be repositioned and the phantom reassembled. “Since several exposures are recommended to attain more reliable dosimetric values, measuring the effective dose by TLD is very laborious, time consuming and prone to mistakes” (Nardi, et al., 2018, p. 771). EBT2 gafchromic film (a type of self-developing film that can be used to measure radiation dose) has also been used as a dosemeter for insertion within the phantom. The use of EBT2 gafchromic film is subject to the same limitations as TLDs i.e. ensuring there is an appropriate calibration and needing to remove and assess the doses after each exposure.

MOSFETS and photodiodes are electronic dosemeters that can be used to measure the radiation doses within the phantom. Using these means there is no need to remove the dosemeter after each scan as the doses can be assessed while they remain in the phantom. This has the advantage of reducing the need to repeatedly set up the dosemeters in the phantom and allows for more scans to be investigated in a shorter time.

When choosing a dosemeter it is important to understand how it will respond to the radiation beams it is exposed to. The sensitivity of a detector is the minimum air kerma that is required to produce a signal (Hourdakis & Nowotny, 2014). The linearity of a detector refers to how linear the response of the detector is to a range of air kerma. The energy dependence of a dosemeter refers to the variation in response of the detector to different beam qualities. An ideal dosemeter would have a high sensitivity (allowing small air kerma values to be measured), have a linear response to air kerma and have a low energy dependence. Table 3 summarises these for the types of dosemeter encountered in the literature review.

Table 3 Summary of sensitivity, linearity and energy dependence for dosemeters encountered in the literature review

Dosemeter Type	Sensitivity	Linearity	Energy Dependence
TLD (LiF:Mg,Ti) (ThermoFisher, 2016)	10 µGy	10µGy – 1Gy	Varies across range for diagnostic radiology
TLD (LiF:Mg,Cu,P) (ThermoFisher, 2016)	1 µGy	1µGy – 10 Gy	Varies across range for diagnostic radiology
EBT2 Gafchromic Film (Ashland Inc., 2021)	1 mGy	Non-linear response – requires calibration curve	Requires calibration to be undertaken for energy being investigated
MOSFET TN-1002RD (Koivisto, et al., 2015)	1.7 mGy	Linear with no corrections in the range 0.24mGy – 17.5mGy	Not statistically significant
p-n photodiodes (Aoyama, et al., 2002)	20 µGy	0.03mGy – 10mGy	10%/10keV

The results from papers that have used anthropomorphic phantoms for patient dose calculation have been split by anatomical region into head and neck, chest and abdomen and the effective doses for the various anatomical regions are summarised in Table 4. These results show that for the same anatomical region there are a range of effective doses delivered, even on the same piece of equipment.

Table 4 Summary of the Range of Effective Doses for each Anatomical Region

Reference	Equipment	Phantom and Dosemeter	Anatomical Region	E (mSv)
(Piergallini, et al., 2018)	Philips Allura Xper FD20	Rando Phantom and TLD	Head	0.584
(Nardi, et al., 2017)	Newtom 5G	Rando Phantom and TLD	Head	0.3
(Chu, et al., 2014)	Siemens Axiom Artis	Rando Phantom and TLD	Head	3.91
(Wang, et al., 2014)	Philips Allura Xper FD20	CIRS Phantom and MOSFET	Head	0.8-1.6
(Bai, et al., 2013)	Siemens Axiom Artis dTA	Rando Phantom and TLD	Head	0.3 (0.12 – 0.43)
(Koyama, et al., 2010)	Shimadzu BRANSIST Safire	Koyoto Kagaku Phantom and Photodiodes	Head	1.2
(Nardi, et al., 2017)	Newtom 5G	Rando Phantom and TLD	Ear	0.3
(Nardi, et al., 2017)	Newtom 5G	Rando Phantom and TLD	C-Spine	0.3
(Choo, et al., 2013)	Philips Allura Xper FD20	Rando Phantom and EBT2 Gafchromic	Lung	5.72 ± 4.19
(Steuwe, et al., 2016)	Siemens Artis Zeego	Rando Phantom and TLD	Abdomen	4.9 ± 1.1
(Schegerer, et al., 2014)	Siemens Artis Zee	Rando Phantom and TLD	Abdomen	0.35 – 17.10
(Koyama, et al., 2010)	Shimadzu BRANSIST Safire	Koyoto Kagaku Phantom and Photodiodes	Abdomen (17in) Abdomen (9in)	4.0 5.2

These results demonstrate large ranges of E even where the same region is imaged on the same piece of equipment. This range is due to the range of exposure parameters that are used to acquire the images. Wang et al. investigated 7 protocols which use different kV, mA, time, frame rate, field size and spectral filters and found doses for neurovascular imaging ranging from 0.16mSv to 1.6mSv (Wang, et al., 2014). Schegerer et al. also found a large range of E depending on CBCT protocol used with abdomen CBCT doses ranging from 0.35mSv to 17.10mSv (Schegerer, et al., 2014). These results highlight a limitation to the use of this method as the results generated are specific to the equipment and exposure parameters used.

The use of an anthropomorphic phantom for measurement of E is also limited due to the size of the phantom, meaning that the calculated E in the phantom may not be the same as the E in a patient population. Other patient specific factors such as the 'gender' of the phantom can also have an impact on the calculated E, particularly in the thoracic, abdomen and pelvis regions. For the thoracic regions the Absorbed Dose in breast tissue can have a large impact on E due to the relatively large tissue weighting factor. In the abdomen and pelvis regions the differences are due to the dose to the gonads with the ovaries located in the abdomen while the testes are in the pelvis. Four of the studies used a male phantom (Rando Alderson Male, CIRS model 701-D and Kyoto Kagaku THRA1) while the other three studies did not specify the gender but did specify that the Rando Alderson Phantom was used. A summary of the construction and physical aspects of the phantoms are summarised in Table 5. Other phantoms, such as paediatric size, are also available but were not encountered in the literature review.

Table 5 Specifications for the Various Anthropomorphic Phantoms Included in the Literature Review

	RANDO Woman	**RANDO Man**	**CIRS 701-D Adult Male**	**Kyoto Kagaku THRA1**
Height (cm)	163	175	173	170
Mass (kg)	54	73.5	73	60
Arms?	No	No	No	No
Legs?	No	No	No	No
Soft Tissue	Propriety urethane with effective atomic number which simulates muscle with randomly distributed fat		Resins and polymers to simulate any human tissue	Human soft tissue substitute (WE0211)
Lung Tissue	As for soft tissue but with density that simulates lung tissue			Lung Substitute (LP-430)
Bone	Natural human skeleton			Bone Substitute (BE-303)
Reference	(The Phantom Laboratory)		(CIRS)	(Kyoto Kagaku Co. LTD)

There are limitations to using the phantom and dosemeter method when determining E in patients. The process of setting up the phantoms and measuring doses is a time consuming one, even where electronic dosemeters are used. The results these generate are only applicable to that particular system and exposure parameters used and only applicable in a patient group that match the size of the phantom that has been used. The advantage of this method is that a dose inside a patient sized phantom can be directly measured (rather than calculated or simulated) and by using appropriate weighting factors to calculate E which would not be possible in a patient.

7.5. Monte Carlo Simulation

Monte Carlo simulations use a computer software based approach to simulate the radiation transport through a patient to allow the Absorbed Dose to each organ and thus E to be evaluated. An advantage of using a Monte Carlo approach over anthropomorphic phantoms is that after developing the program it is possible to simulate a wide range of examinations or exposure parameters. Therefore Monte Carlo simulation has been deemed a "much more powerful tool for the production of conversion coefficients than measurements taken using anthropomorphic phantoms" (Dance & Castellano, 2014, p. 573).

When used for patient dosimetry it is important to ensure that the various components of the imaging system are accurately modelled. These include the X-ray source (including energy spectra and filtration), the geometry of the system and the patient. The computer code that simulates the photon interactions will also need to be accurate to ensure the correct dosimetric results (Bliznakova, et al., 2018). It is therefore very important that any Monte Carlo simulation is properly validated prior to use.

As with using physical anthropomorphic phantoms, there is a choice of computational anthropomorphic phantoms than can be used in the Monte Carlo simulation. There are three distinct categories of computational phantom that may be used, mathematic (geometrical), voxel or hybrid phantom. Mathematical phantoms represent the patient's body and organs as a combination of solid shapes while voxel phantoms are based on human anatomy derived from 3D images (such as CT or Magnetic Resonance Imaging (MRI)) which have the various organs segmented on a voxel by voxel basis. Voxel phantoms offer a more realistic human anatomy while the organ shape and positions in mathematical phantoms are criticised as being unrealistic (Dance & Castellano, 2014). Hybrid phantoms combine the mathematical and voxel approaches to constructing the phantom, using 3D anatomical models to produce polygon mesh surfaces to represent the anatomy.

Twelve of the papers reviewed used Monte Carlo methods to calculate the radiation doses received from CBCT. These are summarised in Table 6. Eleven of the papers used the Monte Carlo program PCXMC (STUK, 2011) with a mathematical phantom while the other used the BEAMnrc program (Rogers, et al., 1994) with a voxel phantom. Three of the papers quoted DAP to E conversion factors. However as these are specific to the equipment and protocol that was used in the study caution should be used as the results may not apply generally to CBCT for the given anatomical region. The range of E quoted in Table 6 again highlights the role that protocol selection plays in the overall E delivered to the patient.

The use of Monte Carlo methods for patient dose calculation has some advantages over using an anthropomorphic phantom and dosemeters. These include the ability to simulate a wide range of examinations and exposure parameters without having the time consuming task of setting up the phantom and assessing the radiation doses. The phantom that is used in the Monte Carlo simulation can be manipulated to simulate different patient sizes and body compositions. The limitations of Monte Carlo simulations include accuracy in modelling the patient anatomy and the radiation transfer through the patient. This means the simulation geometry may be difficult and time consuming to set up initially. Validation is required to ensure the results from the simulation are meaningful.

Table 6 Summary of Papers using Monte Carlo Simulations for Effective Dose Calculations

Reference	Equipment	Monte Carlo Code	Phantom Type	Anatomical Region	Effective Dose (mSv)	Conversion Factor (mSv/Gycm²)
(Xiong, et al., 2018)	Toshiba Infinix C-Arm	BEAMnrc	Voxel (Zubal)	Head	54.2 (Eye dose)	-
(Hwang, et al., 2018)	BRANSIST Safire VC17	PCXMC	Mathematical (based on Cristy and Eckerman phantom)	Abdomen	3.5	0.29 (BMI < 25) 0.26 (BMI 25 – 30) 0.23 (BMI ≥ 30)
(Stanzi, et al., 2018)	No details			Chest	11.6	-
(Sailer, et al., 2015)	Philips Allura Xper FD20			Abdomen	4.3	0.31 (All) 0.34 (Upper) 0.25 (Lower)
(Wang, et al., 2014)	Philips Allura XperCT FD20			Head	0.62 – 1.87	0.025 – 0.076
(Bai, et al., 2013)	Siemens Axiom Artis dTA			Head	0.3 (0.12 – 0.43)	0.030 – 0.035
(Podnieks & Negus, 2012)	Siemens Axiom Artis Zee			Upper Abdomen Middle Abdomen Lower Abdomen	13 10 12	-
(Strocchi, et al., 2012)	Philips Allura XperCT FD20			Chest	7.88 (3 arcs)	-

Table 6 Continued

Reference	Equipment	Monte Carlo Code	Phantom Type	Anatomical Region	Effective Dose (mSv)	Conversion Factor (mSv/Gycm²)
(Abul-Kasim, et al., 2012)	Medtronic O-Arm	PCXMC	Mathematical (based on Cristy and Eckerman phantom)	Thoracic Spine Lumbar Spine Whole Spine	0.2 – 11 0.1 – 8.6 0.3 - 20	-
(Petersen, et al., 2012)	Medtronic O-Arm			Paediatric Spine	0.5 (low dose) 8.3 (medium dose)	-
(Braak, et al., 2011)	Philips Allura XperCT FD20			Upper Thorax Lower Thorax Upper Abdomen Lower Abdomen	4.3 (2.7 – 5.8) 7.8 (4.5 – 11.2) 5.7 (4.6 – 6.8) 5.8 (2.9 – 8.8)	-
(Suzuki, et al., 2009)	GE Innova 4100			Abdomen	2.1 (155cm phantom) 3.2 (163cm phantom) 4.2 (175cm phantom)	0.31 (155cm phantom) 0.30 (163cm phantom) 0.28 (175cm phantom)

7.6. Conversion Factors

The use of either physical anthropomorphic phantoms or Monte Carlo simulations is a time consuming process when calculating E in diagnostic radiology. For other X-ray imaging modalities (e.g. general radiography, fluoroscopy, CT and mammography) Monte Carlo simulations have been used to produce tables of conversion factors which can be applied to a measurable dose metric to calculate E (e.g. NRPB-R262 (Hart, et al., 1994) and HPA-CRCE-012 (Hart, et al., 2010) for diagnostic radiology and fluoroscopy examinations). If this process could be used for CBCT it would represent a quick method of calculating E in the clinical environment. Three of the Monte Carlo and two of the anthropomorphic phantom papers reviewed in the previous sections calculated conversion factors to allow this process to be undertaken. In addition eight papers included in this review have used previously published conversion factors in the calculation of E. These are summarised in Table 7.

The majority of CBCT equipment displays DAP and AK_{ref}. However there are some that display DLP for the CBCT portion of the exposure. The conversion factors that are used to convert these metrics into E have been determined either using physical anthropomorphic phantoms with a dosemeter or Monte Carlo methods. From the previous sections it has been shown that it is important to ensure that appropriate conversion factors are used.

Three of the studies have used DLP as the dose metric when applying conversion factors. CTDI and thus DLP measurements involve the use of narrow beams in a Perspex phantom and so are not necessarily transferrable to CBCT in which a much larger beam of X-rays is employed (International Commission on Radiological Protection, 2015). These studies have used conversion factors that have been established for conventional CT scanning. The influence of the different geometries between conventional CT and CBCT has not been mentioned in the papers. Due to these differences the use of conventional CT conversion factors is not appropriate for CBCT applications.

The paper by Lange, et. al. details a method for measuring the DLP which is not the conventionally used method. Their method uses TLDs placed on a foam-plastic thoracolumbar spine model to determine the beam characteristics. In air measurements were then made and fitted to the beam characteristics determined from the TLD measurements and converted to a skin surface measurement. This is different from the conventional method of measuring the CTDI in a Perspex phantom and multiplying by the scan length. As this is not the appropriate method for measuring a DLP the conversion factors produced may not be reproducible and caution should be applied to their use. The other papers used the value of DLP that was produced by the scanner the accuracy of which is also subject to the limitations of beam size in the method used (International Commission on Radiological Protection, 2015).

Two of the studies, Perry et. al. and McKay et. al. used conversion factors that have been established for planar fluoroscopy examinations rather than specifically for CBCT. The limitation of using this dose conversion method has been acknowledged in both papers; “radiation dose conversions are not well established for CBCT and there are multiple assumptions made when converting standard dose measurements (DAP or DLP) to E” (Perry, et al., 2017, p. 1598) and “Radiation dose conversions for cone beam CT are challenging and not fully standardised” (McKay, et al., 2016, p. 57). In the remaining studies the conversion factors were either matched for equipment type or were determined as part of the study. Where equipment was matched it wasn’t stated if the acquisition parameters used were the same.

The literature review has highlighted the importance of knowing how any conversion factors that are used have been established and how these can be implemented in the correct manner in order to ensure that the calculated E is accurate.

Table 7 Summary of Papers using Conversion Factors to Determine Effective Dose

Reference	Equipment	Anatomical Region	Conversion Factor	Reference for conversion factor
(Fior, et al., 2019)	Philips XPer FD20	Chest	DAP to E 0.31mSv/Gycm²	(Strocchi, et al., 2012)
(Farah, et al., 2018)	Medtronic O-Arm	Spine	DLP to E 0.0015mSv/mGycm	(Bongartz, et al., 2004) Conversion factor for MDCT
(Hwang, et al., 2018)	BRANSIST Safire VC17	Abdomen (BMI<25) (BMI25-30) (BMI≥30)	DAP to E 0.29mSv/Gycm² 0.26mSv/Gycm² 0.23mSv/Gycm²	Monte Carlo as part of study
(Perry, et al., 2017)	Philips Angiography	Femur, Tibia, Foot Pelvis	DAP to E 0.01mSv/Gycm²	(Castellano, et al., 1995) (McParland, 1998) Conversion factor for fluoroscopy not CBCT
(Petersen, et al., 2018)	GE Innova 4100	Abdomen	DAP to E 0.3mSv/Gycm²	(Suzuki, et al., 2009)
(Costa, et al., 2016)	Medtronic O-Arm	Spine	DLP to E using IMPACT CT spreadsheet	IMPACT CT Conversion factors for CT
(McKay, et al., 2016)	Philips XPer Guide	Abdomen and Pelvis	DAP to E 0.22mSv/Gycm²	(Compagnone, et al., 2012) Conversion factor for single plane not CBCT using GE Innova 3100 or Siemens Angiostar Plus
(Rotolo, et al., 2016)	Philips XPer FD20	Chest	DAP to E 0.31mSv/Gycm²	(Strocchi, et al., 2012)
(Wang, et al., 2014)	Philips XPer FD20	Head	DAP to E 0.025 – 0.076 mSv/Gycm²	CIRS phantom measurements as part of study

Table 7 Continued

Reference	Equipment	Anatomical Region	Conversion Factor	Reference for conversion factor
(Sailer, et al., 2015)	Philips XPer FD20	Abdomen(All) (Upper) (Lower)	0.31mSv/Gycm² 0.34mSv/Gycm² 0.25mSv/Gycm²	Monte Carlo as part of study
(Choo, et al., 2013)	Philips XPer FD20	Chest	DAP to E 0.45mSv/Gycm²	Rando phantom measurements as part of study
(Lange, et al., 2013)	Medtronic O-Arm	Spine	DLP to E 0.0153mSv/mGycm	(Deak, et al., 2010) Conversion factors for CT
(Bai, et al., 2013)	Siemens Axiom Artis dTA	Head	DAP to E 0.030 – 0.035 mSv/Gycm²	Monte Carlo as part of study

7.7. Literature Review – Discussion

Nardi et. al. published a systematic review into radiation doses in non-dental CBCT (Nardi, et al., 2018). The equipment included in this review did not include any C-arm systems and the examinations were limited to ear, paranasal sinuses, ankle, wrist, knee and C-spine. These applications were excluded from this review as they were undertaken on equipment that was designed for either dental or extremity CBCT applications. The conclusion "Effective doses varied significantly because of different exposure settings of CBCT units and different dosimetry systems used to estimate dose" (Nardi, et al., 2018, p. 765), however, is similar to what has been found in this literature review.

The use of either anthropomorphic phantoms or Monte Carlo simulations have been used to measure or simulate E that is received by patients when undergoing CBCT imaging. Each of these methods has also been used to establish conversion factors to convert a dose metric displayed on the CBCT unit to E. The use of conversion factors represents a relatively simple method to calculate E for patients undergoing CBCT. However due to the range of equipment and exposure parameters that are available conversion factors quoted may not be suitable even for the same examination. The objective of this work is to produce such a table of conversion factors that can be applied to a wide range of CBCT equipment to calculate E for a range of examinations.

To achieve this, for each anatomical region the influence of applied kV, added filtration, radiation field size, number of projections and angular range of the exposure would need to be determined and accounted for.

8. Aims and Objectives

The literature review has shown that there are limited resources available to enable a simple calculation of patient radiation doses for CBCT when used in diagnostic and interventional radiology. The aim of this work is to produce a set of conversion factors to allow a conversion from the dose metric displayed on the system to E for the various anatomical sites where CBCT is clinically used. The objectives to achieve this aim are:

1. To investigate and establish the method to be used to produce the conversion factors.
2. Investigate the current clinical use of CBCT in diagnostic and interventional radiology to ensure that the full range of clinical applications is included.
3. Review the current equipment in the UK capable of undertaking CBCT examinations and establishing the exposure parameters used.
4. Set up and validate the chosen method for calculating conversion factors for the clinical examinations and equipment.
5. Calculate the conversion factors for the clinical examinations.

9. Methodology

9.1. Choice of Dose Calculation Method

From the literature review it was found that there are two different methods widely used for the calculation of E in diagnostic radiology, i.e. Monte Carlo simulations or anthropomorphic phantoms with dosemeters inserted. Due to the time consuming process of setting up and reading the dosemeters it was decided that for this work the calculation of E would be undertaken using the Monte Carlo method. This also has the advantage of being able to simulate a wide range of examinations using various equipment settings without requiring access to the clinical equipment. To ensure that the Monte Carlo simulations had been correctly set up it was decided that two of the examinations would be verified using an anthropomorphic phantom with suitable dosemeters.

9.2. Monte Carlo Simulations

The literature review showed that for Monte Carlo simulations different simulation packages and codes can be used to determine E. The literature review revealed two Monte Carlo packages had been used; BEAMnrc and PCXMC. Other Monte Carlo packages for the calculation of E also exist which have different methods for simulating the photon and charged particle transport through different media. The Monte Carlo codes allow for the modelling of different particles and can be set to simulate different types of interaction based on the application. The greater the number of particle types or interactions included will have an impact on the time taken to undertake the simulation. A balance between the accuracy required for the given task, the types of radiations that need to be simulated, the number of incident photons and the time taken needs to be achieved.

For diagnostic radiology applications X-ray photons with energies up to 140keV are of primary concern. This limits the types of interaction required for the simulation to photo-electric absorption, Rayleigh scattering and Compton scattering. Following a photo-electric

absorption event a Monte Carlo code can be set-up to follow the electron history. However for diagnostic radiology energies it is “sufficient in most cases to assume that energy deposited after a photon interaction is locally absorbed” (Dance & Castellano, 2014, p. 573). This assumption is based on the limited range of the secondary electron within the patient due to the relatively low energies used and provides a time saving when running the simulation.

In order to calculate E a computational phantom is required for the Monte Carlo simulation. As discussed in section 7.5 there are two categories of phantom that can be used; a mathematical or voxel phantom. Voxel phantoms give a realistic patient geometry and organ positions as they are based on real patient data while mathematical phantoms represent the organs as a combination of simple geometric shapes which are easier to specify when setting up the simulation.

For this work E to patients undergoing CBCT examinations was calculated using the Monte Carlo simulation software PCXMC Rotation, Version 2.0.1.5 Rotation (STUK, 2012). PCXMC is a Monte Carlo program used for calculating organ doses and E delivered from diagnostic radiology X-ray examinations from the Radiation and Nuclear Safety Authority of Finland (Tapiovaara & Siiskonen, 2008). PCXMC was chosen for this work as it has a easy to use interface, can be set up to simulate rotational scans using a variety of geometries and radiation qualities and has been previously validated for diagnostic radiology (Tapiovaara & Siiskonen, 2008).

For organ dose and E calculations PCXMC uses mathematical phantoms from Christy and Eckerman (Cristy & Eckerman, 1987) that cover a range of ages from new born to adult. It is also possible to specify the height and mass of the phantom to customise for different patient demographics. The standard adult hermaphrodite phantom has been used which has a height of 178.6cm and a mass of 73.2kg.

The Photon transport used in PCXMC is fully described in the documentation accompanying the program (Tapiovaara & Siiskonen, 2008). Photons are simulated to be emitted from a point source and are constrained to a solid angle that is defined by the field size dimensions which the user selects. The user can specify the filtration that is present in the beam with up to two different filter materials included. The specifications for the different CBCT equipment were reviewed to obtain the filters that are used clinically. There was some variation in the total beam filtration (3 – 3.5mm Al equivalent) and a range of spectral filters (0 – 1mmCu) included. These combinations can all be simulated in PCXMC. The X-ray spectra is then calculated using the Birch and Marshall method (Birch & Marshall, 1979) taking into account the applied kV, tube angle and the filtration.

PCXMC uses pseudo random numbers to simulate the initial photon direction, distance between interactions, type of interaction and scattering angle with associated energy loss. The photons are followed through the phantom until the energy falls below 2keV where it is forced to be fully absorbed or until it exits the phantom without entering it again. To reduce the simulation time PCXMC simulates organ doses for monochromatic photons in increments of 10keV and then uses interpolation to ascertain the dose for energies between these values.

9.3. PCXMC Monte Carlo Set-up and Validation

A review of the current clinical applications for CBCT was undertaken from both the literature and local clinical practice to determine the examinations to be simulated. The review found that the most commonly performed examinations utilising CBCT imaging were of the head, heart, kidneys, liver, abdominal aorta and prostate. These represent scanning in the major body parts; the head, thorax, abdomen and pelvis. Extremity and dental CBCT is performed at some sites using dedicated equipment, but this is out of the scope of this work.

Technical reference manuals for each piece of CBCT equipment currently available in the UK (Supply Chain Coordination Limited, 2019) were obtained to allow the Monte Carlo simulations to be set up according to geometries and beam conditions available. These are summarised in Table 8. This includes equipment from Canon (formally Toshiba), GE, Philips, Siemens and Ziehm.

Table 8 Summary of Acquisition Parameters to be Investigated

Parameter	**Values Investigated**
kV	60-120
Frame rate (f/s)	30
Number of frames	150, 300, 313, 600, 632
Field Sizes at detector (cm)	48, 40, 32, 30, 20, 16, 12
Focus to Isocentre distance (cm)	75, 71, 82
Added Filter (mm Cu)	0, 0.1, 0.2, 0.3, 0.5, 0.6, 0.9, 1.0
Angle of Acquisition	180°, 200°

For CBCT imaging all the systems use an angular range that is less than 360° with the majority rotating through the PA projection (for a patient lying supine). For some projections the attenuation of the table needed to be accounted for in the Monte Carlo simulations. To achieve this the dose metric and beam filtration were adjusted for the attenuation and filtration provided by the table. The attenuation of the table was measured using an ionisation chamber positioned free in air at a distance of 100cm from the focal spot. Exposure factors of 85 kV and 13 mAs were used and the AK was measured. The measurements were repeated five times and the average AK for each set used to determine the table attenuation. This was repeated twice at 125 kV and 91 mAs to determine the energy dependence. Due to the operation of the equipment it was not possible to vary the factors manually which has limited the range of energies used. These measurements have been made without backscatter included in the beam as this is how the dose metrics are defined. The results of these measurements are given in Table 9. The impact of the angle

of incidence and thus the path length through the table have not been considered. These measurements provide a factor to apply to the dose metric to simulate the beam passing through the table. For the extra filtration provided by the table, information was obtained from the equipment manuals.

Table 9 Results from measurements to determine the attenuation of the table using a Philips system

	kV	mAs	Additional Filtration	Mean Output (µGy)	Table Attenuation Factor
No Table	85	13	0.1mm Cu	343.3	0.836
Through Table				287.1	
No Table	125	91	0.1mm Cu	6216	0.848
Through Table				5271	

To determine which projections these factors are applied to, raw projection images from a CBCT scan were visually analysed and the angle of projections which passed through the table were recorded. Where the table is partially included in the X-ray beam a threshold of greater than 50% was used to determine if it was included in the simulation.

When setting up PCXMC the total number of photons that are simulated can be specified. This represents a trade-off between the percentage error in the simulation and the computational time required. PCXMC calculates the organ doses for batches of monochromatic photons in energies in steps of 10keV. The absorbed energy is obtained as an average of these batches and the statistical error is estimated from the standard deviation of the batches. An investigation was undertaken to determine an appropriate number of photons to use for the simulations. The same simulation (Philips Allura, Liver exam, 120kV, 313 projections) run was conducted and the results are shown in Figure 3. Initially there is a sharp reduction in the error but after 10,000 photons per projection there is a more gradual reduction in error with a significant increase in simulation time. The PCXMC user guide recommends a minimum of 10,000 photons to be used and suggests 20,000 photons for a balance between computational time and accuracy (Tapiovaara & Siiskonen,

2008). Based on this investigation 20,000 photons per projection were used to keep the total calculation time low while keeping the simulation error below 1%.

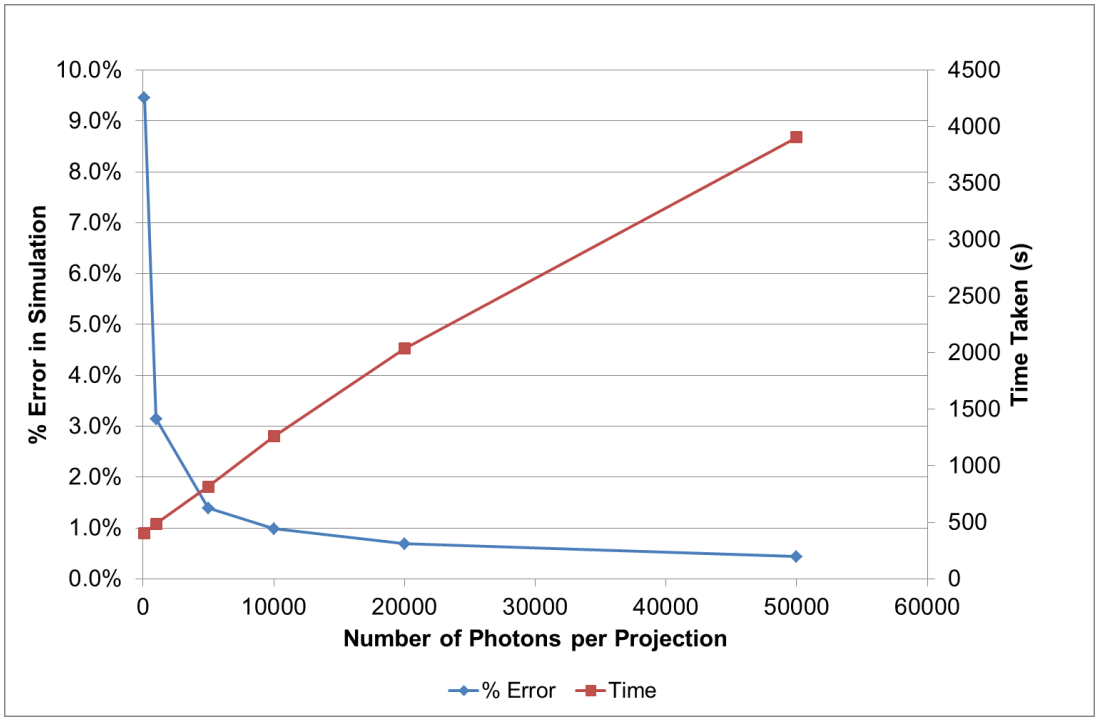

Figure 3 Results from Investigation into the Simulation Error and Time Taken for Different Numbers of Photons Simulated

PCXMC allows for different input dose parameters to be used; AK_{ref}, DAP, Exposure at Reference Distance, Exposure-Area Product and Current-Time Product (mAs). In diagnostic radiology in the UK AK_{ref} and DAP are commonly used parameters and are displayed on the equipment and so have been chosen for the input values for the Monte Carlo simulations. Although the mAs is also displayed on the system the PCXMC user manual states that using this method could introduce up to a 30% error (Tapiovaara & Siiskonen, 2008, p. 14) in the calculation depending on how the system has been calibrated at set-up. It was therefore decided not to use this as an input for this work. Changes in the tube current or exposure time per frame will have a linear impact on the DAP and AK_{ref} so changes in these parameters will be accounted for by the conversion factors.

PCXMC has options that allow the arms to either be present or removed from the phantom. In clinical practice the patient would be imaged with their arms out of the X-ray beam if possible as the presence of the arms can introduce artefacts into the images. When setting up the simulations the arms were removed from the phantom to represent best clinical practice.

9.3.1. PCXMC Geometry

The geometries in PCXMC rotation are defined relative to the phantom with the x-coordinate being patient's right (negative) to left (positive), y-coordinate being patient AP (negative) to PA (positive) and z-coordinate being along the body from foot (negative) to head (positive). The origin (x=0, y=0 and z=0) represents the middle of the base of the trunk of the phantom. The angle of the incident beam is defined as 0º being left-lateral, 90º is PA, 180º right-lateral and 270º AP. The incident beam can also be angled in the Cranio-caudal direction with positive being cranial rotation and negative being caudal direction. The radiation field in PCXMC rotation is defined using the Focus to Rotation Distance (FRD), Beam Width and Height at the rotation distance, coordinates for centre of radiation beam at FRD, rotation angle and caudo-crainal angle.

On the individual pieces of equipment the field size is defined at the detector and may be defined as either a diagonal (corner to corner) or the length of the side of the square field size. PCXMC however requires the field size to be defined as beam height (z-axis) and width (perpendicular to z-axis) at the FRD. This was achieved by applying a simple geometric conversion to the field size that was defined at the detector. For rectangular (rather than square) fields with the field size defined as a diagonal measurement the dimensions of the field were obtained from the equipment documentation before the geometric conversion was applied.

9.3.2. PCXMC Set-up

To undertake the simulations for this work PCXMC was set to run in batch mode known as autocalc with all of the individual projections being defined in a Spreadsheet (AutocalcRotation) which is provided with PCXMC rotation. This allows the input parameters to be provided, uses Macros to produce first the definition files for PCXMC, runs the simulation and finally copies the results into the spreadsheet. To vary some of the parameters (e.g. number of photons, anode angle and filter materials) required the Macros to be modified. A summary of the input parameters is given in Table 10. Full details on the PCXMC set-up used for this work are in Appendix 3.

Table 10 Summary of the various input parameters required for the PCXMC simulations

Parameter	Description	Fixed or variable	Comments
Hospital	Parameter to identify scan.	Variable.	Used here to define equipment used.
Examination	Description of examination.	Variable.	
Projection	Parameter to define the incident angle of the x-ray beam around the patient.	Variable.	Angle defined relative to the patient as detailed in section 9.3.1.
Oblique Angle	Parameter to define the cranio-caudal angle of the incident x-ray beam.	Variable.	Set to 0º for all projections in the work.
Patient Number	Parameter to identify scan.	Variable.	Used here as a unique identifier for each exam.
Patient Height	Parameter to define the individual patient height.	Variable.	For majority of the work this was set to default (0).
Patient Weight	Parameter to define the individual patient mass.	Variable.	For majority of the work this was set to default (0).
Patient Age	Parameter to define the individual patient age.	Variable.	For majority of the work this was set to default (30) to represent an adult.
X-ray tube voltage	Parameter to define the x-ray kVp used in the simulation.	Variable.	For this work considered range 60kV – 120kV in 10 kV steps.
Filtration (mm Al)	Parameter to define the inherent filtration for the x-ray beam.	Fixed for each piece of equipment.	Value used based on review of the documentation.
Additional Filter (mm Cu)	Parameter to define the additional copper filtration for the x-ray beam.	Variable.	Values used based on review of the documentation – 0, 0.1, 0.2, 0.3, 0.5. 0.6, 0.9 and 1.0.
FRD	Parameter to define the focus to rotation distance.	Fixed for each piece of equipment.	Value used based on review of the documentation.

Parameter	Description	Fixed or variable	Comments
X-ray beam width	Parameter to define the x-ray beam width (perpendicular to z-axis) at the FRD.	Variable.	Value used based on review of the documentation.
X-ray beam height	Parameter to define the x-ray beam height (parallel to z-axis) at the FRD.	Variable.	Value used based on review of the documentation.
Xref	Parameter to define the x coordinate of the centre of the x-ray beam.	Fixed.	Set to 0 based on clinical use of the equipment.
Yref	Parameter to define the y coordinate of the centre of the x-ray beam.	Fixed.	Set to 0 based on clinical use of the equipment.
Zref	Parameter to define the z coordinate of the centre of the x-ray beam.	Variable.	Used to define the location of the scan along the z-axis.
Arms in Phantom	Parameter to define if arms are included in the scan.	Fixed.	0 – arms excluded was used for majority of this work.
Input Dose quantity	Parameter to define the dose metric used as an input.	Fixed.	For this work EAK (air kerma at reference point (no backscatter) and DAP have been used.
Input Dose Value	Parameter to define the quantity of the dose metric.	Variable.	Set so the total for a CBCT scan is either EAK = 1Gy @ AK_{ref} or DAP = 1Gycm².
Number of photons	Defines the number of photons used in the simulation for each projection. Is varied by changing Macro.	Variable.	For majority of this work used 20,000.
Tube Target Angle	Defines the angle of the target in the x-ray tube. Is varied by changing Macro.	Fixed for each piece of equipment.	Default value used.

9.4. Thermoluminescent Dosemeter Calibration

Lithium Fluoride doped with Magnesium TLDs (Thermofisher TLD100) were used for measurements in a Rando Man Phantom (The Phantom Laboratory). The TLDs were provided, processed and reported by the local Approved Dosimetry Service (ADS). The ADS is part of the Radiation Protection Service (RRPPS) at University Hospitals Birmingham NHS Foundation Trust (University Hospitals Birmingham NHS Foundation Trust, 2020).

The ADS calibrate the TLDs using a Caesium-137 gamma source with photon energy of 661.7 keV (Lockheed Martin, 2002). The TLDs have previously been characterised by the ADS (Aveyard & Katsidzira, 2016) which has shown that the LiF TLDs over-respond at the energies used in diagnostic radiology. The response, using international standard narrow beam X-ray spectra (ISO 4037-3, 1999), is shown in Figure 4.

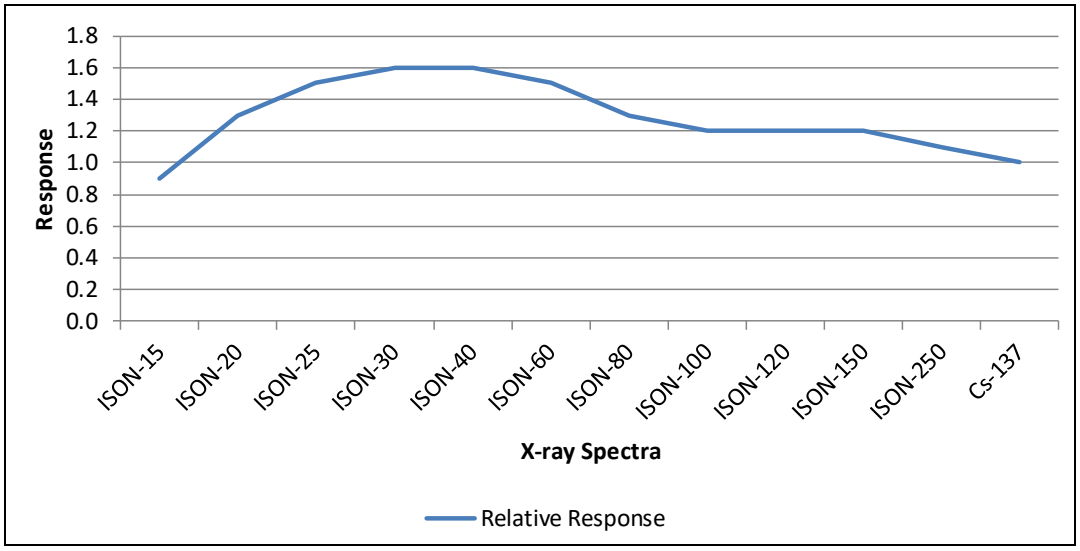

Figure 4 Response of TLDs to X-ray Spectra Relative to Cs-137 Reproduced from (Aveyard & Katsidzira, 2016)

For the Rando Phantom measurements a Philips Allura Xper FD 20 Angiography system (Philips Healthcare, Best, The Netherlands) was used. CBCT images were acquired using the default acquisition parameters for both head and liver scans which are detailed in Table 11.

Table 11 Clinical Acquisition Parameters used for Head and Liver CBCT Imaging using the Philips Allura Xper FD 20 Angiography System

Parameter	Xper CT Cerebral High Dose	Xper CT Abdomen Low Dose
kV	120	120
mA	250	175
ms	5	7
Frame rate (f/s)	30	30
Added Filter	1mm Cu + 1mm Al	1mm Cu + 1mm Al
Angle of Acquisition	-90 to +90	-90 to +90
Total time (s)	20.8	10.3
Total frames	624	310

To determine the correction factor to compensate for the TLD response the beam characteristics for the ISON and clinical spectra were compared (see Table 12).

Table 12 Beam Characteristics for ISON Narrow Beam and Broad Clinical Beam Conditions from (ISO 4037-3, 1999) and (Aveyard & Katsidzira, 2016)

X-Ray Spectra	Applied kV	Filter	Mean Energy (keV)	HVL (mm Al)	Response (rel. to Cs-137)
ISON-20	20	1.025 mm Al	16	0.3	1.3
ISON-25	25	2.05 mm Al	20	0.6	1.5
ISON-30	30	4.10 mm Al	24	1.1	1.6
ISON-40	40	0.22 mm Cu	33	2.3	1.6
ISON-60	60	0.63 mm Cu	48	5.6	1.5
ISON-80	80	2.00 mm Cu	65	9.6	1.3
ISON-100	100	5.04 mm Cu	83	12.8	1.2
ISON-120	120	1.03 mm Sn & 5.05 mm Cu	100	14.9	1.2
Cs-137	N/A	N/A	662	6.5mm Pb	1
Clinical	120	2.9 mm Al & 1 mm Cu & 94 mm PMMA	63	7.6	To be determined

For each ISON and clinical beam the spectra were simulated using the Siemens simulation of X-ray spectra software (Siemens Healthineers, 2020). These were compared to ascertain their suitability for correcting the TLD results obtained using a clinical beam (Figure 5). It can be seen that the ISON spectra are sufficiently different to the clinical spectra and so these correction factors cannot be applied to the results.

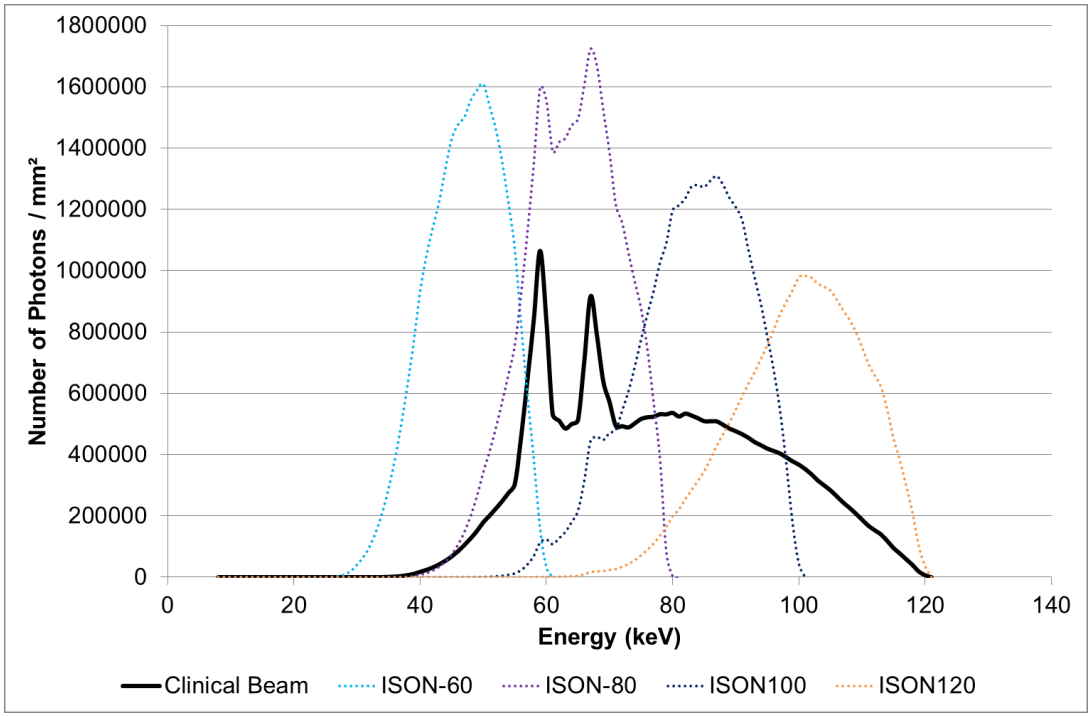

Figure 5 Comparison of X-ray Spectra for the Relevant ISON and Clinical Beams

A calibration factor for the clinical beam was determined by recreating the beam and scatter conditions in the Rando phantom. To determine the calibration factor TLDs and ionisation chamber (6cc Radcal Accu Pro) were positioned centrally 9.4cm deep in an 18.8cm Perspex phantom with 1mmCu and 1mmAl filter added to the beam. Twenty five repeated measurements were performed with the TLDs being replaced for each measurement.

The results from the TLD calibration showed a difference between the reported personal dose equivalent ($Hp_{0.07}$) and that measured using an ionisation chamber. The dose distributions for twenty five repeated measurements are given in Figure 6. These results indicate a difference between the means of 34.5% (3.14mSv ($Hp_{0.07}$) and 2.33mGy (Air Kerma)). A statistical analysis was undertaken on the measurements. For this the null hypothesis was set to there being no statistically significant difference between the two sets of results.

SPSS (IBM, 2013) was used to undertake a two sample t-test on the results against the null hypothesis. A Levene's test for equality of variances showed that the two data sets have

statistically different variances and a t-test for unequal variances was undertaken. The t-test gave strong evidence against the null hypothesis with a p value of 0.000. A calibration factor of 0.743 (i.e. 1/1.345) was applied to the raw TLD results and the two sample t-test was repeated. This gave little evidence against the null hypothesis with a p value of 0.984. The statistical analysis shows that for the clinically used spectra, the TLD readings over-estimate the dose by a factor of 1.345.

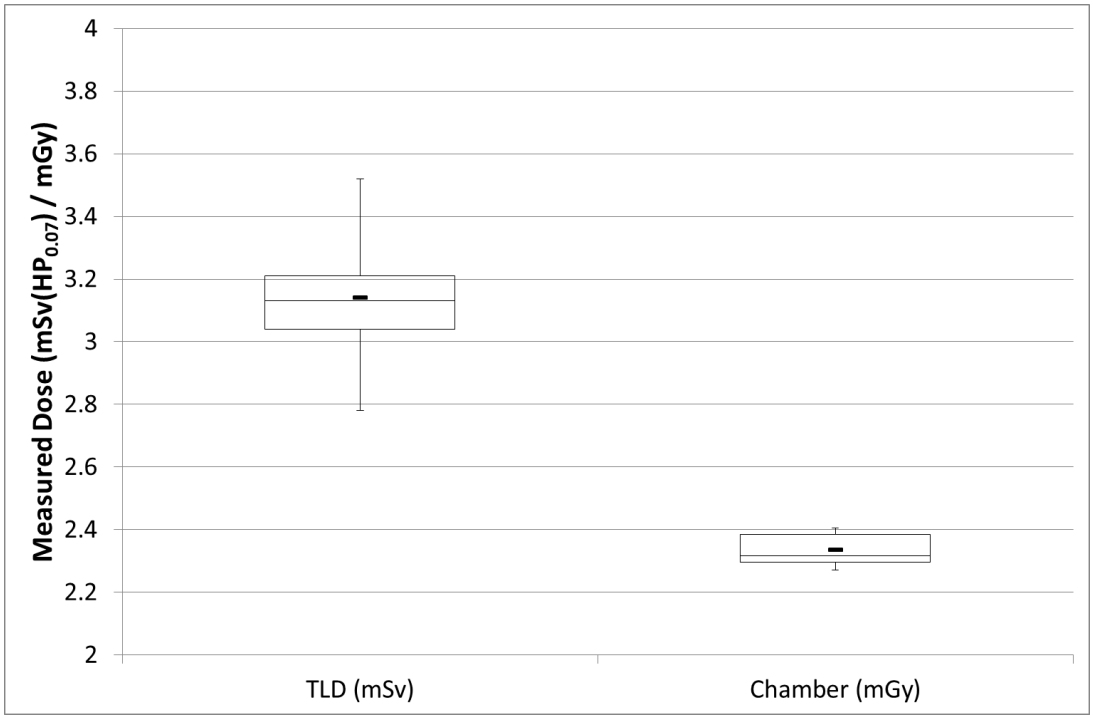

Figure 6 Comparison between TLD Results (HP0.07) and Ionisation Chamber Measurements made using Clinical X-ray Acquisition Parameters.

In addition to the differences between the chamber and TLD measurements there is also a range of results produced by the TLDs for a given exposure. These results give a standard error (defined as twice the standard deviation divided by the mean value) of 9.8%

The Calibration factor that has been derived can be used to convert $HP_{0.07}$ to AK. However this cannot necessarily be used to measure an absorbed dose in the phantom due to differences in the definitions of AK and D. AK is a measure of the energy that is transferred from uncharged particles (x-ray photons) to the air while D is a measure of the energy

deposited in the matter. Energy is transferred from the x-ray photons to electrons within the matter. If the electrons leave the organ then the absorbed dose will not be equal to the kerma. To evaluate the impact this will have on the measurement of absorbed dose, the ratios of absorbed dose in various media to absorbed dose in air has been investigated. These ratios are given in Table 13 and show that for the range of energies encountered in various body tissues the absorbed dose in the various media is within 10% of the absorbed dose in air. As the ratios are within the uncertainty of the TLD measurements these have not been applied to the TLD results. The absorbed dose has been calculated as $D = 0.743 \times TLD$.

Table 13 Ratios of absorbed dose in various media to absorbed dose in air from (Institute of Physical Sciences in Medicine, 1992, p. 23)

Medium	50kV (2.0mm Al)	80kV (2.5mmAl)	120kV (4.0mmAl)
Water	1.02	1.02	1.11
Striated muscle	1.05	1.06	1.07
IRCU reference man soft tissue	0.95	0.96	1.0
ICRU sphere tissue	0.94	0.95	1.05
Skeletal muscle	1.05	1.05	1.06

9.5. Rando Phantom Measurements

In order to validate the results from Monte Carlo simulations, measurements using a physical anthropomorphic phantom, the Rando Man phantom were made. This phantom contains a skeleton and propriety urethane with density to simulate lungs and soft tissue. The phantom used represents a male with a height of 175cm and mass of 73.5kg. The Rando phantom consists of 36 slabs which have spaces within them to allow dosimeters to be positioned to measure the dose within the phantom during an X-ray exposure.

The method of Scalzetti et al (Scalzetti, et al., 2008) was used to obtain mean organ doses in the Rando phantom using TLDs. Prior to any TLD measurements, the Rando phantom was placed on the table and positioned using fluoroscopy. Anatomical landmarks were used

to ensure that the positioning was matched with the positioning used for the Monte Carlo simulations. The positioning of the Rando phantom was marked on the table so this could be reproduced once the TLDs were positioned in the phantom.

The TLDs were positioned within the phantom at various locations corresponding to organs of interest. The Rando phantom was then scanned using the clinical protocols for head and liver given in Table 11 with the TLDs being replaced between the scans. For the head scan 61 TLDs were placed in the phantom covering organs from the top of the skull to the bottom of the lungs. For the liver scans 110 TLDs were placed covering the organs from the top of the lungs to the bottom of the phantom. Full details of the positioning of the TLDs is given in Appendix 4.

The TLDs were then read at the ADS and the previously determined calibration factor (0.743) was applied to the results. The average dose within each organ was calculated and the ICRP103 organ weighting factors (ICRP, 2007) applied and summed to calculate E. The organ and effective doses for the head and liver CBCT scans are given in Table 14 and Table 15. The uncertainty in these results is the uncertainty in the TLD readings (which was calculated in section 9.4 to be 9.8%) multiplied by the organ weighting factor. The ADS has a minimum dose (0.2mSv) below which the results are assigned a '*' rather than numerical value. Where a '*' has been reported a value of 0.2mSv has been used as the uncertainty in the results. To convert the uncertainty in the TLD readings to the uncertainty in E the uncertainty in TLD reading for each organ has been multiplied by the organ weighting factor then summed across all the organs.

Some of the organs used to calculate E have only been partially irradiated in the CBCT scans e.g. bone marrow, bone surface and skin. For these organs the mass irradiated was estimated as a proportion of the total organ. For the various organs these proportions have been obtained from (Cristy & Eckerman, 1987).

Table 14 Calculation of Effective Dose in Rando Phantom for Head CBCT scan

	Weighting Factor	Corrected TLD Dose (mGy)	Weighted Dose (mSv)	Uncertainty (mSv)
Bone Marrow	0.12	1.32	0.16	0.015
Colon	0.12	0.00	0.00	0.024
Lung	0.12	0.58	0.07	0.007
Stomach	0.12	0.00	0.00	0.024
Breast	0.12	0.00	0.00	0.024
Remainder	0.12	1.69	0.20	0.010
Gonads	0.08	0.00	0.00	0.016
Bladder	0.04	0.00	0.00	0.008
Oesophagus	0.04	3.63	0.15	0.014
Liver	0.04	0.00	0.00	0.008
Thyroid	0.04	3.63	0.15	0.014
Bone Surface	0.01	1.32	0.01	0.001
Brain	0.01	15.87	0.16	0.016
Salivary Glands	0.01	14.76	0.15	0.014
Skin	0.01	1.61	0.02	0.002

Effective Dose: 1.06 ± 0.20mSv

Table 15 Calculation of Effective Dose in Rando Phantom for Liver CBCT scan

	Weighting Factor	Corrected TLD Dose (mGy)	Weighted Dose (mSv)	Uncertainty (mSv)
Bone Marrow	0.12	1.63	0.20	0.019
Colon	0.12	3.33	0.40	0.039
Lung	0.12	1.58	0.19	0.019
Stomach	0.12	7.08	0.85	0.083
Breast	0.12	0.66	0.08	0.008
Remainder	0.12	3.98	0.48	0.047
Gonads	0.08	0.16	0.01	0.001
Bladder	0.04	0.19	0.01	0.001
Oesophagus	0.04	0.59	0.02	0.002
Liver	0.04	6.74	0.27	0.026
Thyroid	0.04	0.00	0.00	0.008
Bone Surface	0.01	1.63	0.20	0.002
Brain	0.01	0.00	0.00	0.008
Salivary Glands	0.01	0.00	0.00	0.008
Skin	0.01	0.95	0.01	0.001

Effective Dose: 2.71 ± 0.27mSv

9.6. Monte Carlo Validation

To validate the PCXMC set-up the head and liver scans performed on the Rando phantom were simulated and the results compared. Simulations were run using the total DAP and AK_{ref}. The results from the validation are given in Figure 7 which shows agreement with Rando measurements within the errors in measurement and simulation.

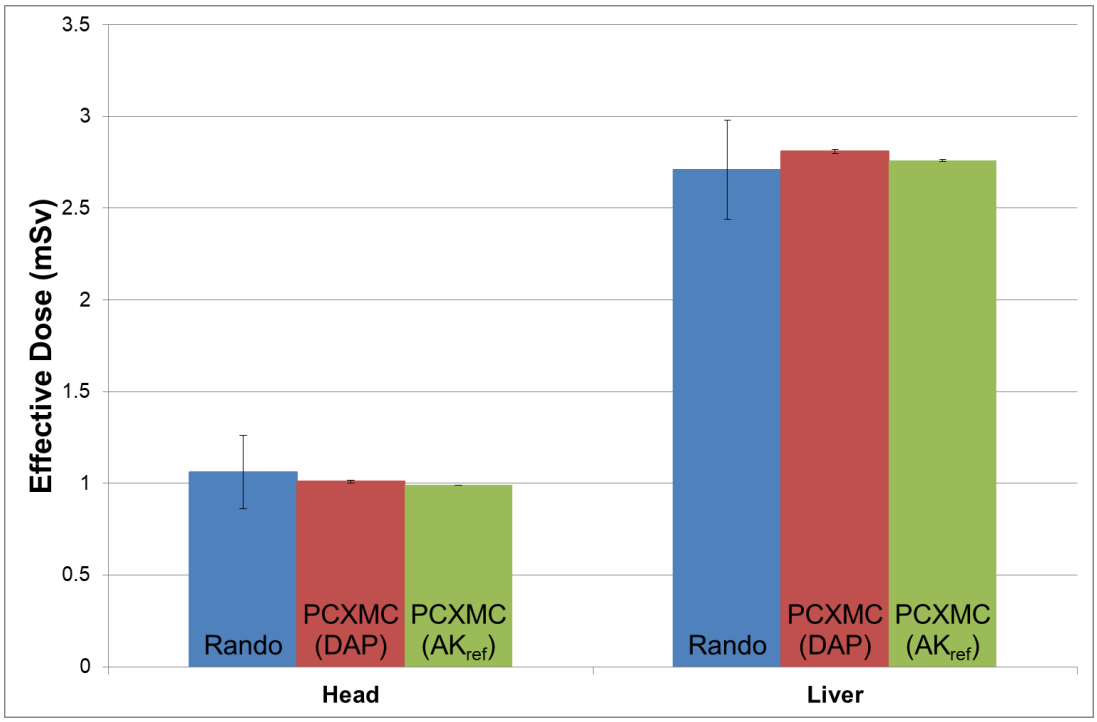

Figure 7 Validation of PCXMC Simulations

While the overall E was found to be in agreement the individual organ doses used to calculate E were also investigated. The comparisons are shown in Figure 8 and Figure 9. These show that while the effective doses are similar for both methods there are some organs which have very different absorbed doses. For head scans the organ with the greatest difference was the bone surface. There are several factors that lead to this difference. For the Rando measurements I was unable to position the TLDs within the bone. Instead the TLD was positioned inside the skull resulting in a lower measured dose by the TLD. In addition to this cortical bone has a higher atomic number than both soft tissue and air resulting in more photoelectric interactions. As the TLDs have been calibrated to

absorbed dose in air this will result in measuring a lower absorbed dose in the bone. The accuracy of measured absorbed dose in bone will also be affected by how close the TLD has been positioned to the bone. At the interface between the bone and the soft tissue there is no longer electronic equilibrium. This will result in a higher absorbed dose in this tissue, however if the TLD is placed away from the interface this will not be measured. PCMXC accounts for this in the calculation of bone marrow dose by using a energy dependent kerma to dose conversion factor but this is not done for other tissues. For the liver scans the biggest difference in organ dose is seen in the oesophagus. This difference is likely due to the positioning of the TLDs in the Rando phantom being more superior to the location within the PCXMC phantom. Version 2.0 of PCXMC uses a Cristy Phantom that was modified by Eckerman and Ryman to include the oesophagus (Tapiovaara & Siiskonen, 2008). The difference in dose within the liver is likely due to the limited number of measurements taken through the organ.

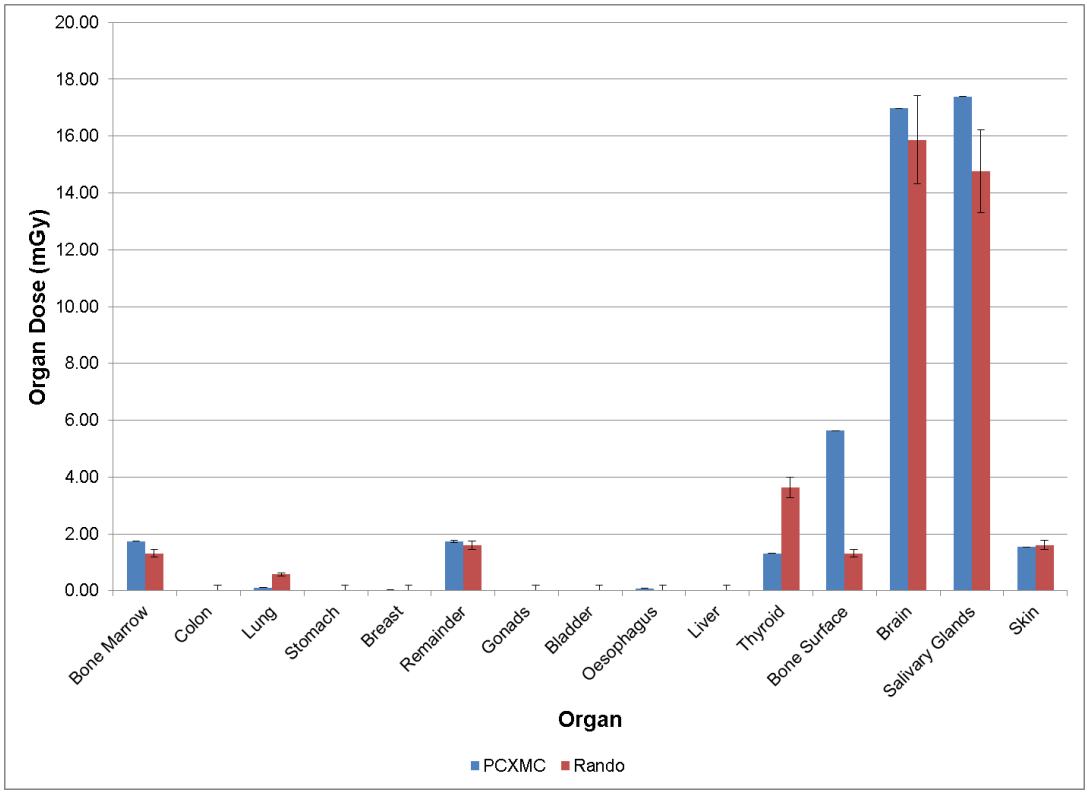

Figure 8 Comparison of Simulated and Measured Organ Doses for Head Scan

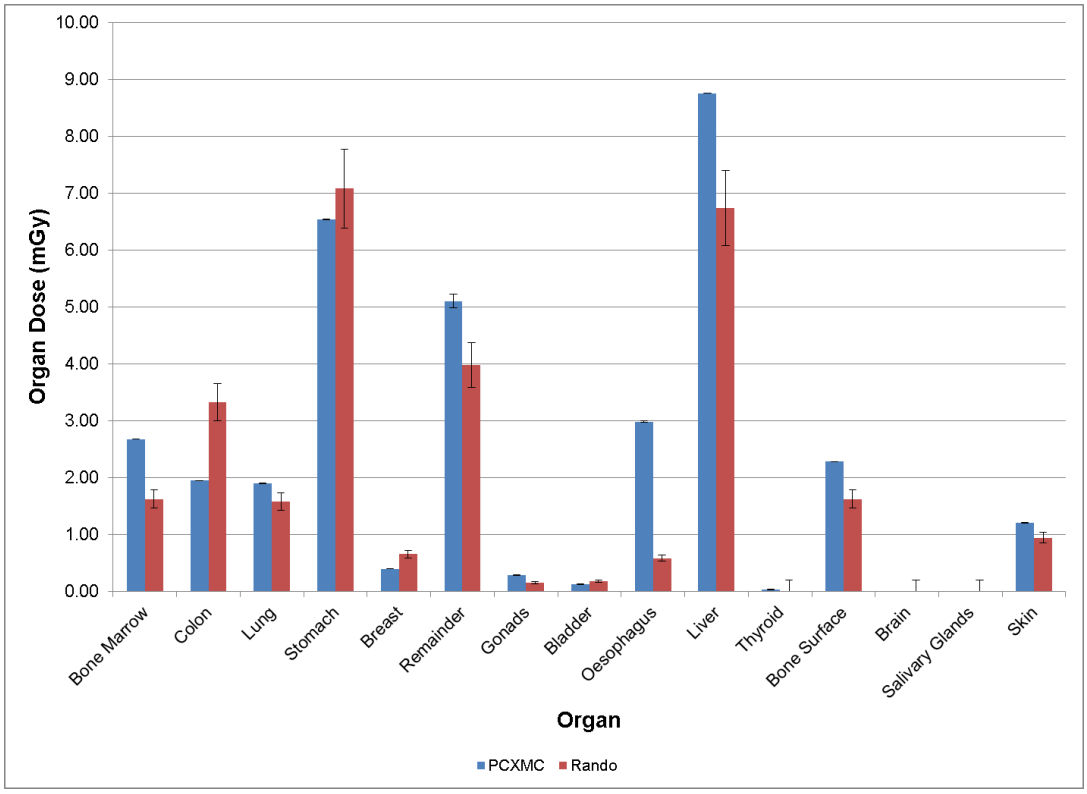

Figure 9 Comparison of Simulated and Measured Organ Doses for Liver Scan

Once the results were validated PCXMC was set-up for the various scan parameters covering the range provided by the different equipment. For each set of simulations the dose metric was set to either 1Gycm² (DAP) or 1Gy @ interventional reference point (AK_{ref}) to provide normalised doses. The interventional reference point is defined in the international standard as "15cm from the isocentre in the direction of the focal spot" (ISO 60601-2-43, 2020, p. 30). For DAP this involved dividing the total DAP by the number of projections and then adjusting where appropriate for the table. For Air Kerma PCXMC requires the Air Kerma at the isocentre rather than the international reference point. To achieve this the AK_{ref} was first corrected for distance to the isocentre and then divided by the number of projections and where appropriate adjusted for the table. Simulations were run for a range of applied kV, additional filtrations and X-ray field sizes. The impact of the number of projections was also investigated as some equipment allows the user to select this.

10. Results

10.1. Introduction

Simulations were undertaken using PCXMC for the parameters detailed in Table 16. A total of 1,090,399 projections representing 3211 examinations were simulated. These represent the various parameters used clinically for equipment that is currently available for CBCT scanning. For each CBCT examination E from the individual projections were summed to provide the total E for the examination.

Table 16 Summary of Acquisition Parameters Investigated

Parameter	Values Investigated
kV	60, 70, 80, 90, 100, 110, 120
Additional Spectral Filter (mmCu)	0, 0.1, 0.2, 0.3, 0.5, 0.6, 0.9, 1.0
X-ray field size at Flat Panel (cm)	48, 27, 22, 15, 11(diagonal) 40, 20, 16 (side of square)
Dose Metric	Air Kerma, Dose Area Product
Focus to Isocentre Distance (cm)	75, 81, 82
Number of projections	300, 313, 400, 632
Anatomy	Head, Heart (Thorax), Kidney (Upper Abdomen), Liver (Upper Abdomen), Prostate (Pelvis)
Patient table	In primary beam, out of primary beam

For some body parts such as the head it is possible that the X-ray field size can exceed the patient, particularly for the larger sizes. For this work it is assumed that the operator will ensure that the X-ray field size used is appropriately collimated as this is important radiographic practice to ensure patient doses are kept as low as reasonably practicable. To ensure that this was the case, simulated projections were assessed in PCXMC to ensure the X-ray beam falls within the patient. Therefore the maximum field size was determined from

the projection which included the largest patient dimension e.g. for head scans where the phantom is larger in the Anterior-Posterior (AP) or Posterior-Anterior (PA) direction the lateral view was used. This is shown in Figure 10. It is acknowledged that this may result in some of the X-ray beam not intercepting the patient in all the projections. However this may occur in the clinical setting to ensure that all the required anatomy is included in the CBCT images.

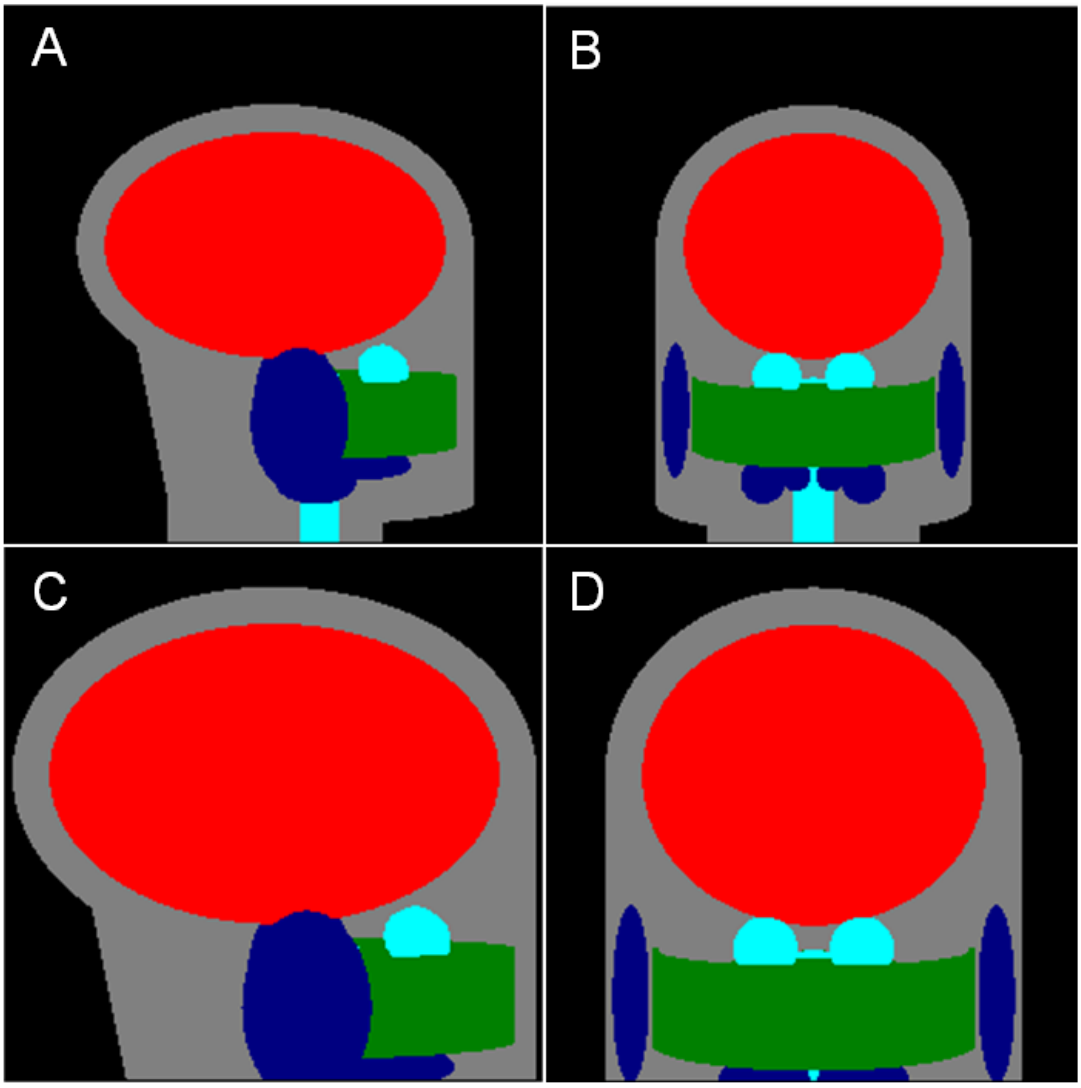

Figure 10 Comparison of Maximum Field Size for Head Examinations Showing Uncollimated Lateral (A) Uncollimated AP (B), Collimated Lateral (C) and Collimated AP (D) views

10.2. Monte Carlo Error Analysis

The results from the Monte Carlo simulations have an error associated with them. As discussed in section 9.3 the error in the calculation can be reduced by increasing the number of photons in the simulation. This represents the statistical uncertainty in the Monte Carlo method due to the stochastic processes that are simulated. The statistical uncertainties are larger when the doses in the organs are lower. Twenty thousand photons per projection was chosen as this represented a good compromise between simulation time and statistical error with the aim to keep this around 1%.

When providing an estimate of patient dose there will also be differences based on the use of a mathematical phantom in the Monte Carlo simulations. These differences are due to the inaccurate representation of the human anatomy by the mathematical phantom. For PCXMC comparisons have previously been made with results from a human voxel phantom by Tapoivaara and Siiskonen. They found the difference between the two data sets were in agreement within 20% across the organ doses (Tapiovaara & Siiskonen, 2008, p. 33) using entrance Air Kerma as the dose metric for a range of X-ray field sizes. They note that some organs had higher with bone representing the greatest difference (PCXMC being 50% greater) while other organs (thyroid, skin, lungs and liver) had an agreement of 5 – 10% for energies above 20keV.

For the results produced in this work the overall uncertainty for a conversion factor for E will be in the order of 20% (i.e. averaged over all the organs and taking into account the statistical error in the Monte Carlo simulation).

10.3. Discussion of Dose Metrics Used

When making the choice of which dose metric to use for producing conversion factors it is important to consider the physical parameters measured and the impact that these will have on any conversion factor. The two used in this work AK_{ref} and DAP are common parameters in diagnostic radiology and are displayed on the equipment. For applications such as dose monitoring the DAP has the advantage that it doesn't vary with distance and gives an assessment of both the radiation dose delivered and the collimation (or size) of the X-ray field used. The AK_{ref} is measured under specific conditions and represents a radiation dose in scatter free conditions at a fixed point 15cm from the isocentre in the direction of the X-ray source (ISO 60601-2-43, 2020).

E depends on the radiation output, the area of the radiation field and the organs that are irradiated. Therefore for the same body part and AK_{ref} a larger radiation field area will result in a larger effective dose (assuming all other factors are constant). To take this into account the conversion factor for AK_{ref} simulations should be normalised to the X-ray field area at the isocentre.

10.4. Effect of Number of Projections on Conversion Factor

To assess the impact that the number of projections in a CBCT run has on the conversion factor simulations were performed for the range of examinations using the GE protocols. Simulations with 150, 300 or 600 projections per scan were performed as these represent the greatest range of projections. In all cases a DAP of 1Gycm² was used for the whole examination to keep the normalisation. To ensure that the results are applicable across the range of X-ray field sizes this was assessed for both the largest and smallest field sizes available. The results are given in Table 17 which shows that within the errors the total number of projections has no impact on the conversion factor.

Table 17 Assessment of Total Number of Projections on Effective Dose Conversion Factor

Exam	Number of Projections	Conversion Factor (E/Gycm²)	Simulation Error (E/Gycm²)
Head	150	0.068	0.00109
	300	0.068	0.00108
	600	0.068	0.00109
Heart	150	0.337	0.00207
	300	0.336	0.00206
	600	0.338	0.00193
Kidney	150	0.287	0.00220
	300	0.286	0.00219
	600	0.288	0.00220
Liver	150	0.351	0.00210
	300	0.350	0.00209
	600	0.350	0.00210
Prostate	150	0.098	0.00169
	300	0.097	0.00167
	600	0.098	0.00168

Knowledge of this means that for equipment which allows variation in the number of projections acquired simulations of the different options don't need to be undertaken. Further simulations were performed to investigate this further. Results for varying numbers of projections simulated from 3 to 600 are given in Figure 11 and show that while there is considerable variation at low numbers after 100 projections the effective dose conversion factor stabilises. Given the time taken to undertake these simulations this represents a significant time saving for this piece of work as not all variations in number of projections need to be simulated.

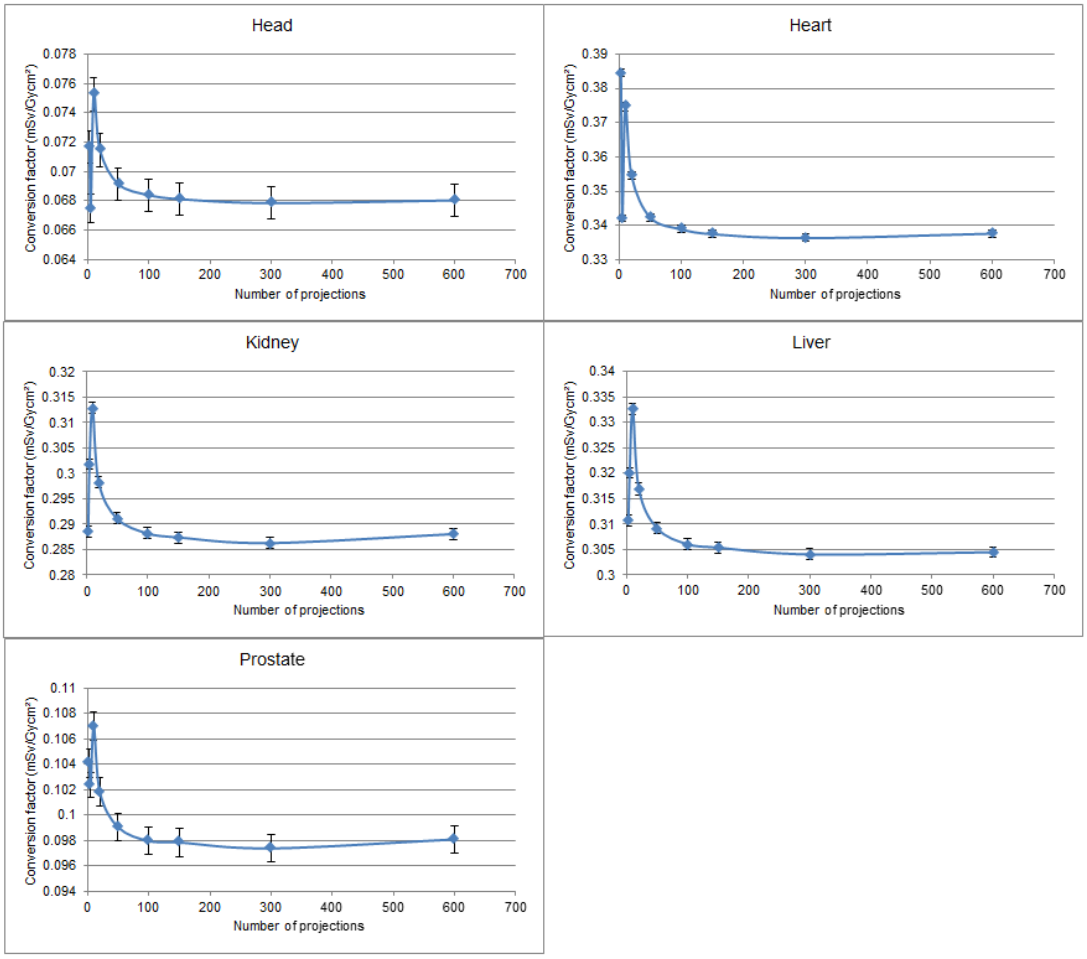

Figure 11 Influence of Number of Projections Simulated on Effective Dose Conversion Factor

10.5. Effect of Scan Orientation on Conversion Factor

The different types of equipment are set up to perform a CBCT scan with the primary X-ray beam either passing through the table before the patient (i.e. through a PA view) or after the patient (through an AP view). Any views with the primary beam passing through the table before the patient will be subject to beam attenuation and hardening. In addition to this the organs within the patient will be subject to different radiation doses due to their location within the patient and any attenuation provided by other organs. The impact of these on the conversion factor was investigated. The results for 120kV and 0.1mmCu filtration are shown

in Figure 12 for all examinations. Similar results are also seen for the other kVs and additional filtrations.

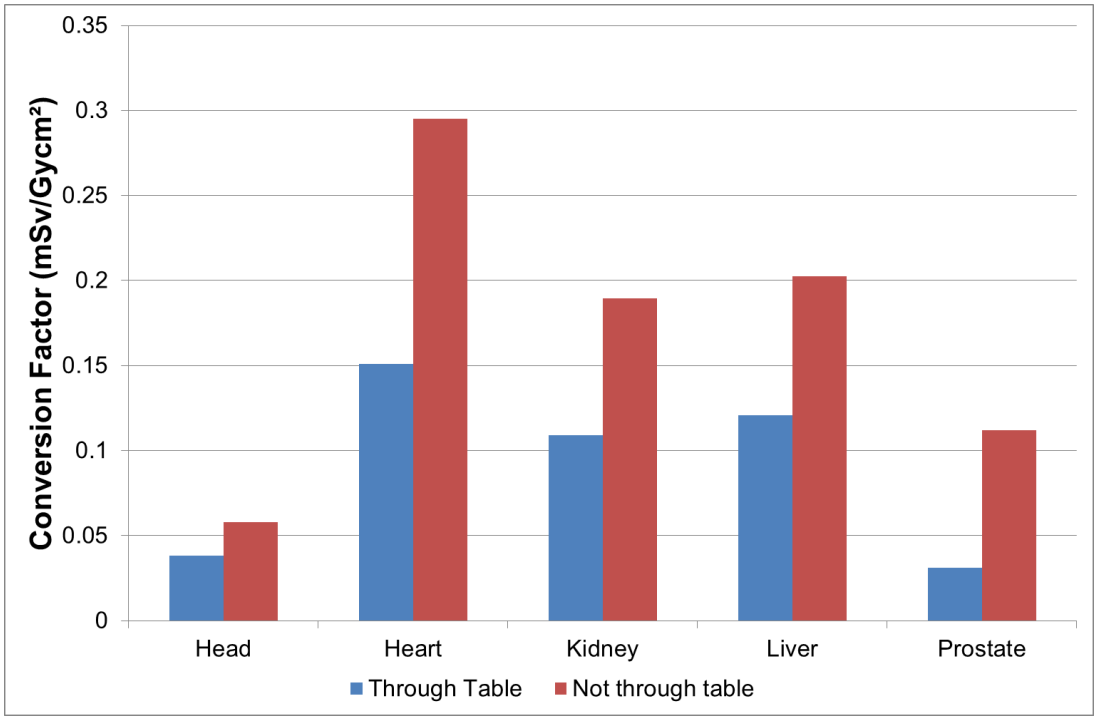

Figure 12 Differences between Conversion Factors for CBCT Examinations Performed either the Primary Beam Through or not Through the Table for 120kV and 0.1mm Additional Copper Filtration with the Patient Positioned Supine

The results show that for the different examinations being simulated scanning with either the primary beam passing through or not through the table has an inconsistent effect on conversion factors. This was investigated by looking at the individual organ dose conversion factors with the greatest difference in dose for each scan. A summary of the organ dose conversion factors with the 5 largest differences for 120kV and 0.1mmCu filtration is given in Table 18.

Table 18 Comparison of Organ Dose Conversion Factor Differences for Examinations Performed with Primary Beam either Through or not Through the Table with the Patient Positioned Supine.

Head Examinations					
Organ Dose (mGy/Gycm²)	Oral Mucosa	Salivary Glands	Brain	Extrathoracic airways	Skeleton
Not Through Table	1.87	1.73	1.51	0.94	0.61
Through Table	0.08	1.14	1.02	0.55	0.40
Difference	1.07	0.59	0.50	0.39	0.21

Heart Examinations					
Organ Dose (mGy/Gycm²)	Breasts	Thymus	Heart	Adrenals	Spleen
Not Through Table	1.72	1.62	1.62	0.33	0.20
Through Table	0.36	0.35	0.64	0.74	0.39
Difference	1.36	1.26	0.98	-0.41	-0.19

Kidney Examinations					
Organ Dose (mGy/Gycm²)	Stomach	Gall Bladder	Kidneys	Adrenals	Liver
Not Through Table	1.51	1.49	0.75	0.39	1.09
Through Table	0.53	0.54	1.62	0.91	0.67
Difference	0.98	0.95	-0.87	-0.52	0.42

Liver Examinations					
Organ Dose (mGy/Gycm²)	Stomach	Gall Bladder	Kidneys	Liver	Adrenals
Not Through Table	1.72	1.39	0.74	1.45	0.58
Through Table	0.56	0.51	1.60	0.79	1.19
Difference	1.16	0.88	-0.86	0.66	-0.61

Prostate Examinations					
Organ Dose (mGy/Gycm²)	Testicles	Prostate	Urinary Bladder	Colon	Muscle
Not Through Table	2.33	1.34	1.06	0.24	0.25
Through Table	0.23	0.49	0.35	0.20	0.22
Difference	2.10	0.85	0.72	0.04	0.03

For head examinations the radiosensitive organs with the greatest Absorbed Dose are the salivary glands, brain and skeleton (bone surface). These all have an organ weighting factor of 0.1. If head examinations are performed through the PA orientation these organs will be exposed to a lower radiation dose due to attenuation and beam hardening provided by the table.

For examinations of the heart the largest contribution to the increased dose for the AP view scans will be from the breast dose which has an organ weighting factor of 0.12. Other organs located in the anterior of the body (thymus and heart) also see an increase in dose when an AP scan is undertaken. It can also be seen from Table 18 that the some organs located in the posterior of the body (adrenal glands and spleen) show an increase in dose when a PA rotation is undertaken. These organs contribute less to E as they are included in the 13 remainder organs and so only have a weighting factor of 0.009 each.

Examinations of the kidneys and liver show a similar pattern of organ dose differences with the anterior organs (stomach, gall bladder and liver) having increased doses for the AP scans and posterior organs (kidneys and adrenal glands) having increased doses for the PA scans. Of these organs the stomach is the most radiosensitive with a weighting factor of 0.12 followed by the liver at 0.04. The other organs are included in the remainder organs. This combined with the additional attenuation of the table account for the differences in effective dose.

The prostate examination shows the greatest difference in effective dose conversion factor (Figure 12). For PA scans the primary beam is intercepted by the bones of the pelvis which provides shielding for the radiosensitive organs (colon (weighting factor 0.12), gonads (weighting factor 0.08) and bladder (weighting factor 0.04)) within the beam. An increase (up to a 10 times) in dose to the testes is seen when an AP scan is undertaken as compared to a PA scan. This is due to their location on the surface of the body meaning they are in the primary beam for AP scans.

For these simulated scans it has been assumed that the patient is positioned supine. However the patient may be positioned prone in which case scans through the AP view will pass through the table before the patient. Simulations have been undertaken to investigate the impact that the both the table and the patient orientation have on the scans. This involved additional simulations of PA scans without a table (patient prone) and AP scans with a table (patient supine). Results from these are summarised in Table 19.

Table 19 Summary of the impact of the table and scan orientation on the E to DAP dose conversion factors.

No Table			
Organ	AP Scan (mSv/Gycm²) – Supine	PA Scan (mSv/Gycm²) – Prone	% increase from PA
Head	0.085	0.078	9%
Heart	0.453	0.339	34%
Kidney	0.353	0.261	35%
Liver	0.373	0.285	31%
Prostate	0.182	0.093	97%
Through Table			
Organ	AP Scan (mSv/Gycm²) – Prone	PA Scan (mSv/Gycm²) – Supine	% increase from PA
Head	0.064	0.056	14%
Heart	0.401	0.270	49%
Kidney	0.307	0.224	37%
Liver	0.321	0.240	34%
Prostate	0.151	0.075	102%
AP Scan			
Organ	No Table (mSv/Gycm²) – Supine	Through Table (mSv/Gycm²) – Prone	% increase without table
Head	0.085	0.064	33%
Heart	0.453	0.401	13%
Kidney	0.353	0.307	15%
Liver	0.373	0.321	16%
Prostate	0.182	0.151	21%
PA Scan			
Organ	No Table (mSv/Gycm²) – Prone	Through Table (mSv/Gycm²) – Supine	% increase without table
Head	0.078	0.056	39%
Heart	0.339	0.270	25%
Kidney	0.261	0.224	17%
Liver	0.285	0.240	19%
Prostate	0.093	0.075	24%

These results show that for head examinations scanning through the table has a bigger impact (33% - 39%) on the conversion factors than scanning through an AP or PA view

(10% - 14%). This implies that for the head the impact of the table accounts for more of the differences in conversion factor than the positioning of the organs. For the other examinations the opposite is true with the table having a smaller (13 – 25%) impact on the conversion factor than scanning through an AP or PA view (31% - 102%). This implies that for these scans the location of the organs has a bigger influence on the effective dose conversion factor than the impact of the table. In all cases either scanning through the table or using a PA view resulted in a lower conversion factor.

Table 20 shows the differences in conversion factors between scans performed through or not through the table for the different kVs simulated. For all examinations the difference between the conversion factors acquired through or not through the table increased as the kV was increased. When expressed as a percentage difference however the differences decrease with increasing kV for all examinations except the head where the percentage difference was constant with increasing kV. These results show that there is not a consistent difference with varying kV and so this will be investigated further.

The difference in conversion factor between the two geometries is sufficiently large enough that the results are presented as two different sets of examinations. This is due to differences in the dose distribution within the patient in addition to the attenuation and beam hardening provided by the table. Knowledge of these differences provides an opportunity for optimisation of patient dose if a rotation with the primary beam passing through the table can be performed.

Table 20 Variation of Conversion Factor with Varying kV for Examinations Performed Through or Not Through the Table for a Patient Positioned Supine.

kV	Conversion Factor (mSv/Gycm²)			
	Not Through Table	**Through Table**	**Difference**	**% Difference**
Head				
60	0.064	0.041	0.023	44%
70	0.075	0.048	0.027	43%
80	0.083	0.054	0.030	43%
90	0.090	0.058	0.032	43%
100	0.094	0.061	0.034	43%
110	0.098	0.063	0.035	44%
120	0.100	0.064	0.036	44%
Heart				
60	0.371	0.194	0.177	63%
70	0.416	0.228	0.187	58%
80	0.452	0.257	0.195	55%
90	0.478	0.278	0.200	53%
100	0.497	0.293	0.203	51%
110	0.510	0.305	0.205	50%
120	0.520	0.313	0.206	50%
Kidney				
60	0.259	0.146	0.113	56%
70	0.306	0.179	0.127	52%
80	0.346	0.208	0.138	50%
90	0.375	0.230	0.145	48%
100	0.395	0.245	0.150	47%
110	0.411	0.257	0.154	46%
120	0.423	0.266	0.157	46%
Liver				
60	0.276	0.161	0.115	53%
70	0.325	0.195	0.130	50%
80	0.366	0.224	0.142	48%
90	0.396	0.246	0.150	47%
100	0.418	0.261	0.156	46%
110	0.433	0.273	0.160	45%
120	0.445	0.282	0.163	45%

Table 20 Continued

kV	Conversion Factor (mSv/Gycm²)			
	Not Through Table	**Through Table**	**Difference**	**% Difference**
Prostate				
60	0.143	0.043	0.100	107%
70	0.163	0.056	0.107	98%
80	0.180	0.067	0.113	91%
90	0.192	0.075	0.117	87%
100	0.201	0.082	0.119	84%
110	0.207	0.086	0.121	82%
120	0.212	0.090	0.122	81%

10.6. Effect of Beam Half Value Layer on Dose Area Product to Effective Dose Conversion Factor

The Half Value Layer (HVL) of an X-ray beam gives an indication of how penetrating the radiation is and is affected by the choice of applied kV and additional filtration added to the beam. For diagnostic radiology this is measured in terms of mm of Aluminium (mm Al) that are required to attenuate half of the incident X-rays. A larger HVL indicates that the X-ray beam is more penetrating. HVL was chosen for comparison as it allows the different combinations of kV and additional filtration to be assessed together.

Table 21 gives a sample of kV and filtration options representing the Siemens equipment and HVLs have been found using simulation (Siemens Healthineers, 2020). The results for the different examinations with the smallest field sizes defined at the detector (10cm x 10cm, 10.5cm x 10.5cm and 12.5cm x 12.5cm) are shown in Figure 13.

Table 21 Impact of kV and Added Filtration on the HVL of an X-ray Beam

kV	mm Al	mm Cu	HVL
60	2.5	0.1	3.617
60	2.5	0.2	4.277
60	2.5	0.3	4.767
60	2.5	0.6	5.723
60	2.5	0.9	6.295
70	2.5	0.1	4.251
70	2.5	0.2	5.04
70	2.5	0.3	5.628
70	2.5	0.6	6.772
70	2.5	0.9	7.456
80	2.5	0.1	4.881
80	2.5	0.2	5.778
80	2.5	0.3	6.437
80	2.5	0.6	7.69
80	2.5	0.9	8.417
90	2.5	0.1	5.458
90	2.5	0.2	6.426
90	2.5	0.3	7.125
90	2.5	0.6	8.431
90	2.5	0.9	9.183
100	2.5	0.1	5.974
100	2.5	0.2	6.984
100	2.5	0.3	7.706
100	2.5	0.6	9.04
100	2.5	0.9	9.813
110	2.5	0.1	6.448
110	2.5	0.2	7.488
110	2.5	0.3	8.224
110	2.5	0.6	9.583
110	2.5	0.9	10.383
120	2.5	0.1	6.889
120	2.5	0.2	7.948
120	2.5	0.3	8.694
120	2.5	0.6	10.074
120	2.5	0.9	10.898

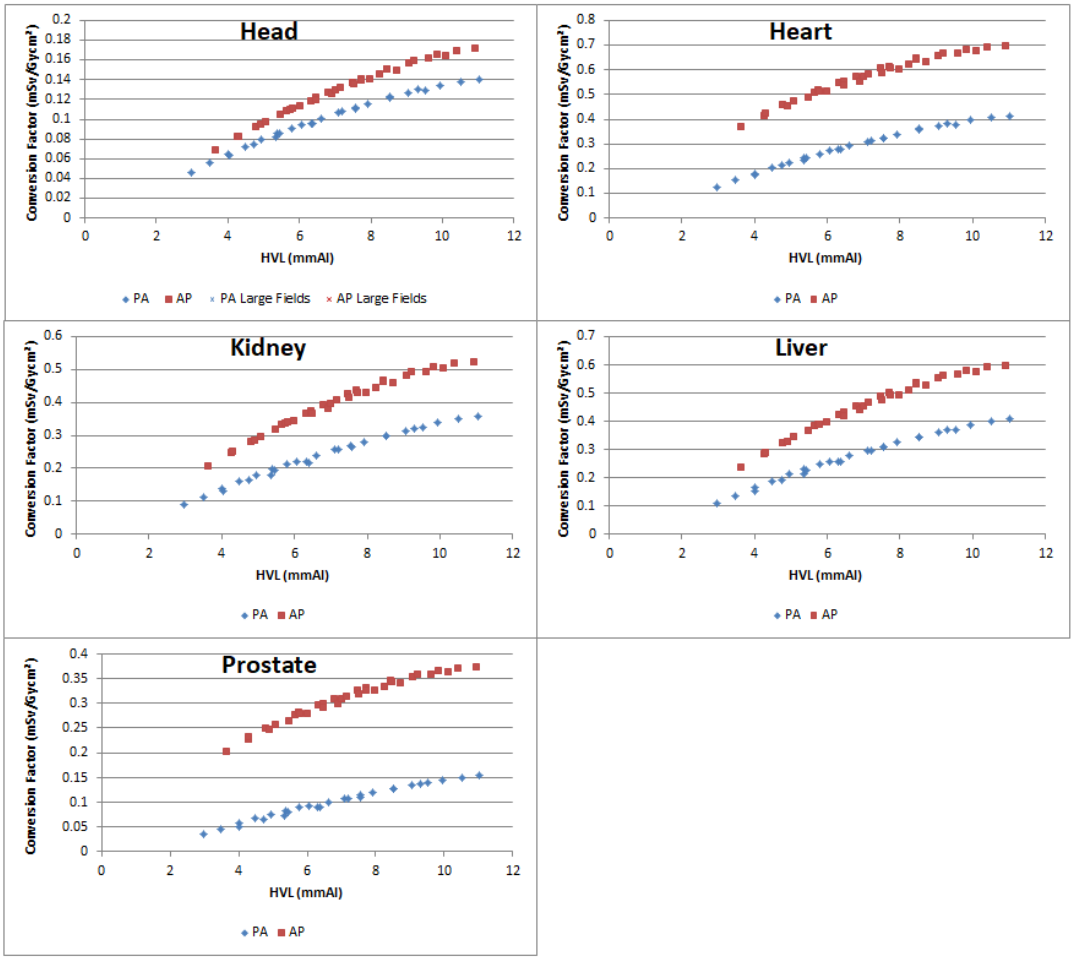

Figure 13 Variation of Conversion Factor with Varying HVL for AP and PA Examinations Using the Smallest Field Size

It can be seen from the graphs that when the field size is kept constant the conversion factor increases with increasing HVL. These results represent the full range of kV and additional filtrations simulated. This trend was found for the all the field sizes investigated. This is to be expected as although the DAP remains the same the photons incident on the phantom have a higher average energy for a higher HVL beam. These higher energy X–rays are more likely to undergo scattering events than photoelectric absorption.

These results show that if there is to be a generalised conversion factor for CBCT examinations then one of the variables that needs to be considered is the beam quality as defined by the HVL.

10.7. Effect of Field Size on Dose Area Product to Effective Dose Conversion Factor

For each body region simulations were undertaken for a range of X-ray field sizes that are currently available to assess the impact this has on the conversion factor. When specifying DAP the irradiated field size is included in the dose metric. This leads to a relationship between the irradiated area and the incident radiation dose when the total DAP is kept constant (i.e. increasing the field size while keeping the DAP constant will result in a decrease in the incident radiation dose). In addition to the dose the area of the X-ray field plays a part in the effective dose with a larger area leading to increase in the volume of imaged and neighbouring organs in the beam. If the incident dose if kept constant a larger field size will result in a larger DAP and, provided the primary beam falls within the patient, a larger E. This leads to the possibility of there being a relationship between field size and E that may not be initially intuitive. Simulations were undertaken using a range of X-ray field sizes to include the largest and smallest available. These are given in Table 22. Figure 14 shows how the conversion factor varies with HVL for the simulated X-ray field sizes. For some examinations (e.g. heart and prostate) it can be seen that the field size has an impact on the conversion factor while for others (e.g. head) the field size has little impact.

Table 22 Field sizes simulated as defined at the detector and calculated at the rotation distance

Field size at the detector	FDD (cm)	FRD (cm)	Field size at FRD
40cm x 40cm	120	82	27.33 cm x 27.33cm
40cm x 30cm	120	81	26.67cm x 19.91cm
37cm x 30cm	120	75	23.25cm x 18.44cm
27cm x 27cm	100	55	15cm x 15cm
31cm x 31cm	120	82	21.6cm x 21.6cm
23cm x 23cm	120	75	14.38cm x 14.38cm
19cm x 19cm	120	81	12.89cm x 12.89cm
15cm x 15cm	120	81	10.13cm x 12.13xm
12.5cm x 12.5cm	120	75	7.78cm x 7.78cm
12cm x 12cm	120	82	8.2cm x 8.2cm

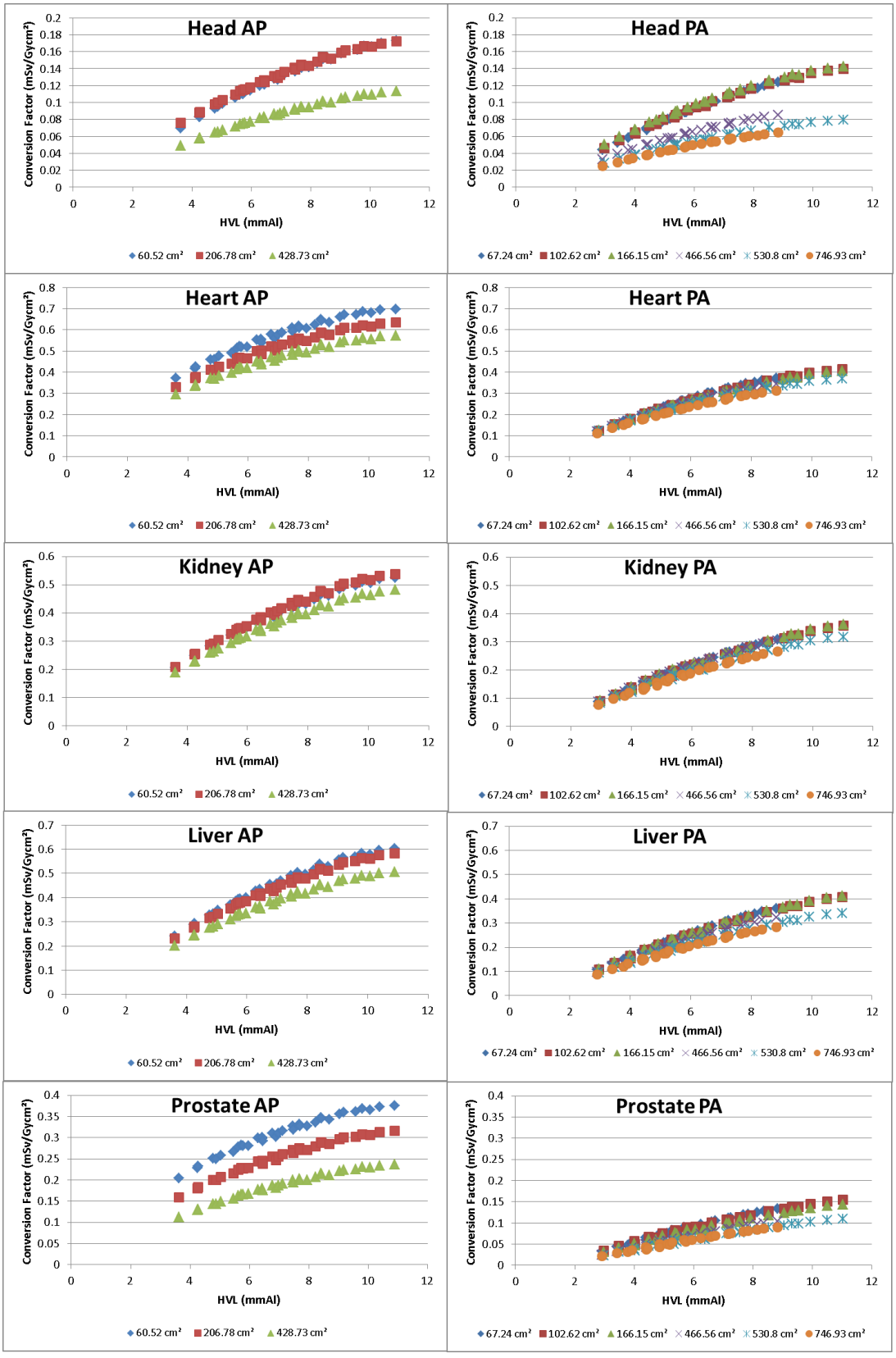

Figure 14 Variation of Conversion Factor with HVL for all Simulated X-ray Field Sizes

Figure 14 shows that the differences in field size are more pronounced for those examinations performed through the AP view. The reasons behind the differences in conversion factor for some examinations were investigated. As the trends are the same for the different beam HVLs this was done for examinations undertaken at 120kV using 0.9mmCu filtration for both AP and PA scans and summarised in Table 23. The percentage difference has been defined as the difference between the maximum and minimum divided by the mean. It was found that the conversion factors for the smaller field sizes were bigger than those for the large field sizes for all the examinations.

Table 23 Comparison of Mean and Range of Conversion Factors with Varying X-ray Field Size for Examinations Undertaken using 120kV with 0.9mmCu Filtration

AP	Conversion Factor (mSv/Gycm²)			% Difference
	Mean	Minimum	Maximum	
Head	0.17	0.17	0.17	0.4%
Heart	0.63	0.57	0.70	19.9%
Kidneys	0.52	0.48	0.54	10.9%
Liver	0.56	0.51	0.60	16.8%
Prostate	0.31	0.24	0.38	44.6%

PA	Conversion Factor (mSv/Gycm²)			% Difference
	Mean	Minimum	Maximum	
Head	0.14	0.14	0.14	2.0%
Heart	0.40	0.37	0.41	11.3%
Kidneys	0.35	0.32	0.36	12.9%
Liver	0.39	0.34	0.41	18.4%
Prostate	0.14	0.11	0.15	33.0%

Further investigations were undertaken to determine the reasons for these differences by considering the organs with the biggest differences in dose conversion factor. These are shown in Table 24 where it can be seen that for each examination the organs with the biggest difference in dose are located near the anatomy that is being imaged. For DAP conversion factors a smaller field size with the same DAP reading will mean that organs within the field of view will be exposed to a higher radiation dose when compared to the use of a large field. When considering E the organ weighting factor also needs to be taken into consideration. To determine the impact on E the organ dose difference has been multiplied by the tissue weighting factor to obtain the weighted difference.

Table 24 Organs with the Largest Differences in Radiation Dose as the X-ray Field Size is Varied

Head

	Brain	**Oral mucosa**	**Salivary glands**	**Extrathoracic airways**
Organ Dose Difference (mGy/Gycm²)	0.747	-0.743	-0.692	0.471
Weighting Factor	0.010	0.009	0.010	0.009
Weighted Difference	0.007	-0.007	-0.007	0.004

Heart

	Heart	**Thymus**	**Breasts**	**Oesophagus**
Organ Dose Difference (mGy/Gycm²)	2.099	1.044	0.753	0.551
Weighting Factor	0.009	0.009	0.120	0.040
Weighted Difference	0.019	0.010	0.090	0.022

Kidney

	Gall bladder	**Stomach**	**Kidneys**	**Colon**
Organ Dose Difference (mGy/Gycm²)	2.584	0.379	0.327	0.286
Weighting Factor	0.009	0.120	0.009	0.120
Weighted Difference	0.024	0.045	0.003	0.034

Liver

	Pancreas	**Gall bladder**	**Spleen**	**Stomach**
Organ Dose Difference (mGy/Gycm²)	1.773	1.085	0.717	0.541
Weighting Factor	0.009	0.009	0.009	0.120
Weighted Difference	0.016	0.010	0.006	0.065

Table 24 Continued

Prostate

	Prostate	**Testes**	**Urinary bladder**	**Colon**
Organ Dose Difference (mGy/Gycm²)	3.119	3.054	0.574	0.177
Weighting Factor	0.009	0.040	0.040	0.120
Weighted Difference	0.029	0.122	0.023	0.021

The results given above are for examinations performed where the X-ray field has been collimated to fit the phantom. For the head examinations the larger available field sizes extend beyond the limits of the phantom and so the use of the largest available field size was investigated to demonstrate the effect of poor collimation on the conversion factor for these examinations. The results for these examinations can be seen in Figure 15. Where the large field size is used the conversion factor is on average 37.5% lower (range 24.7% to 48.0%) compared with the collimated fields. This is due to less of the X-ray beam being incident on the patient but still contributing to the incident DAP reading resulting in the smaller conversion factor.

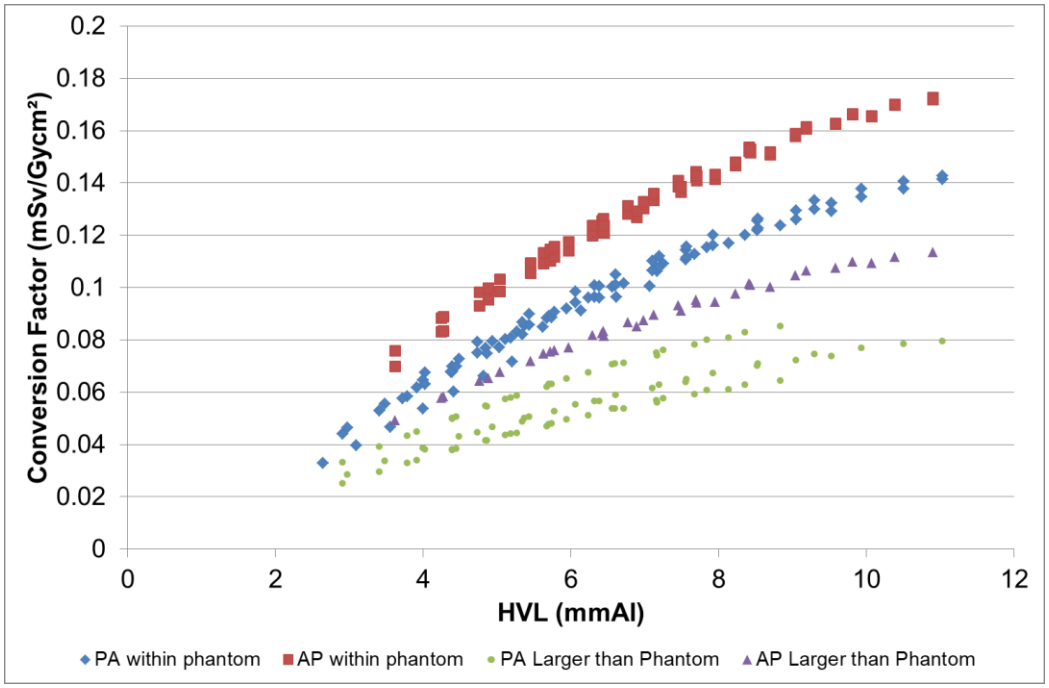

Figure 15 Impact of collimation on the conversion factors for head examinations showing a decrease in conversion factor when the X-ray field is greater than the phantom size.

As collimation of the X-ray beam represents good radiographic practice and should be undertaken for patient examinations it has been decided to report the conversion factors for the collimated X-ray beams only. Should the users not collimate appropriately and the reported conversion factors are used this could result in an over estimation of E and thus any risks associated with the exposure.

10.8. Derivation of Conversion Factor for Dose Area Product to Effective Dose using Half Value Layer

For the majority of examinations investigated it was seen that the irradiated field size had limited effect on the conversion factor provided the beam was collimated to the patient. It is therefore postulated that the relationship between the HVL and conversion factor can be found without knowledge of the field size. For this to be valid, results obtained would have to be in agreement with the simulated conversion factor to within ± 20%. To determine this

relationship Excel was used to provide a fit to the results. For each anatomical region the conversion factor was plotted against HVL for all the examinations simulated. It was found that a logarithmic relationship provided the best fit to the results. The formulae for the various examinations are given in Table 25 along with the range of differences (% difference is defined as 100 x (conversion factor from formula – PCXMC conversion factor)/PCXMC conversion factor) arising from the use of these as compared to the PCXMC results. Comparisons of the calculated conversion factor with the PCXMC conversion factor are given in Figure 16 and Figure 17.

Table 25 Formulae for Dose Area Product to Effective Dose Conversion Factor using Beam HVL and Differences from PCXMC Results

Exam	**Conversion factor formula**	**Range of difference from PCXMC**
AP Head	CF = 0.0949Ln(HVL) – 0.0523	-8% – 3.3%
AP Heart	CF = 0.287 Ln(HVL) – 0.0363	-11.4% – 14.3%
AP Kidney	CF = 0.2992 Ln(HVL) – 0.1898	-7.0% – 9.9%
AP Liver	CF = 0.3237 Ln(HVL) – 0.1988	-9.9% – 14.2%
AP Prostate	CF = 0.1428 Ln(HVL) – 0.0260	-23.0% – 40.5%
PA Head	CF = 0.0797 Ln(HVL) – 0.0493	-25.3% – 15.3%
PA Heart	CF = 0.2237 Ln(HVL) – 0.1403	-19.0% – 11.1%
PA Kidney	CF = 02068 Ln(HVL) – 0.156	-26.1% – 16.9%
PA Liver	CF = 0.2292 Ln(HVL) – 0.1719	-31.2% – 18.6%
PA Prostate	CF = 0.0848 Ln(HVL) – 0.0736	-45.2 – 42.2%

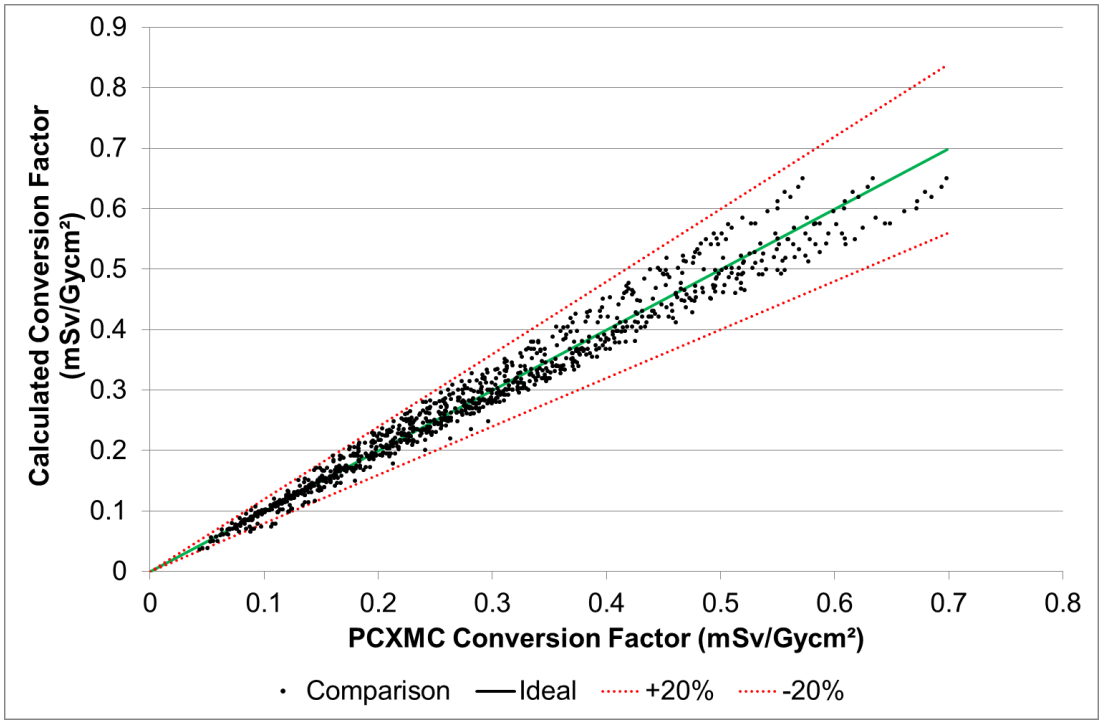

Figure 16 Comparison of PCXMC Conversion Factor with Calculated Conversion Factor for Head, Heart, Kidney and Liver Examinations Performed both Through and Not Through the Table with an Ideal Fit and ± 20% Deviation

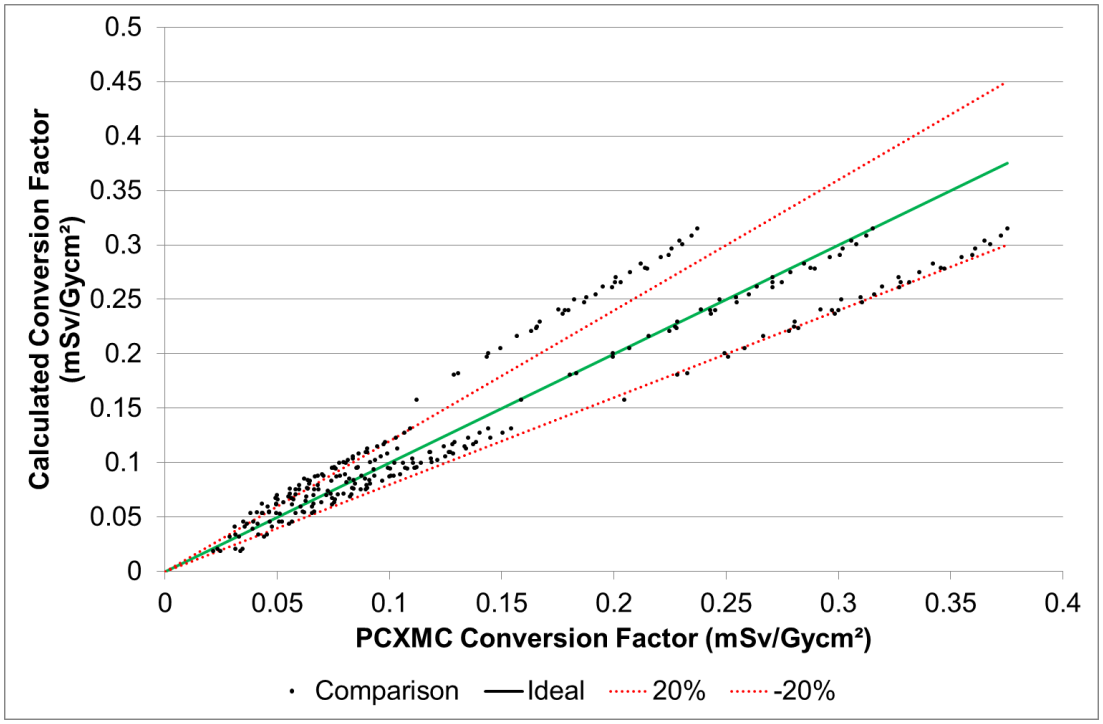

Figure 17 Comparison of PCXMC Conversion Factor with Calculated Conversion Factor for Prostate Examinations Performed both Through and Not Through the Table with an Ideal Fit and ± 20% Deviation

For prostate examinations the field size differences lead to large (greater than 20%) differences in the calculated conversion factor when compared to that produced from PCXMC. It is therefore not possible to use this method to determine the conversion factors without introducing large errors.

The impact of area on the conversion formula was assessed for all the examinations and the formulae were updated. These are given in Table 26 where A is the field area in cm² at the isocentre, with the results summarised in Figure 18. These results show greater agreement with the majority of results within ± 20% from those produced by PCXMC. The greatest differences were found in the examinations performed with a HVL less than 3mmAl (equivalent to 60kV and 0mm additional copper filtration) where the scan was undertaken through the table. For these beams the impact of the attenuation and beam hardening of the table will be greater which would account for the underestimate of the conversion factor

which is seen. The range of differences in brackets in Table 26 have had these low HVL results removed.

Table 26 Updated Formulae for Dose Area Product to Effective Dose Conversion Factor using Beam HVL and X-ray Area at the Isocentre (A) and Differences from PCXMC Results. Results in Brackets are with the Beam HVL Less than 3mmAl Removed

Exam	Conversion factor formula	Range of difference from PCXMC
AP Head	CF = (-0.00004A + 0.1007)Ln(HVL) + 0.0001A – 0.0658	-4.8% – 3.2% (-4.8% – 3.2%)
AP Heart	CF = (-0.00005A +0.0982)Ln(HVL) - 0.00004A – 0.0268	-2.6% - 6.8% (-2.6% – 6.8%)
AP Kidney	CF = (-0.00008A + 0.3166)Ln(HVL) + 0.00005A – 0.2008	-6.8% – 4.8% (-6.8% – 4.8%)
AP Liver	CF = (-0.0001A + 0.3582)Ln(HVL) + 0.00009A – 0.2193	-1.0% – 14.7% (-1.0% – 14.7%)
AP Prostate	CF = (-0.0001A + 0.1698)Ln(HVL) - 0.0001A – 0.0019	-1.9% – 9.8% (-1.9% – 9.8%)
PA Head	CF = (-0.00008A + 0.0836)Ln(HVL) + 0.00001A – 0.0497	-13.4% – 10.4% (-8.3% – 10.4%)
PA Heart	CF = (-0.00007A +0.2373) Ln(HVL) + 0.00007A – 0.1484	-14.9% – 4.8% (-7.9% – 4.8%)
PA Kidney	CF = (-0.00006A + 0.2273)Ln(HVL) + 0.00006A – 0.1703	-19.7% – 15.3% (-12.2% – 15.3%)
PA Liver	CF = (-0.00009A + 0.2478)Ln(HVL) + 0.00008A – 0.1816	-22.7% – 12.9% (-11.9% – 12.9%)
PA Prostate	CF = (-0.00005A +0.0982) Ln(HVL) + 0.00004A – 0.0816	-38.4% – 19.4% (-20.8% – 19.4%)

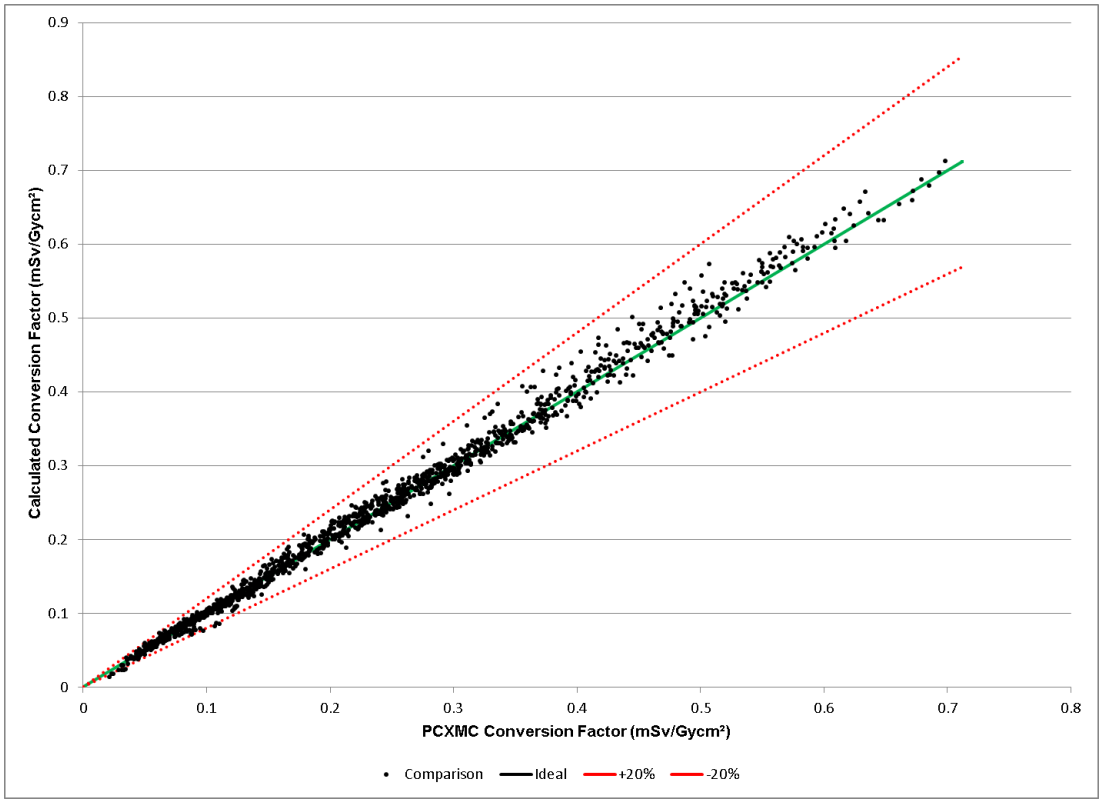

Figure 18 Comparison of PCXMC Conversion Factor with Updated Calculated Conversion Factors for Head, Heart, Kidney, Liver and Prostate Examinations both Through and Not Through the Table with an Ideal Fit and ± 20% Deviation

If the beam HVL and field size are known the formulae given in Table 26 provide a convenient way of calculating the appropriate conversion factor for each given examination. For the majority of examinations simulated these will produce a conversion factor that is within 20% of those produced from PCXMC. Due to the attenuation present within the patient it is unlikely that scans in the lower abdomen and pelvis regions would use these lower HVL X-ray beams. If the area of the X-ray beam is not known the formulae in Table 25 provide an alternative method however the errors in the conversion factor are increased. To calculate E the conversion factor determined from the formula in either Table 25 or Table 26 should be multiplied by the DAP in Gycm².

10.9. Variation of Dose Area Product to Effective Dose Conversion Factor with kV and Additional Filtration

While the use of HVL to describe the radiation beam is a convenient way to display the results from this work it is a less practical method for general use as this requires the HVL for the beam to be determined. To make the application of conversion factors more convenient they will be analysed by the applied kV and additional filtration.

The results are given in Table 27 (for examinations performed through the table) and Table 28 (for examinations not performed through the table) and show the average conversion factor and the range for the given additional copper filtration. The range of results represents the variations in inherent filtration found in the different systems along with the impact that field size has on the conversion factor. To calculate E the appropriate conversion factor should be selected from either Table 27 or Table 28 and multiplied by the DAP in Gycm².

Table 27 Conversion factors (DAP to Effective Dose) for varying kV and Additional Copper Filtration for Examinations Performed with Primary Beam Through the Table

	Additional Copper Filtration (mmCu)					
kV	**0**	**0.1**	**0.2**	**0.3**	**0.5**	**1.0**
Head (mSv/Gycm²)						
60	0.047 (0.044 - 0.050)	0.056 (0.054 - 0.058)	0.066 (0.063 - 0.068)	0.075 (0.075 - 0.075)	0.084 (0.082 - 0.087)	0.098 (0.096 - 0.101)
70	0.056 (0.053 - 0.060)	0.066 (0.063 - 0.070)	0.078 (0.075 - 0.081)	0.089 (0.089 - 0.089)	0.099 (0.096 - 0.101)	0.113 (0.111 - 0.116)
80	0.065 (0.062 - 0.069)	0.076 (0.072 - 0.080)	0.089 (0.086 - 0.092)	0.100 (0.100 - 0.100)	0.110 (0.108 - 0.112)	0.125 (0.123 - 0.126)
90	0.073 (0.070 - 0.077)	0.084 (0.079 - 0.089)	0.098 (0.094 - 0.101)	0.109 (0.109 - 0.109)	0.118 (0.116 - 0.120)	0.132 (0.130 - 0.133)
100	0.080 (0.077 - 0.083)	0.090 (0.084 - 0.096)	0.105 (0.101 - 0.108)	0.115 (0.115 - 0.115)	0.124 (0.122 - 0.125)	0.136 (0.135 - 0.138)
110	0.086 (0.083 - 0.089)	0.095 (0.089 - 0.102)	0.110 (0.106 - 0.113)	0.120 (0.120 - 0.120)	0.128 (0.126 - 0.129)	0.139 (0.138 - 0.141)
120	0.091 (0.088 - 0.094)	0.099 (0.092 - 0.106)	0.114 (0.111 - 0.117)	0.124 (0.124 - 0.124)	0.131 (0.129 - 0.132)	0.141 (0.140 - 0.143)
Heart (mSv/Gycm²)						
60	0.121 (0.113 - 0.125)	0.159 (0.151 - 0.168)	0.181 (0.170 - 0.198)	0.209 (0.194 - 0.220)	0.230 (0.223 - 0.234)	0.271 (0.260 - 0.277)
70	0.148 (0.136 - 0.153)	0.191 (0.180 - 0.204)	0.217 (0.202 - 0.238)	0.247 (0.228 - 0.263)	0.272 (0.260 - 0.279)	0.316 (0.300 - 0.326)
80	0.174 (0.159 - 0.180)	0.221 (0.206 - 0.237)	0.248 (0.231 - 0.274)	0.280 (0.257 - 0.300)	0.306 (0.290 - 0.315)	0.348 (0.328 - 0.361)
90	0.197 (0.179 - 0.205)	0.245 (0.228 - 0.264)	0.273 (0.253 - 0.301)	0.303 (0.278 - 0.327)	0.329 (0.311 - 0.340)	0.368 (0.346 - 0.383)
100	0.217 (0.196 - 0.227)	0.264 (0.245 - 0.286)	0.292 (0.270 - 0.322)	0.321 (0.293 - 0.347)	0.345 (0.325 - 0.358)	0.382 (0.357 - 0.397)
110	0.234 (0.212 - 0.245)	0.280 (0.259 - 0.304)	0.306 (0.284 - 0.338)	0.333 (0.305 - 0.361)	0.357 (0.335 - 0.371)	0.390 (0.364 - 0.407)
120	0.249 (0.225 - 0.261)	0.293 (0.270 - 0.318)	0.318 (0.295 - 0.351)	0.343 (0.313 - 0.373)	0.366 (0.342 - 0.380)	0.396 (0.369 - 0.413)

Table 27 Continued

	Additional Copper Filtration (mmCu)					
kV	**0**	**0.1**	**0.2**	**0.3**	**0.5**	**1.0**
Kidney (mSv/Gycm²)						
60	0.087 (0.078 - 0.091)	0.125 (0.109 - 0.145)	0.135 (0.122 - 0.148)	0.159 (0.146 - 0.166)	0.176 (0.167 - 0.183)	0.213 (0.201 - 0.221)
70	0.110 (0.099 - 0.116)	0.156 (0.136 - 0.180)	0.168 (0.151 - 0.183)	0.196 (0.179 - 0.204)	0.216 (0.204 - 0.225)	0.258 (0.242 - 0.269)
80	0.134 (0.120 - 0.142)	0.186 (0.161 - 0.213)	0.198 (0.179 - 0.216)	0.228 (0.208 - 0.238)	0.250 (0.234 - 0.261)	0.292 (0.272 - 0.305)
90	0.155 (0.139 - 0.165)	0.210 (0.182 - 0.241)	0.222 (0.201 - 0.241)	0.252 (0.230 - 0.264)	0.274 (0.255 - 0.286)	0.314 (0.291 - 0.328)
100	0.174 (0.156 - 0.185)	0.230 (0.199 - 0.263)	0.241 (0.218 - 0.261)	0.269 (0.245 - 0.283)	0.291 (0.271 - 0.305)	0.328 (0.303 - 0.344)
110	0.190 (0.170 - 0.202)	0.246 (0.213 - 0.282)	0.256 (0.232 - 0.276)	0.283 (0.257 - 0.297)	0.304 (0.282 - 0.318)	0.339 (0.312 - 0.355)
120	0.204 (0.183 - 0.217)	0.259 (0.224 - 0.297)	0.268 (0.243 - 0.289)	0.293 (0.266 - 0.308)	0.314 (0.290 - 0.328)	0.346 (0.318 - 0.362)
Liver (mSv/Gycm²)						
60	0.101 (0.088 - 0.110)	0.132 (0.121 - 0.149)	0.155 (0.135 - 0.177)	0.180 (0.161 - 0.198)	0.204 (0.184 - 0.217)	0.245 (0.220 - 0.260)
70	0.127 (0.109 - 0.139)	0.164 (0.149 - 0.184)	0.191 (0.167 - 0.218)	0.219 (0.195 - 0.243)	0.248 (0.222 - 0.263)	0.294 (0.263 - 0.312)
80	0.152 (0.131 - 0.167)	0.194 (0.175 - 0.218)	0.224 (0.196 - 0.255)	0.253 (0.224 - 0.281)	0.284 (0.254 - 0.302)	0.330 (0.294 - 0.351)
90	0.176 (0.151 - 0.193)	0.219 (0.197 - 0.247)	0.250 (0.219 - 0.284)	0.278 (0.246 - 0.310)	0.310 (0.276 - 0.330)	0.353 (0.313 - 0.375)
100	0.196 (0.168 - 0.215)	0.239 (0.214 - 0.270)	0.270 (0.237 - 0.306)	0.297 (0.261 - 0.332)	0.329 (0.292 - 0.349)	0.369 (0.326 - 0.392)
110	0.214 (0.183 - 0.234)	0.255 (0.228 - 0.288)	0.286 (0.251 - 0.324)	0.311 (0.273 - 0.348)	0.342 (0.303 - 0.364)	0.379 (0.334 - 0.403)
120	0.229 (0.196 - 0.251)	0.269 (0.240 - 0.304)	0.299 (0.263 - 0.338)	0.322 (0.282 - 0.360)	0.352 (0.311 - 0.375)	0.386 (0.340 - 0.411)
Prostate (mSv/Gycm²)						
60	0.028 (0.022 - 0.035)	0.038 (0.031 - 0.048)	0.045 (0.035 - 0.058)	0.053 (0.043 - 0.066)	0.063 (0.050 - 0.072)	0.078 (0.062 - 0.089)
70	0.037 (0.029 - 0.045)	0.050 (0.041 - 0.062)	0.059 (0.046 - 0.075)	0.068 (0.056 - 0.084)	0.080 (0.064 - 0.091)	0.097 (0.078 - 0.110)
80	0.047 (0.036 - 0.057)	0.062 (0.050 - 0.076)	0.071 (0.056 - 0.090)	0.081 (0.067 - 0.100)	0.094 (0.075 - 0.107)	0.111 (0.090 - 0.127)
90	0.056 (0.043 - 0.067)	0.071 (0.058 - 0.087)	0.081 (0.064 - 0.102)	0.091 (0.075 - 0.112)	0.104 (0.084 - 0.119)	0.121 (0.098 - 0.137)
100	0.063 (0.050 - 0.076)	0.079 (0.065 - 0.097)	0.089 (0.071 - 0.111)	0.099 (0.082 - 0.121)	0.112 (0.090 - 0.127)	0.128 (0.103 - 0.145)
110	0.070 (0.055 - 0.083)	0.086 (0.070 - 0.105)	0.096 (0.076 - 0.119)	0.105 (0.086 - 0.129)	0.118 (0.095 - 0.134)	0.132 (0.107 - 0.150)
120	0.076 (0.060 - 0.090)	0.091 (0.075 - 0.111)	0.101 (0.081 - 0.125)	0.109 (0.090 - 0.134)	0.122 (0.098 - 0.139)	0.136 (0.109 - 0.154)

Table 28 Conversion factors (DAP to Effective Dose) for varying kV and Additional Copper Filtration for Examinations Performed with Primary Beam not Through the Table

	Additional Copper Filtration (mmCu)				
kV	**0.1**	**0.2**	**0.3**	**0.6**	**0.9**
Head (mSv/Gycm²)					
60	0.073 (0.070 - 0.076)	0.086 (0.083 - 0.089)	0.096 (0.093 - 0.098)	0.112 (0.110 - 0.115)	0.122 (0.120 - 0.124)
70	0.086 (0.083 - 0.088)	0.101 (0.098 - 0.103)	0.111 (0.109 - 0.113)	0.130 (0.128 - 0.131)	0.140 (0.138 - 0.141)
80	0.098 (0.095 - 0.100)	0.114 (0.112 - 0.116)	0.125 (0.123 - 0.126)	0.143 (0.142 - 0.144)	0.153 (0.152 - 0.154)
90	0.108 (0.106 - 0.109)	0.124 (0.122 - 0.125)	0.135 (0.133 - 0.136)	0.152 (0.151 - 0.153)	0.161 (0.161 - 0.161)
100	0.116 (0.114 - 0.117)	0.132 (0.130 - 0.133)	0.142 (0.141 - 0.143)	0.158 (0.158 - 0.159)	0.166 (0.166 - 0.166)
110	0.122 (0.121 - 0.124)	0.138 (0.137 - 0.139)	0.147 (0.147 - 0.148)	0.163 (0.162 - 0.163)	0.170 (0.170 - 0.170)
120	0.128 (0.127 - 0.129)	0.142 (0.142 - 0.143)	0.151 (0.151 - 0.152)	0.165 (0.165 - 0.166)	0.172 (0.172 - 0.173)
Heart (mSv/Gycm²)					
60	0.332 (0.295 - 0.372)	0.382 (0.341 - 0.425)	0.415 (0.371 - 0.461)	0.471 (0.423 - 0.521)	0.501 (0.450 - 0.553)
70	0.374 (0.334 - 0.417)	0.428 (0.383 - 0.475)	0.463 (0.416 - 0.513)	0.523 (0.470 - 0.577)	0.553 (0.498 - 0.610)
80	0.412 (0.369 - 0.458)	0.468 (0.419 - 0.518)	0.503 (0.452 - 0.556)	0.561 (0.505 - 0.618)	0.589 (0.531 - 0.649)
90	0.443 (0.397 - 0.492)	0.498 (0.447 - 0.550)	0.532 (0.478 - 0.587)	0.585 (0.527 - 0.645)	0.610 (0.550 - 0.672)
100	0.468 (0.420 - 0.518)	0.520 (0.467 - 0.574)	0.552 (0.497 - 0.609)	0.601 (0.541 - 0.661)	0.623 (0.562 - 0.685)
110	0.488 (0.438 - 0.540)	0.537 (0.483 - 0.593)	0.566 (0.510 - 0.625)	0.611 (0.550 - 0.672)	0.630 (0.568 - 0.694)
120	0.504 (0.453 - 0.557)	0.550 (0.495 - 0.607)	0.577 (0.520 - 0.636)	0.617 (0.556 - 0.679)	0.635 (0.572 - 0.698)

Table 28 Continued

	Additional Copper Filtration (mmCu)				
kV	**0.1**	**0.2**	**0.3**	**0.6**	**0.9**
Kidney (mSv/Gycm²)					
60	0.202 (0.189 - 0.210)	0.246 (0.230 - 0.255)	0.276 (0.259 - 0.287)	0.331 (0.311 - 0.344)	0.362 (0.340 - 0.376)
70	0.243 (0.228 - 0.253)	0.293 (0.275 - 0.304)	0.327 (0.306 - 0.340)	0.386 (0.363 - 0.402)	0.418 (0.393 - 0.435)
80	0.282 (0.264 - 0.292)	0.334 (0.313 - 0.347)	0.369 (0.346 - 0.384)	0.428 (0.402 - 0.446)	0.459 (0.430 - 0.478)
90	0.313 (0.293 - 0.326)	0.366 (0.343 - 0.381)	0.400 (0.375 - 0.417)	0.456 (0.427 - 0.475)	0.483 (0.452 - 0.504)
100	0.339 (0.317 - 0.353)	0.390 (0.365 - 0.406)	0.422 (0.395 - 0.440)	0.474 (0.444 - 0.494)	0.499 (0.467 - 0.520)
110	0.360 (0.337 - 0.374)	0.408 (0.382 - 0.425)	0.439 (0.411 - 0.457)	0.486 (0.455 - 0.507)	0.509 (0.476 - 0.531)
120	0.377 (0.353 - 0.393)	0.422 (0.395 - 0.440)	0.451 (0.423 - 0.470)	0.495 (0.463 - 0.516)	0.515 (0.482 - 0.538)
Liver (mSv/Gycm²)					
60	0.225 (0.202 - 0.241)	0.273 (0.246 - 0.292)	0.306 (0.276 - 0.328)	0.366 (0.330 - 0.391)	0.399 (0.360 - 0.427)
70	0.270 (0.243 - 0.289)	0.324 (0.292 - 0.346)	0.361 (0.325 - 0.386)	0.425 (0.384 - 0.454)	0.460 (0.415 - 0.491)
80	0.311 (0.280 - 0.333)	0.368 (0.332 - 0.394)	0.406 (0.366 - 0.434)	0.470 (0.424 - 0.502)	0.503 (0.454 - 0.537)
90	0.345 (0.311 - 0.369)	0.402 (0.363 - 0.430)	0.440 (0.396 - 0.470)	0.500 (0.451 - 0.534)	0.530 (0.477 - 0.565)
100	0.373 (0.336 - 0.399)	0.428 (0.386 - 0.458)	0.464 (0.418 - 0.495)	0.520 (0.468 - 0.555)	0.546 (0.492 - 0.583)
110	0.396 (0.356 - 0.423)	0.448 (0.404 - 0.479)	0.481 (0.433 - 0.514)	0.533 (0.480 - 0.569)	0.557 (0.501 - 0.594)
120	0.414 (0.373 - 0.443)	0.464 (0.418 - 0.495)	0.495 (0.445 - 0.528)	0.542 (0.488 - 0.578)	0.564 (0.507 - 0.602)
Prostate (mSv/Gycm²)					
60	0.159 (0.112 - 0.205)	0.182 (0.131 - 0.233)	0.198 (0.143 - 0.251)	0.225 (0.165 - 0.282)	0.240 (0.177 - 0.298)
70	0.179 (0.129 - 0.228)	0.205 (0.149 - 0.258)	0.222 (0.163 - 0.278)	0.251 (0.187 - 0.310)	0.266 (0.199 - 0.327)
80	0.198 (0.144 - 0.249)	0.224 (0.166 - 0.280)	0.242 (0.180 - 0.300)	0.270 (0.203 - 0.332)	0.284 (0.215 - 0.347)
90	0.213 (0.157 - 0.267)	0.239 (0.178 - 0.297)	0.256 (0.192 - 0.316)	0.282 (0.214 - 0.346)	0.295 (0.225 - 0.360)
100	0.225 (0.167 - 0.281)	0.251 (0.188 - 0.310)	0.266 (0.201 - 0.328)	0.291 (0.221 - 0.355)	0.302 (0.231 - 0.368)
110	0.235 (0.175 - 0.292)	0.259 (0.195 - 0.320)	0.274 (0.207 - 0.336)	0.296 (0.226 - 0.361)	0.307 (0.235 - 0.372)
120	0.244 (0.182 - 0.301)	0.266 (0.201 - 0.327)	0.280 (0.212 - 0.342)	0.300 (0.229 - 0.365)	0.309 (0.237 - 0.375)

10.10. Effect of Half Value Layer and Field Size on Reference Air Kerma to Effective Dose Conversion Factor

The results from simulations normalised to AK_{ref} were analysed as previously done for the DAP dose metric (section 10.7) and are presented in Figure 19. As would be expected the results show an increasing conversion factor with increasing HVL as is seen for the DAP conversion factors. These results however show a much greater impact with varying field sizes. This result is expected as the dose metric does not provide any indication of the field size used.

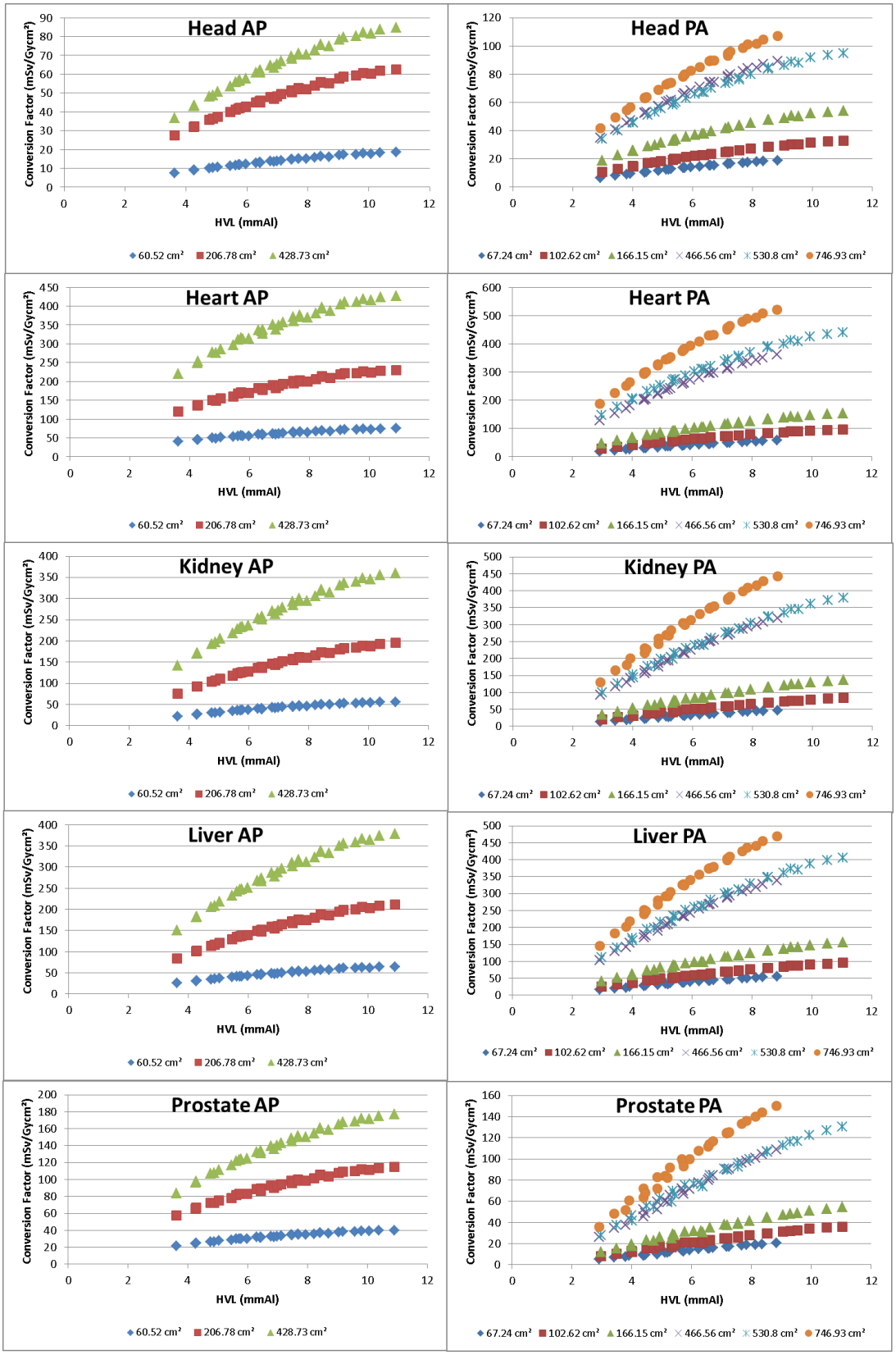

Figure 19 Results for Conversion Factors using the Reference Air Kerma as a Dose Metric

Given this greater variation in conversion factor and in order to achieve a generalised conversion factor they were normalised to the X-ray field area at the isocentre. Results from this are given in Figure 20 and show similar trends to those using DAP as the dose metric. This is not unexpected and allows for a simpler variation of conversion factor to be established. The downside to using this method is that the field size used will need to be known for the conversion factors to be used.

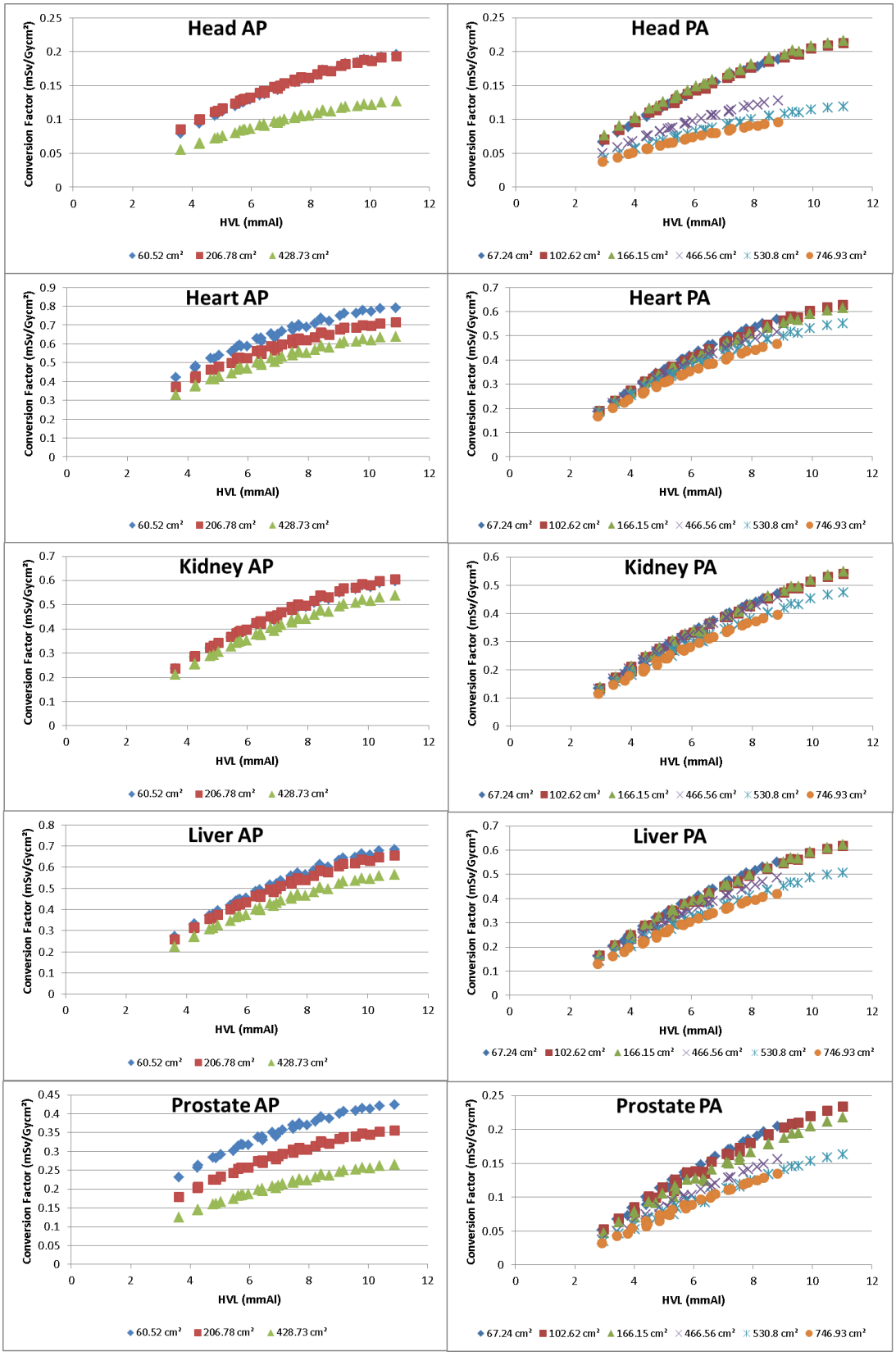

Figure 20 Conversion Factor for Reference Air Kerma Normalised to the X-ray Field Size

Following the normalisation by field area it can be seen in Figure 20 there is still a field size variation for most of the examinations. A summary for one set of exposure parameters (120kV and 0.9mmCu filtration) is provided in Table 29. (% difference is defined as 100 x (maximum - minimum)/mean). This shows a similar range in effective dose conversion factor as was seen for the DAP results (see Table 18 and Table 23). To calculate the effective dose the conversion factor is multiplied by the AK_{ref} and the x-ray area at the isocentre.

Table 29 Comparison of Mean and Range of Conversion Factors with Varying X-ray Field Size for the Different Examinations Simulated

AP	Conversion Factor (mSv/Gy/cm²)			% Difference
	Mean	Minimum	Maximum	
Head	0.11	0.11	0.11	0.9%
Heart	0.40	0.36	0.45	21.5%
Kidneys	0.33	0.30	0.34	11.8%
Liver	0.36	0.32	0.38	18.6%
Prostate	0.20	0.15	0.24	45.8%

PA	Conversion Factor (mSv/Gy/cm²)			% Difference
	Mean	Minimum	Maximum	
Head	0.09	0.09	0.09	1.8%
Heart	0.26	0.24	0.27	12.9%
Kidneys	0.23	0.21	0.24	14.3%
Liver	0.25	0.22	0.27	19.7%
Prostate	0.09	0.07	0.10	34.5%

Normalising the conversion factor by field area at the isocentre introduces additional calculations into the effective dose calculation as the x-ray area is not displayed on the equipment. Field size at the detector is displayed which would provide an alternative quantity to normalise the conversion factors. The use of field size rather than area has been considered, but this introduces additional complications as the focus to detector distance is not fixed and different equipment defines the field size using different methods. For some equipment the field size is defined by the length of the side of the x-ray field while others define the field size as the diagonal distance between the corners of the x-ray field. It was

found that the conversion factors vary by the field size squared and so using this method produces an area that would still need to be calculated at a standard distance. This would change the conversion factors by a factor of $(^{FIsoD}/_{FDD})^2$.

10.11. Derivation of Conversion Factor for Reference Air Kerma to Effective Dose using Half Value Layer and Beam Area

The results given in Figure 20 show that for AK_{ref} the conversion factor is influenced by both the field size and the beam HVL. The process used in section 10.8 was used to produce a method to calculate the conversion factor for E. In section 10.10 both the not normalised by area (Figure 19) and normalised by area (Figure 20) conversion factors were analysed. For AK_{ref} only the not normalised by area conversion factors have been produced. These factors require the area to be known regardless of whether or not the conversion factor is normalised so to keep the conversion simpler only the not normalised factors are considered. Using this method means the conversion factor can be used with the AK_{ref} from the system to calculate E. The conversion factor formulae are given in Table 30 and the differences from PCXMC are shown in Figure 21 (% difference is defined as 100 x (conversion factor from formula – PCXMC conversion factor)/PCXMC conversion factor).

Table 30 Formulae for Reference Air Kerma to Effective Dose Conversion Factor Using Beam HVL and X-ray Area at the Isocentre (A) and Differences from PCXMC Results. Results in Brackets are with the Beam HVL Less than 3mmAl Removed

Exam	Conversion factor formula	Range of difference from PCXMC
AP Head	(0.0564A + 0.371) Ln(HVL) – 0.0246A – 0.8088	-5.0% – 2.3% (-5.0% – 2.3%)
AP Heart	(0.1587A + 3.3493) Ln(HVL) – 0.0279A + 0.6056	-6.7% – 11.1% (-6.7% – 11.1%)
AP Kidney	(0.1706A + 3.1444) Ln(HVL) – 0.1076A – 2.1628	-9.1% – 16.1% (-9.1% – 16.1%)
AP Liver	(0.1747A + 4.7044) Ln(HVL) – 0.1069A – 3.0408	-9.7% – 16.5%

		(-9.7% – 16.5%)
AP Prostate	(0.0689A + 3.2312) Ln(HVL) – 0.031A + 1.8917	-13.9% – 23.3% (-13.9% – 23.3%)
PA Head	(0.0484A + 0.1359) Ln(HVL) – 0.0198A – 0.6092	-14.4% – 5.9% (6.4% – 5.9%)
PA Heart	(0.1206A + 4.1226) Ln(HVL) – 0.0611A – 3.8526	-13.2% – 15.2% (-7.4% – 15.2%)
PA Kidney	(0.1152A + 3.728) Ln(HVL) – 0.0807A – 3.4818	-24.8% – 24.4% (-14.5% – 24.4%)
PA Liver	(0.1175A + 5.4678) Ln(HVL) – 0.0772A – 4.7272	-21.3% – 25.8% (-12.2% – 25.8%)
PA Prostate	(0.0402A + 2.5522) Ln (HVL) – 0.0338A + 1.8917	-35.1% – 32.7% (-18.1% – 32.7%)

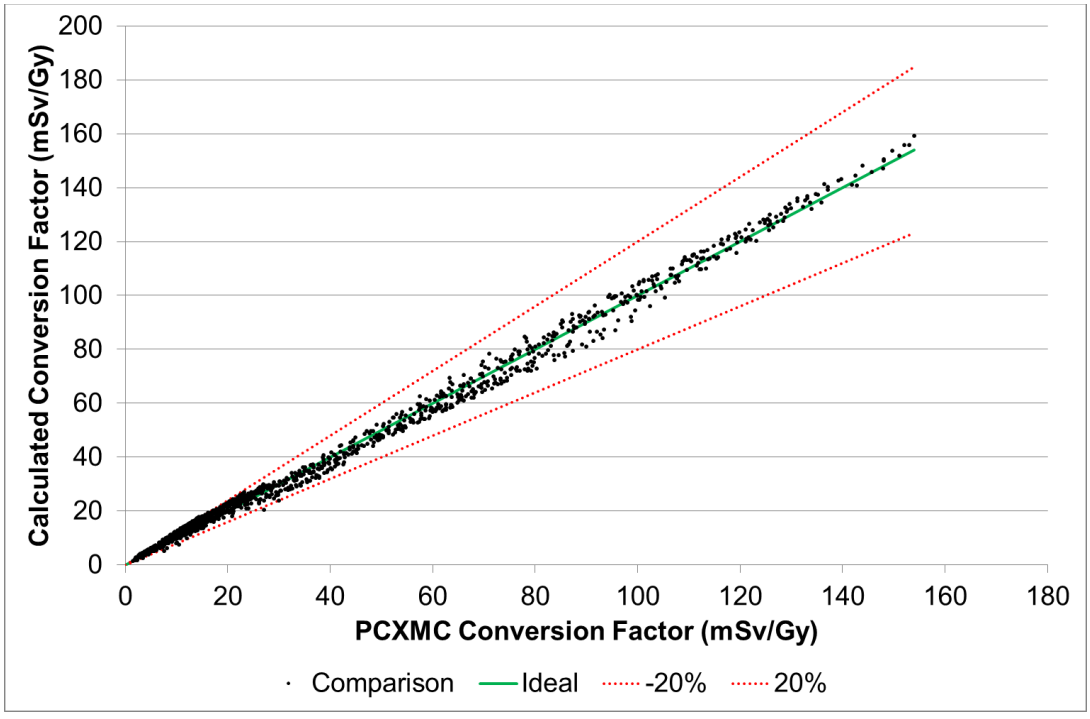

Figure 21 Comparison of PCXMC Conversion Factor with Calculated Conversion Factors for Head, Heart, Kidney, Liver and Prostate Examinations with an Ideal Fit and ± 20% Deviation

These results are similar to those seen for the DAP conversion factor (Table 26) with examinations performed with a beam HVL below 3mmAl through the table having the greatest difference from the PCXMC result. The remaining high percentage differences are for examinations with a small conversion factor where similar small differences represent a larger percentage. To calculate E the conversion factor determined from the formula in Table 30 should be multiplied by the AK_{ref} in Gy.

10.12. Variation of Reference Air Kerma to Effective Dose Conversion Factor with kV and Additional Filtration

As discussed previously (section 10.9) the HVL of the X-ray beam is not always known. It is therefore useful to have the conversion factors detailed in terms of kV and additional filtration. Table 31 and Table 32 give the mean and range of normalised conversion factors for the various beam conditions. Unlike those in Table 27 and Table 28 these have been normalised to the X-ray beam area at the isocentre and so will need this additional information to be used when calculating E. The range given in brackets represents the range of conversion factors resulting from the different variations in inherent filtration and field size. To calculate E the conversion factor determined from the formula in Table 31 or Table 32 should be multiplied by the AK_{ref} in Gy and by the X-ray field area at the isocentre in cm^2.

Table 31 Normalised Conversion Factors (Reference Air Kerma to Effective Dose) for Varying kV and Additional Copper Filtration for Examinations Performed with the Primary Beam Through the Table

	Additional Copper Filtration (mmCu)					
kV	**0**	**0.1**	**0.2**	**0.3**	**0.5**	**1.0**
Head (mSv/Gy/cm²)						
60	0.031 (0.029 - 0.033)	0.033 (0.028 - 0.039)	0.044 (0.042 - 0.045)	0.050 (0.050 - 0.050)	0.056 (0.054 - 0.057)	0.065 (0.064 - 0.066)
70	0.037 (0.035 - 0.039)	0.040 (0.033 - 0.046)	0.052 (0.050 - 0.054)	0.059 (0.059 - 0.059)	0.065 (0.064 - 0.067)	0.075 (0.074 - 0.076)
80	0.043 (0.041 - 0.045)	0.045 (0.037 - 0.054)	0.059 (0.057 - 0.061)	0.067 (0.067 - 0.067)	0.073 (0.071 - 0.074)	0.082 (0.081 - 0.084)
90	0.048 (0.047 - 0.051)	0.050 (0.041 - 0.059)	0.065 (0.062 - 0.067)	0.073 (0.073 - 0.073)	0.078 (0.077 - 0.079)	0.087 (0.086 - 0.088)
100	0.053 (0.051 - 0.055)	0.054 (0.044 - 0.064)	0.069 (0.067 - 0.072)	0.077 (0.077 - 0.077)	0.082 (0.081 - 0.083)	0.090 (0.089 - 0.091)
110	0.057 (0.055 - 0.059)	0.057 (0.046 - 0.068)	0.073 (0.071 - 0.075)	0.080 (0.080 - 0.080)	0.085 (0.084 - 0.086)	0.092 (0.091 - 0.093)
120	0.060 (0.059 - 0.062)	0.059 (0.048 - 0.071)	0.076 (0.073 - 0.078)	0.083 (0.083 - 0.083)	0.086 (0.086 - 0.087)	0.093 (0.093 - 0.094)
Heart (mSv/Gy/cm²)						
60	0.080 (0.073 - 0.082)	0.099 (0.080 - 0.112)	0.119 (0.111 - 0.132)	0.137 (0.126 - 0.147)	0.151 (0.145 - 0.155)	0.178 (0.169 - 0.183)
70	0.097 (0.088 - 0.101)	0.119 (0.096 - 0.136)	0.143 (0.132 - 0.159)	0.163 (0.149 - 0.176)	0.179 (0.169 - 0.184)	0.208 (0.195 - 0.215)
80	0.114 (0.103 - 0.119)	0.138 (0.112 - 0.158)	0.163 (0.150 - 0.183)	0.184 (0.167 - 0.200)	0.201 (0.189 - 0.208)	0.229 (0.214 - 0.239)
90	0.129 (0.116 - 0.136)	0.153 (0.124 - 0.176)	0.180 (0.165 - 0.201)	0.200 (0.181 - 0.218)	0.216 (0.202 - 0.225)	0.242 (0.225 - 0.253)
100	0.143 (0.128 - 0.150)	0.165 (0.135 - 0.191)	0.192 (0.176 - 0.215)	0.211 (0.191 - 0.231)	0.227 (0.211 - 0.237)	0.251 (0.232 - 0.263)
110	0.154 (0.138 - 0.163)	0.175 (0.143 - 0.202)	0.202 (0.185 - 0.226)	0.220 (0.198 - 0.241)	0.235 (0.218 - 0.245)	0.257 (0.237 - 0.269)
120	0.164 (0.146 - 0.174)	0.183 (0.149 - 0.212)	0.209 (0.192 - 0.234)	0.226 (0.204 - 0.248)	0.240 (0.223 - 0.251)	0.260 (0.240 - 0.273)

Table 31 Continued

	Additional Copper Filtration (mmCu)					
kV	**0**	**0.1**	**0.2**	**0.3**	**0.5**	**1.0**
Kidney (mSv/Gy/cm²)						
60	0.057 (0.051 - 0.060)	0.077 (0.071 - 0.082)	0.089 (0.079 - 0.098)	0.105 (0.095 - 0.110)	0.116 (0.108 - 0.120)	0.140 (0.131 - 0.146)
70	0.072 (0.064 - 0.077)	0.097 (0.088 - 0.103)	0.111 (0.098 - 0.122)	0.129 (0.117 - 0.136)	0.142 (0.132 - 0.148)	0.170 (0.157 - 0.177)
80	0.088 (0.078 - 0.093)	0.115 (0.105 - 0.123)	0.130 (0.116 - 0.144)	0.150 (0.135 - 0.159)	0.164 (0.152 - 0.172)	0.192 (0.177 - 0.201)
90	0.102 (0.090 - 0.109)	0.130 (0.119 - 0.139)	0.146 (0.131 - 0.161)	0.166 (0.149 - 0.176)	0.180 (0.166 - 0.189)	0.206 (0.189 - 0.216)
100	0.114 (0.101 - 0.122)	0.142 (0.130 - 0.153)	0.159 (0.142 - 0.174)	0.177 (0.160 - 0.189)	0.192 (0.176 - 0.201)	0.216 (0.197 - 0.227)
110	0.125 (0.111 - 0.133)	0.152 (0.139 - 0.164)	0.169 (0.151 - 0.184)	0.186 (0.167 - 0.198)	0.200 (0.183 - 0.210)	0.223 (0.203 - 0.234)
120	0.134 (0.119 - 0.143)	0.160 (0.146 - 0.173)	0.176 (0.158 - 0.192)	0.193 (0.173 - 0.206)	0.206 (0.188 - 0.217)	0.227 (0.207 - 0.239)
Liver (mSv/Gy/cm²)						
60	0.066 (0.057 - 0.073)	0.083 (0.063 - 0.099)	0.102 (0.088 - 0.118)	0.119 (0.104 - 0.132)	0.134 (0.120 - 0.143)	0.161 (0.143 - 0.172)
70	0.083 (0.071 - 0.092)	0.102 (0.079 - 0.123)	0.126 (0.108 - 0.145)	0.144 (0.127 - 0.162)	0.163 (0.145 - 0.174)	0.193 (0.171 - 0.206)
80	0.100 (0.085 - 0.110)	0.121 (0.095 - 0.146)	0.147 (0.127 - 0.170)	0.167 (0.146 - 0.188)	0.187 (0.165 - 0.199)	0.217 (0.191 - 0.231)
90	0.116 (0.098 - 0.127)	0.137 (0.108 - 0.164)	0.165 (0.142 - 0.189)	0.183 (0.160 - 0.207)	0.204 (0.180 - 0.218)	0.232 (0.204 - 0.248)
100	0.129 (0.109 - 0.142)	0.149 (0.119 - 0.180)	0.178 (0.154 - 0.204)	0.196 (0.170 - 0.221)	0.216 (0.190 - 0.231)	0.242 (0.212 - 0.259)
110	0.141 (0.119 - 0.155)	0.160 (0.127 - 0.192)	0.188 (0.163 - 0.216)	0.205 (0.178 - 0.232)	0.225 (0.197 - 0.240)	0.249 (0.217 - 0.266)
120	0.151 (0.128 - 0.166)	0.168 (0.134 - 0.203)	0.197 (0.171 - 0.225)	0.212 (0.184 - 0.240)	0.232 (0.202 - 0.247)	0.254 (0.221 - 0.271)

Table 31 Continued

	Additional Copper Filtration (mmCu)					
kV	**0**	**0.1**	**0.2**	**0.3**	**0.5**	**1.0**
Prostate (mSv/Gy/cm²)						
60	0.019 (0.014 - 0.023)	0.024 (0.020 - 0.032)	0.030 (0.023 - 0.039)	0.035 (0.028 - 0.044)	0.041 (0.032 - 0.048)	0.051 (0.040 - 0.059)
70	0.025 (0.019 - 0.030)	0.031 (0.027 - 0.041)	0.039 (0.030 - 0.050)	0.045 (0.036 - 0.056)	0.052 (0.041 - 0.060)	0.064 (0.051 - 0.073)
80	0.031 (0.024 - 0.037)	0.038 (0.033 - 0.051)	0.047 (0.036 - 0.060)	0.053 (0.044 - 0.067)	0.062 (0.049 - 0.071)	0.073 (0.058 - 0.084)
90	0.037 (0.028 - 0.044)	0.044 (0.038 - 0.058)	0.054 (0.042 - 0.068)	0.060 (0.049 - 0.075)	0.069 (0.055 - 0.078)	0.080 (0.063 - 0.091)
100	0.042 (0.032 - 0.050)	0.049 (0.042 - 0.065)	0.059 (0.046 - 0.074)	0.065 (0.053 - 0.081)	0.074 (0.059 - 0.084)	0.084 (0.067 - 0.096)
110	0.046 (0.036 - 0.055)	0.053 (0.045 - 0.070)	0.063 (0.050 - 0.079)	0.069 (0.056 - 0.086)	0.077 (0.062 - 0.088)	0.087 (0.069 - 0.099)
120	0.050 (0.039 - 0.060)	0.057 (0.048 - 0.074)	0.067 (0.052 - 0.083)	0.072 (0.059 - 0.090)	0.080 (0.064 - 0.092)	0.089 (0.071 - 0.102)

Table 32 Normalised Conversion factors (Reference Air Kerma to Effective Dose) for Varying kV and Additional Copper Filtration for Examinations Performed with the Primary Beam not Through the Table

	Additional Copper Filtration (mmCu)				
kV	**0.1**	**0.2**	**0.3**	**0.6**	**0.9**
Head (mSv/Gy/cm²)					
60	0.046 (0.045 - 0.048)	0.055 (0.053 - 0.056)	0.061 (0.059 - 0.062)	0.071 (0.070 - 0.073)	0.077 (0.076 - 0.078)
70	0.054 (0.053 - 0.056)	0.064 (0.063 - 0.065)	0.071 (0.070 - 0.072)	0.083 (0.082 - 0.083)	0.089 (0.089 - 0.089)
80	0.062 (0.061 - 0.063)	0.072 (0.071 - 0.073)	0.079 (0.079 - 0.080)	0.091 (0.091 - 0.091)	0.097 (0.097 - 0.097)
90	0.068 (0.067 - 0.069)	0.079 (0.078 - 0.080)	0.086 (0.085 - 0.086)	0.097 (0.097 - 0.097)	0.102 (0.102 - 0.103)
100	0.074 (0.073 - 0.074)	0.084 (0.083 - 0.084)	0.090 (0.090 - 0.091)	0.101 (0.101 - 0.101)	0.106 (0.106 - 0.106)
110	0.078 (0.077 - 0.079)	0.088 (0.087 - 0.088)	0.094 (0.094 - 0.094)	0.103 (0.103 - 0.104)	0.108 (0.108 - 0.108)
120	0.081 (0.081 - 0.082)	0.091 (0.090 - 0.091)	0.096 (0.096 - 0.096)	0.105 (0.105 - 0.106)	0.109 (0.109 - 0.110)
Heart (mSv/Gy/cm²)					
60	0.210 (0.185 - 0.237)	0.242 (0.214 - 0.272)	0.263 (0.233 - 0.295)	0.299 (0.265 - 0.334)	0.318 (0.283 - 0.354)
70	0.237 (0.210 - 0.267)	0.271 (0.241 - 0.304)	0.294 (0.261 - 0.328)	0.331 (0.295 - 0.369)	0.351 (0.313 - 0.390)
80	0.261 (0.231 - 0.293)	0.296 (0.263 - 0.331)	0.319 (0.284 - 0.355)	0.355 (0.317 - 0.395)	0.373 (0.333 - 0.414)
90	0.281 (0.249 - 0.314)	0.315 (0.281 - 0.352)	0.337 (0.300 - 0.375)	0.371 (0.331 - 0.412)	0.387 (0.345 - 0.429)
100	0.297 (0.263 - 0.331)	0.330 (0.293 - 0.367)	0.350 (0.312 - 0.389)	0.381 (0.340 - 0.422)	0.395 (0.353 - 0.437)
110	0.309 (0.275 - 0.345)	0.340 (0.303 - 0.378)	0.359 (0.320 - 0.399)	0.387 (0.346 - 0.429)	0.400 (0.357 - 0.443)
120	0.320 (0.284 - 0.356)	0.348 (0.310 - 0.387)	0.366 (0.326 - 0.406)	0.391 (0.349 - 0.434)	0.402 (0.359 - 0.446)

Table 32 Continued

	Additional Copper Filtration (mmCu)				
kV	**0.1**	**0.2**	**0.3**	**0.6**	**0.9**
Kidney (mSv/Gy/cm²)					
60	0.128 (0.119 - 0.133)	0.156 (0.145 - 0.162)	0.175 (0.163 - 0.182)	0.210 (0.195 - 0.218)	0.229 (0.213 - 0.238)
70	0.154 (0.143 - 0.160)	0.186 (0.172 - 0.193)	0.207 (0.192 - 0.215)	0.245 (0.228 - 0.255)	0.265 (0.246 - 0.276)
80	0.179 (0.166 - 0.185)	0.212 (0.196 - 0.220)	0.234 (0.217 - 0.243)	0.272 (0.252 - 0.283)	0.291 (0.270 - 0.303)
90	0.199 (0.184 - 0.207)	0.232 (0.215 - 0.241)	0.254 (0.235 - 0.264)	0.289 (0.268 - 0.301)	0.307 (0.284 - 0.320)
100	0.215 (0.199 - 0.224)	0.247 (0.229 - 0.257)	0.268 (0.248 - 0.279)	0.301 (0.279 - 0.313)	0.316 (0.293 - 0.330)
110	0.228 (0.211 - 0.237)	0.259 (0.240 - 0.270)	0.278 (0.258 - 0.290)	0.308 (0.286 - 0.322)	0.323 (0.299 - 0.337)
120	0.239 (0.221 - 0.249)	0.268 (0.248 - 0.279)	0.286 (0.265 - 0.298)	0.314 (0.291 - 0.327)	0.326 (0.302 - 0.341)
Liver (mSv/Gy/cm²)					
60	0.143 (0.127 - 0.154)	0.173 (0.154 - 0.187)	0.194 (0.173 - 0.210)	0.232 (0.207 - 0.250)	0.253 (0.226 - 0.273)
70	0.171 (0.153 - 0.185)	0.205 (0.183 - 0.222)	0.229 (0.204 - 0.247)	0.270 (0.241 - 0.291)	0.292 (0.260 - 0.315)
80	0.197 (0.176 - 0.213)	0.234 (0.208 - 0.252)	0.258 (0.230 - 0.278)	0.299 (0.266 - 0.322)	0.319 (0.285 - 0.345)
90	0.219 (0.195 - 0.237)	0.255 (0.228 - 0.276)	0.279 (0.249 - 0.301)	0.317 (0.283 - 0.342)	0.336 (0.299 - 0.363)
100	0.237 (0.211 - 0.255)	0.272 (0.242 - 0.293)	0.294 (0.262 - 0.317)	0.330 (0.294 - 0.356)	0.347 (0.309 - 0.374)
110	0.251 (0.224 - 0.271)	0.284 (0.253 - 0.307)	0.305 (0.272 - 0.329)	0.338 (0.301 - 0.364)	0.353 (0.315 - 0.381)
120	0.263 (0.234 - 0.283)	0.294 (0.262 - 0.317)	0.314 (0.280 - 0.338)	0.344 (0.306 - 0.370)	0.357 (0.318 - 0.385)
Prostate (mSv/Gy/cm²)					
60	0.100 (0.070 - 0.130)	0.115 (0.082 - 0.148)	0.125 (0.090 - 0.160)	0.143 (0.104 - 0.180)	0.152 (0.111 - 0.190)
70	0.113 (0.081 - 0.145)	0.130 (0.094 - 0.164)	0.141 (0.102 - 0.177)	0.159 (0.117 - 0.198)	0.168 (0.125 - 0.208)
80	0.125 (0.090 - 0.159)	0.142 (0.104 - 0.178)	0.153 (0.113 - 0.191)	0.171 (0.128 - 0.211)	0.180 (0.135 - 0.221)
90	0.135 (0.098 - 0.170)	0.152 (0.112 - 0.189)	0.162 (0.121 - 0.201)	0.179 (0.134 - 0.220)	0.187 (0.141 - 0.229)
100	0.143 (0.105 - 0.178)	0.159 (0.118 - 0.197)	0.169 (0.126 - 0.208)	0.184 (0.139 - 0.226)	0.191 (0.145 - 0.234)
110	0.149 (0.110 - 0.186)	0.164 (0.122 - 0.203)	0.174 (0.130 - 0.214)	0.188 (0.142 - 0.230)	0.194 (0.147 - 0.237)
120	0.154 (0.114 - 0.192)	0.169 (0.126 - 0.208)	0.177 (0.133 - 0.218)	0.190 (0.144 - 0.232)	0.196 (0.149 - 0.239)

10.13. Impact of Arms on Conversion Factor

Following best radiographic practice simulations have been undertaken based on scans being undertaken with the arms out of the primary beam. This should be done to reduce image artefacts that would be introduced by the presence of the arms. For CBCT imaging there may be some cases where moving the arms out of the beam may not be clinically appropriate (either due to the procedure, patient compliance or the close proximity of the detector to the patient). The impact of including the arms in the dose calculation was investigated for examinations of the torso. The results from this are shown in Figure 22.

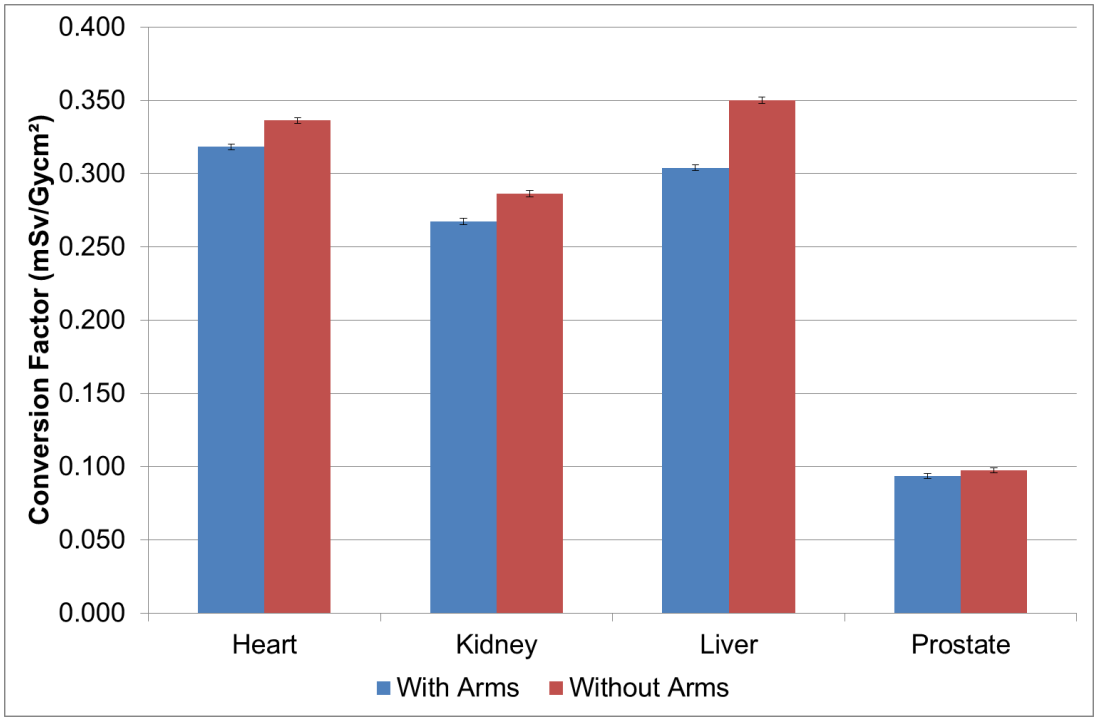

Figure 22 Comparison of Conversion Factor for Examinations Undertaken With or Without the Arms in the Primary Beam

These results show that including the arms in the primary beam results in a decrease in the conversion factor. This would be expected as the arms will attenuate the incident radiation without considerably adding to E due to the arms not containing radiation sensitive organs.

10.14. Impact of x-ray fields extending beyond the body

In sections 10.7 and 10.10 there were simulations which involved an x-ray field size that extended beyond the phantom. For these the conversion factors for either DAP or area normalised AK_{ref} did not vary with field size in the same way as when the field was contained in the phantom. It is postulated that in this case the use of AK_{ref} (not normalised to the field area) conversion factors may be more appropriate if they do not vary with field size when the x-ray field extends beyond the body. Further simulations where the x-ray field extends beyond the patient have been performed to investigate this. Only head scans have been investigated as these were the only body part where the phantom extended beyond the x-ray filed using PCXMC. The results are given in Figure 23. From analysis of the projections in PCXMC for head exams field sizes less than 300 are contained in the phantom while those above extend beyond the phantom. These results show that the conversion factors vary as the x-ray field extends beyond the body. They also show that the conversion factors do not vary proportionally to the field area. Use of AK_{ref} to E conversion factors therefore do not provide an alternative method for calculating E where the field size extends beyond the patient.

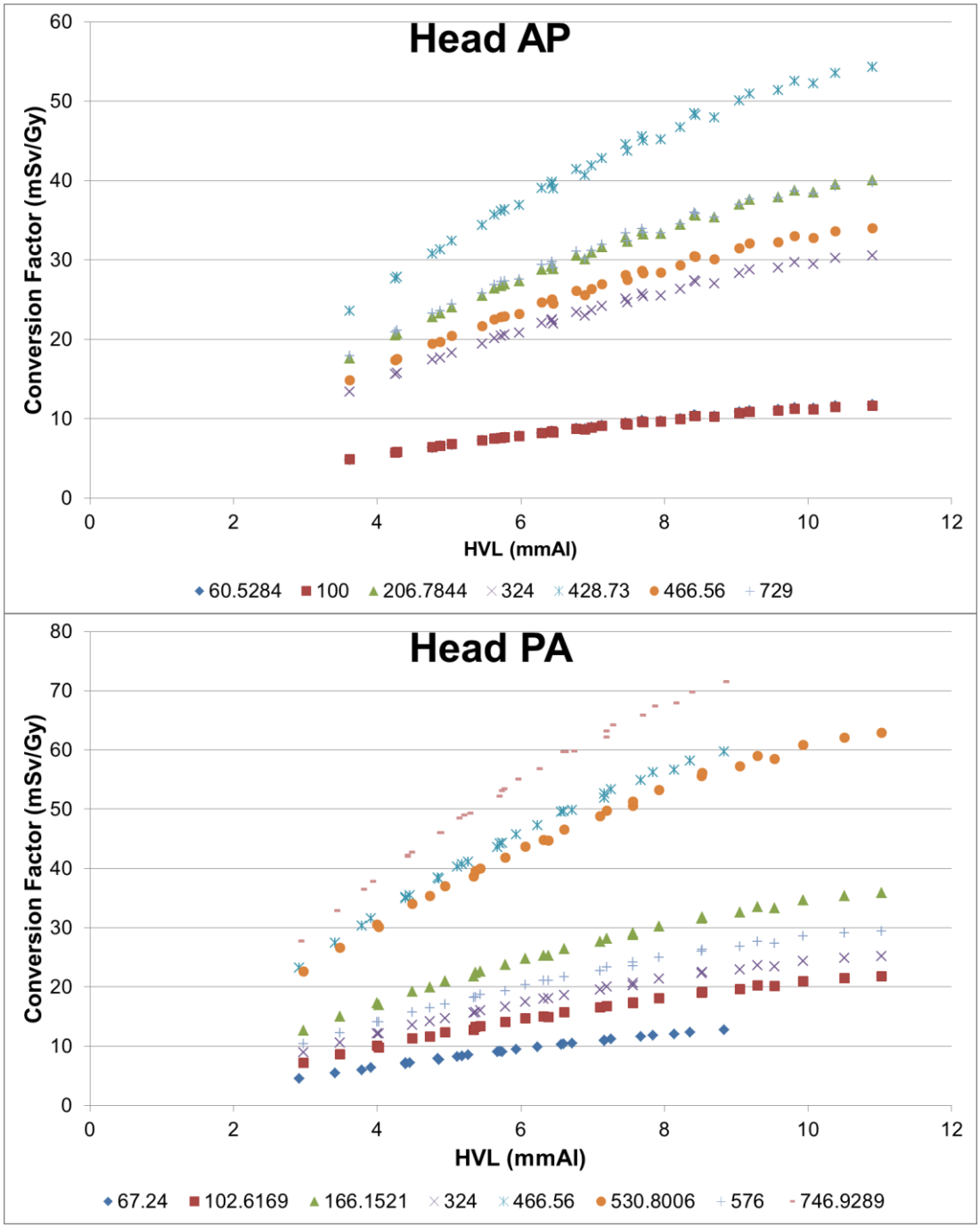

Figure 23 AKref to E conversion factors for head examinations using various x-ray areas

These results have used the pre-set field sizes available on the various systems. In addition to this the x-ray field can be manually adjusted. It is further postulated that if the field size along the length of the phantom remains constant then extending the field beyond the patient will result in a constant AK_{ref} to E conversion factor. Simulations were undertaken to

investigate this. Results are shown in Figure 24 where field sizes greater or equal to 18cm (as measured at the isocentre distance) extend beyond the phantom. These results show that in the scenario there is a constant AK_{ref} to E conversion factor. While this represents a simple method to covert AK_{ref} to E it also involves the use of x-ray fields that are not collimated to the patient which does not represent best practice. It was also not possible to use this method for other body parts due to the limits of the field sizes available not extending beyond the phantom.

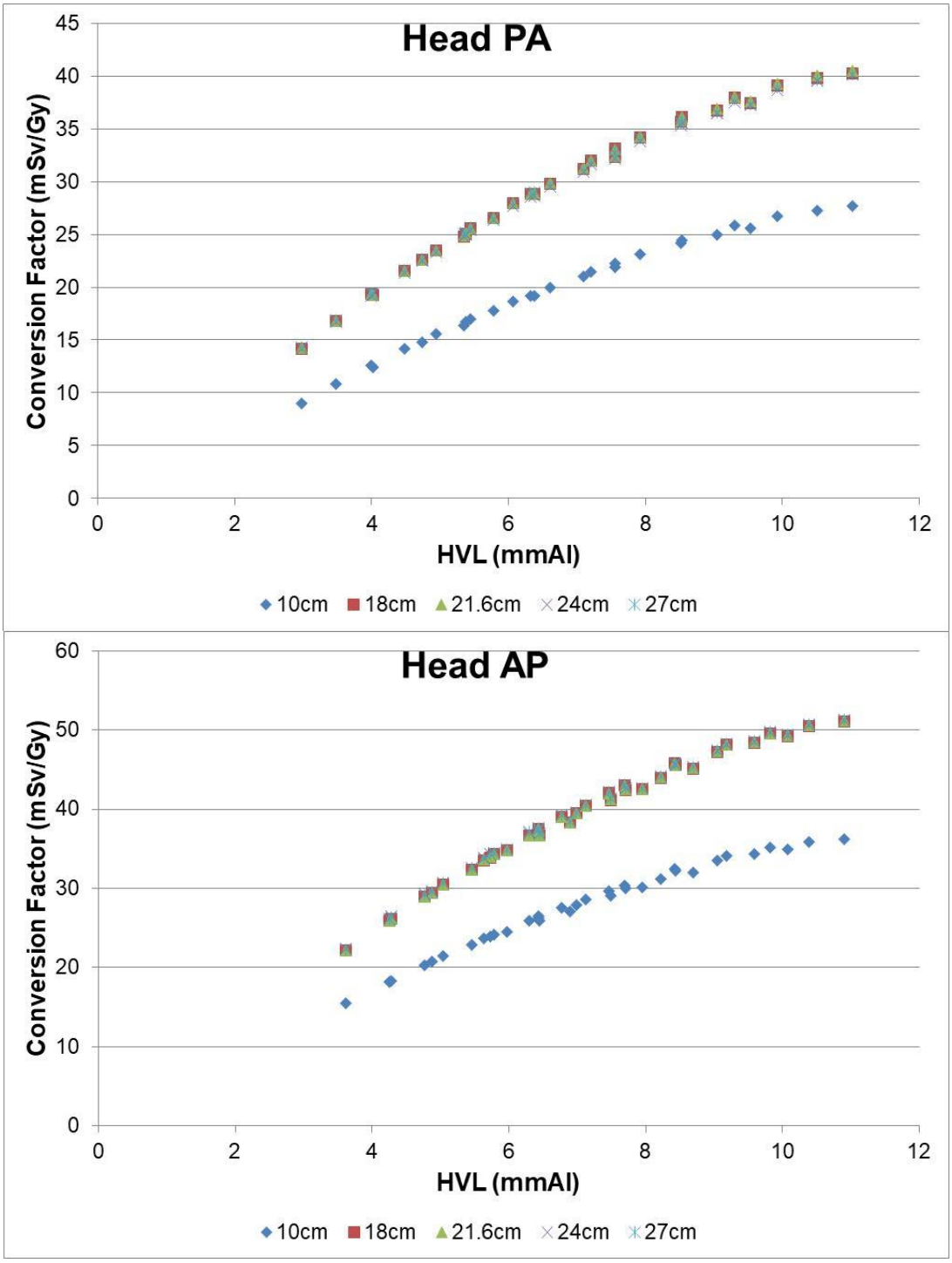

Figure 24 AKref to E conversion factors for head examinations using various X-ray widths while keeping the x-ray length the same

11. Discussion

The results from this work have shown that there are differences in the conversion factors depending on the examination, equipment and exposure parameters used to acquire CBCT images. The results have been presented as both a table of conversion factors based on the applied kV and additional copper filtration and a series of formulae relating to the beam HVL. Tables of conversion factors have also been presented for both DAP and AK_{ref} dose metrics. These both offer a method to convert the displayed dose metric to E. Due to the methods used to determine these conversion factors there are limitations to them that need to be known and understood to ensure their correct use.

11.1. Use of a Standard Size Mathematical Hermaphrodite Phantom

The phantom used for the Monte Carlo simulations represents a patient with height of 178.6cm and a mass of 73.2kg. In England the average height is 175.3cm for males and 161.9cm for females with body mass of 84.6kg (males) and 70.7kg (females) (Moody, 2014). It can be seen that the size of the standard mathematical phantom is not consistent with the average demographics in the English population. The BMI of the phantom (22.9kg/m²) is less than either the average male (27.5kg/m²) or female (27.0kg/m²) which will have an impact on E. A further set of Monte Carlo simulations (120kV, 1mmCu filtration) was undertaken to investigate the impact this may have on the conversion factor and is summarised in Table 33. These simulations only consider the differences in height and mass between the UK male and female populations. These results show that for males the PCXMC standard phantom over estimates the dose while for females the dose is underestimated. When compared to the average for English males and females the conversion factors using the PCXMC standard phantom are within -4% to +2%.

Table 33 Comparison of Conversion Factors using the PCXMC Standard Sized Phantom with those Produced using Phantoms Corresponding to the Average UK Male and Female. All simulations use a hermaphrodite phantom. Figures in Brackets are Percentage Differences from the Standard Phantom).

	Conversion Factor (mSv/Gycm²)			
Examination	**PCXMC Standard**	**UK Male**	**UK Female**	**UK Average**
Head	0.079	0.072 (-9%)	0.084 (+6%)	0.078 (-1%)
Heart	0.369	0.327 (-11%)	0.384 (+4%)	0.356 (-4%)
Kidney	0.318	0.294 (-8%)	0.351 (+10%)	0.322 (+1%)
Liver	0.340	0.315 (-7%)	0.380 (+12%)	0.348 (+2%)
Prostate	0.109	0.099 (-9%)	0.116 (+6%)	0.108 (-1%)

For the Monte Carlo simulations a mathematical hermaphrodite phantom has been used for calculation of E. Limitations due to the geometric representation and locations of organs in a mathematical phantom have been discussed previously in section 10.2. Additionally the use of a hermaphrodite phantom will add some further limitations to the application of conversion factors to both male and female patients for some of the examinations investigated.

For examinations of the thoracic region (e.g. the heart or lungs) the impact of the dose to the breasts has a large influence on E. For male patients with less breast tissue than female patients this can lead to E being over estimated using the conversion factors.

For examinations in the abdomen and pelvis regions the impact of the gonad dose will have an impact on both male and female E. When calculating E using PCXMC the gonad dose is taken as an average of the doses to the ovaries and the testes. In examinations of the abdomen this will result in an underestimate of the gonad dose in females and an overestimate for males as the dose to the ovaries is greater than the testes. The opposite occurs for examinations of the pelvis where the dose to the testes is greater than the ovaries resulting in an overestimate for females and underestimate for males.

To achieve a better estimate of radiation doses in patients the use of male and female voxel phantoms could be used. This would allow for a more specific patient group dose calculation to be undertaken.

11.2. Comparison with Literature Review

From the literature review some of the papers have derived or used E conversion factors for specific examinations. The results from the Monte Carlo simulations undertaken for this work have been compared with the conversion factors found in the literature review and are detailed in Table 34. Where possible the presented conversion factors have been matched to the protocols specified in the reference. Where there is insufficient information provided in the reference a range of possible conversion factors has been given.

Overall the results from this work are comparable to those from the literature review with the exception of the collimated head results from (Wang, et al., 2014) which are investigated further in section 11.2.1. Bai et al. do not mention if they have collimated the X-ray beam and so results here for both the collimated and uncollimated beams have been presented. It can be seen that their results compare with the range of conversion factors from this work if an uncollimated beam is assumed.

Table 34 Comparison between Conversion Factors Reported in the Literature and Conversion Factors Produced in this Work

Reference	Anatomical Region	Conversion Factor (mSv/Gycm²) from reference	Conversion Factor (mSv/Gycm²) from this work	Comments
(Piergallini, et al., 2018)	Head	0.124	0.065 – 0.125	Collimated beam Matched for kV Not matched for filtration
(Wang, et al., 2014)	Head P1 P2 P3 P4 P1 P2 P3 P4 P5 P6	Collimated 0.048 0.047 0.046 0.025 Uncollimated 0.065 0.062 0.070 0.035 0.052 0.043	 0.143 0.143 0.143 0.068 0.079 0.079 0.079 0.039 0.065 0.050	Matched for kV and filtration
(Bai, et al., 2013)	Head	0.030-0.035	0.06 – 0.12 (Collimated) 0.03 – 0.06 (uncollimated)	Matched for kV Not matched for filtration Collimation not mentioned
(Fior, et al., 2019)	Chest	0.31	0.24 – 0.41	Matched for kV Not matched for filtration
(Rotolo, et al., 2016)	Chest	0.31	0.24 – 0.41	Matched for kV Not matched for filtration
(Choo, et al., 2013)	Chest	0.45	0.36 – 0.56	Matched for kV Not matched for filtration

Table 34 Continued

Reference	Anatomical Region	Conversion Factor (mSv/Gycm²) from reference	Conversion Factor (mSv/Gycm²) from this work	Comments
(Hwang, et al., 2018)	Abdomen	0.29 (BMI<25) 0.26 (BMI 25-30) 0.23 (BMI≥30)	0.23 – 0.31	Matched for kV and Filtration. BMI of Rando is 24.
(Petersen, et al., 2018)	Abdomen	0.3	0.18 – 0.36	No data regarding kV or filtration used.
(Sailer, et al., 2015)	Abdomen	0.34	0.31 – 0.36	Matched for kV and filtration

11.2.1. Comparison with Wang et al.

The differences in conversion factor between Wang et al. and this work for collimated beams have been investigated. It is noted that the conversion factors produced have used ICRP60 organ weighting factors compared to the ICRP103 weighting factors used in this work. PCXMC produces effective doses using ICRP60 weighting factors in addition to ICRP103. These results were also analysed and are presented in Table 35. While these show there are some differences between the two methods for producing conversion factors it doesn't account for the differences seen between the collimated and uncollimated beams.

Table 35 Comparison Between Conversion Factors Produced by Wang et al. and this Work using Both ICRP60 and ICRP103 Weighting Factors

Conversion Factor (mSv/Gycm²)	(Wang, et al., 2014) (ICRP60)		This work (ICRP60)		This work (ICRP103)	
	Collimated	Uncollimated	Collimated	Uncollimated	Collimated	Uncollimated
Xper CT Cerebral High Dose	0.048	0.065	0.133	0.069	0.143	0.079
Xper CT Cerebral Low Dose	0.047	0.062	0.133	0.069	0.143	0.079
Xper CT Cerebral Fast High Dose	0.046	0.070	0.133	0.069	0.143	0.079
Xper Intracranial Stent High Dose	0.025	0.035	0.061	0.031	0.068	0.039
Xper Intracranial Stent Low Dose	-	0.052	0.061	0.031	0.068	0.065
3D-RA Cerebral Propeller	-	0.043	0.083	0.043	0.104	0.050
3D-RA Cerebral Roll	-	0.076	0.083	0.043	0.104	0.050

Results from Wang et al. show a decrease in conversion factor for the collimated beams while this work shows an increase in conversion factor. Wang et al. did not include the collimated beams in their PCXMC investigation so a direct like for like comparison cannot be made. Wang et al. included some organ doses in their paper which were compared with those produced from the results of this work and are shown in Table 36.

Table 36 Comparison of Organ Doses for Various Head Scans with Collimated and Uncollimated X-ray Beams

Organ dose (mGy)	Wang et al. 2014		This Work Dose		% Difference	
	Collimated	Uncollimated	Collimated	Uncollimated	Collimated	Uncollimated
XperCT Cerebral High Dose						
Brain	27.3	29.9	24.6	35.4	-10%	18%
Red Bone Marrow	2.4	3.0	2.0	3.7	-17%	22%
Salivary glands	4.6	25.2	17.3	36.4	275%	44%
Thyroid	0.6	2.6	1.0	2.9	65%	13%
XperCT Cerebral Low Dose						
Brain	13.9	14.8	12.4	17.8	-11%	20%
Red Bone Marrow	1.2	1.4	1.0	1.8	-17%	31%
Salivary glands	2.0	12.7	8.7	18.3	334%	44%
Thyroid	0.4	0.9	0.5	1.5	25%	63%
XperCT Cerebral Fast High Dose						
Brain	18	19.8	16.4	23.6	-9%	19%
Red Bone Marrow	1.6	2.0	1.3	2.4	-17%	22%
Salivary glands	2.9	17	11.5	24.3	297%	43%
Thyroid	0.0	1.9	0.7	2.0	-	3%
XperCT Intracranial Stent High Dose						
Brain	22.7	25.1	21.2	29.9	-6%	19%
Red Bone Marrow	2.4	3.2	1.8	3.3	-25%	4%
Salivary glands	2.7	30.1	21.4	43.6	692%	45%
Thyroid	0.1	1.2	0.6	1.9	494%	58%

Results for the XperCT Cerebral scans show comparable results across the range of organs for the uncollimated X-ray beam. When considering the collimated beam it can be seen that the dose to the salivary glands is very much greater in the results from this work when compared to Wang et al. A comparison between the projection images from the two pieces

of work (Figure 25) shows that this is due to the positioning of the salivary glands within the scanned volume. For their work Wang et al. have collimated the X-ray beam and have removed the dosemeter in the salivary glands from the primary beam. In PCXMC the salivary glands sit higher and are partially included in the collimated beam.

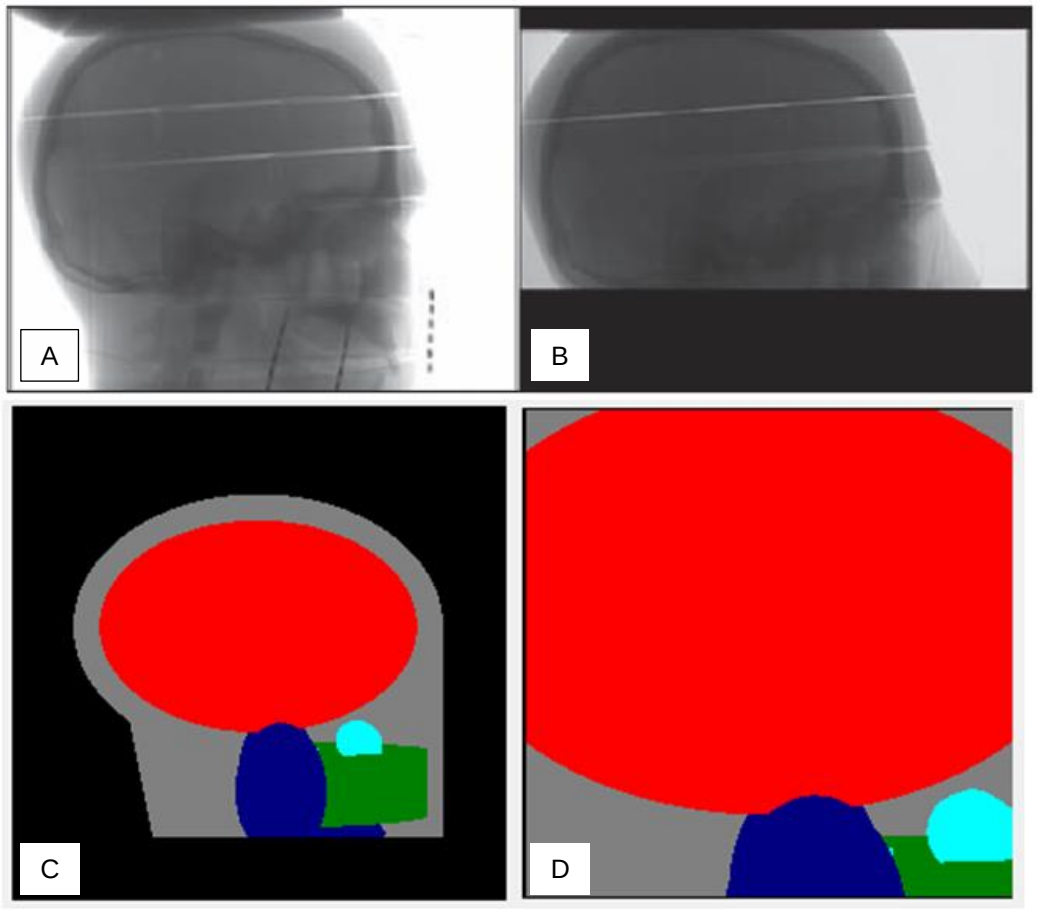

Figure 25 Lateral X-ray Views (produced from (Wang, et al., 2014, p. 1074)) for a) Uncollimated X-ray Beam, b) Collimated X-ray Beam, and PCXMC Simulation for c) Uncollimated X-ray Beam and d) Collimated X-ray Beam. Organs Shown for PCXMC are Brain (red), Salivary Glands (dark blue), Oral Mucosa (green) and Sinus (light blue).

Further simulations were undertaken to match the collimation on PCXMC to that used by Wang et al. for the collimated beam. The results give a conversion factor of 0.041mSv/Gycm². This is a better match to the range 0.046-0.048mSv/Gycm² from Wang et al.

Analysis of these sets of results highlights the limitations to the use of either method for calculating a patient dose. The Monte Carlo method used in this work has limitations due to the mathematical phantom not properly representing the patient. The use of a dosemeter in a phantom is limited to point measurements which may not be a representation of the dose to the whole of the organ. The results also show that a small change of collimation or positioning of the X-ray field can result in a significant change to the effective dose conversion factor.

11.3. Comparison with Rando Phantom Measurements

When initially setting up the Monte Carlo simulations a Rando phantom and TLDs were used to validate the results. To ensure this remained valid the conversion factors produced were used to compare with the initial Rando phantom results. The Rando measurements were made using the parameters given in Table 11 (page 49). From this work there are five different methods for applying conversion factors, which are summarised in Table 37, that have been compared. The results from this comparison are given in Figure 26.

Table 37 Details of the Five Methods for Converting Dose Metric to Effective Dose

	Description	**Reference**
Method 1	Using Table of DAP Conversion Factors	Table 27 and Table 28
Method 2	Using Formula with DAP and HVL	Table 25
Method 3	Using Formula with DAP, Area and HVL	Table 26
Method 4	Using Table of AK_{ref} Conversion Factors	Table 31 and Table 32
Method 5	Using Formula with AK_{ref}, Area and HVL	Table 30

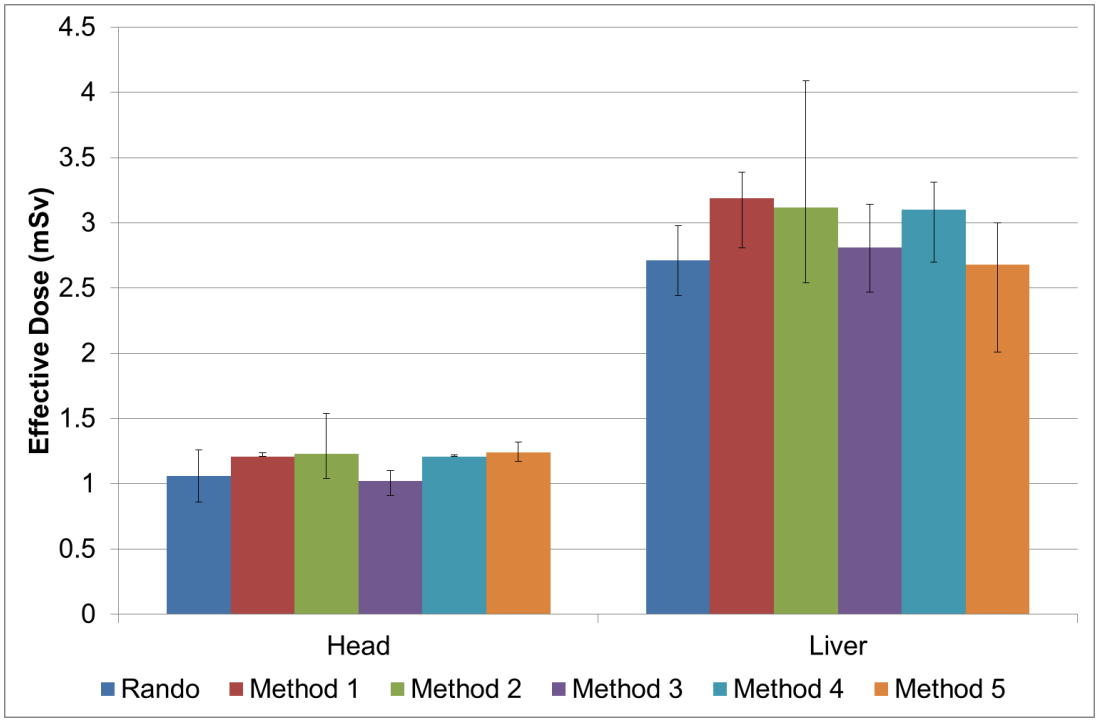

Figure 26 Comparison of Effective Dose Calculations Performed using the 5 Methods Produced in this Work with the Rando Phantom Measurements

This comparison shows that for head and liver examinations there are a range of E produced by the various methods. The error bars shown in Figure 26 show the uncertainty in the TLD readings for the Rando Phantom or the range of conversion factors for the various methods. Figure 26 shows that when these uncertainties and ranges are taken into account there is agreement between the various methods presented and the Rando Phantom measurements.

To determine if these results are statistically significantly different they were assigned a zeta score with the null hypothesis stating there is no difference between each method and the Rando measurements. A zeta less than or equal to two gives little evidence to reject the null hypothesis. The analysis is given in Table 38 and shows zeta to be less than 2 for all methods for both anatomies showing there is little significant difference between the 5 methods and the Rando measurements.

Table 38 Analysis of differences between the different methods and Rando measurements

Method	Effective Dose (mSv)	Difference from Rando (mSv)	Zeta
Head			
Rando	1.06		
Method 1	1.21	0.15	0.74
Method 2	1.23	0.17	0.46
Method 3	1.02	-0.04	0.17
Method 4	1.21	0.15	0.75
Method 5	1.24	0.18	0.84
Liver			
Rando	2.71		
Method 1	3.19	0.48	1.03
Method 2	3.12	0.41	0.41
Method 3	2.81	0.10	0.23
Method 4	3.1	0.39	0.81
Method 5	2.68	-0.03	0.04

11.4. Use of Computed Tomography Dose Index and Dose Length Product as Dose Metrics for Cone Beam Computed Tomography

Some radiology equipment provides CTDI and DLP as the dose metrics instead of reference air kerma and DAP. These dose metrics are defined for conventional CT scanning. They are defined for narrow X-ray beams and measured in standard phantoms. The literature review found papers where conventional CT dose conversion factors had been used to calculate E.

This method may not be suitable due to the differences in equipment geometry, beam shape and beam size. Additionally the CTDI and DLP dose metrics are not defined for these CBCT systems due to the beam size. For systems which perform a partial rotation this will also lead to an uneven distribution in dose through the CTDI phantoms which will not be accounted for with the CT conversion factors. As was shown in section 10.5, conversion factors for scans produced through an AP view were different to those through a PA view due to the differences in the dose distribution through the patient. For CT scans the dose

distribution is assumed to be through the full 360° and so the dose conversion factors will not take this into account.

Given these factors a more specialised Monte Carlo simulation will be required to assess the conversion factors for these systems which are not included in the scope of this work. It may, however, be possible to use the acquisition parameters and Air Kerma measurements made on the system to determine either the AK_{ref} or DAP for a CBCT acquisition which would allow the conversion factors produced by this work to be used. While this is not as simple a solution as using AK_{ref} or DAP directly from the system is does provide a method for patient dose assessment.

11.5. Errors and Uncertainties

Statistical uncertainties from the Monte Carlo calculations have previously been discussed in section 10.2; however these are not the only uncertainties in the conversion factors that have been produced. These include equipment factors (such as variations in the filtration, kV accuracy, use of appropriate collimation), patient factors (such as demographics) and Monte Carlo simulation factors (such as phantom choice and X-ray spectra). Previous work has found that the use of the mathematical phantom results in an average difference of 20% when compared to a voxel phantom (Tapiovaara & Siiskonen, 2008). The use of a hermaphrodite phantom can additionally result in differences between male and female patient populations of -11% and 12% respectively.

The use of conversion factors to calculate E is standard practice in diagnostic radiology. There are published conversion factors for general X-ray, fluoroscopy and CT examinations which have used similar methods to produce them and are summarised in Table 39. All of the references use a mathematical phantom for the calculation of E; however Shrimpton et al. also use adult male and female voxel phantoms.

Table 39 Summary of Methods used for Calculating Conversion Factors in other Applications of Diagnostic Radiology

Application	Reference	Method to Determine Conversion Factor	Phantom Type
General, Fluoroscopy and Interventional	NRPB-R262 (Hart, et al., 1994)	Monte Carlo	Mathematical
	HPA-CRCE-012 (Hart, et al., 2010)	PCXMC (Christy and Eckerman phantom)	Mathematical
	HPA-CRCE-028 (Wall, et al., 2011)	PCXMC (Christy and Eckerman phantom)	Mathematical
CT	(Shrimpton, et al., 2016)	Monte Carlo (HPA18+ phantom)	Mathematical
		Monte Carlo (ICRP adult reference phantoms)	Voxel
	ImPACT Calculator (ImPACT, 2011)	Monte Carlo (Cristy phantom)	Mathematical

It is noted that, with the exception of the ImPACT calculator, the conversion factors used in the references in Table 39 do not take into account the different kV or filtration that may be used when making the X-ray exposure. This work has shown that these have an impact on the conversion factors and so the error associated with their general use for converting the dose metric to E may be increased if different acquisition parameters are used.

HPA-CRCE-028 states that “effective dose should not be used to assess risks to individual patients” (Wall, et al., 2011, p. 2) as this is not the intended purpose. Instead it should be used for comparing the doses to a reference person for different imaging modalities. For this purpose the conversion factors that have been produced in this work provide a suitable comparison due to the similarities in the methods and limitations for the different imaging modalities.

When using conversion factors to calculate E consideration must be given to the uncertainties associated with the dose metric displayed on the equipment. While each

supplier of equipment has tolerances for the accuracy of the displayed metrics the IEC 60580 standard states that the total uncertainty for a DAP meter should be <25% (ISO 60580, 2000). The accuracy of the dose metrics are subject to routine quality assurance checks and when being used to provide a patient dose estimate the accuracy and associated uncertainty should be taken into account.

As has been shown the results from this work are subject to various sources of uncertainty and errors which are summarised in Table 40. Taking all these sources into account the overall uncertainty associated with the use of conversion factors and displayed dose metric to calculate E is estimated at 34%. While this result appears to be large it is comparable to other methods currently accepted for use in diagnostic radiology in the UK where the largest sources of error (use of a mathematical phantom, different patient demographics and DAP/AK meter calibration) will be the same.

Table 40 Sources of uncertainty in calculation and use of conversion factors

Source	Description	Uncertainty
Monte Carlo statistical uncertainty	Uncertainty introduced by the statistical processes in the monte Carlo simulations. This is reduced by increasing the number of photons simulated.	1%
Mathematical Phantom	The use of a mathematical phantom compared to a more realistic voxel phantom	20%
Patient demographics	Differences between standard mathematical phantom and a size specific mathematical phantom representing the average male and female in the UK.	12%
DAP or AK meter calibration	The uncertainty associated with a DAP or AK meter used on the equipment	25%

12. Innovation

Innovation in the NHS is defined as “An idea, service or product, new to the NHS or applied in a way that is new to the NHS, which significantly improves the quality of health and care wherever it is applied” (Department of Health, 2011). This work has produced new conversion factors that allow the radiation doses from a new technique in radiology to be determined. CBCT imaging provided the clinician with additional 3D information during diagnostic and interventional radiology procedures which can be of benefit to the patient.

Knowledge of the radiation doses provides the IR(ME)R practitioner with radiation risk information which will allow them to assess CBCT imaging in the context of justification of the exposure. This is a legal requirement for any medical exposure to ionising radiation and ensures that there is a net benefit to the exposure. Without this knowledge the examination cannot be justified. Additionally the results can be used as part of the optimisation process to ensure that the radiation doses delivered by CBCT are as low as reasonably practicable consistent with the intended purpose. This has the benefit of reducing the radiation risks to patients undergoing these procedures.

When considered in isolation the production of conversion factors does not meet the Department of Health definition of an innovation. However in the context of allowing this new technique to be introduced into clinical practice in a legal way with reduced radiation risks then it can be considered to meet the definition.

13. Conclusion

The results from this work provide a relatively simple method for assessing patient doses for CBCT imaging undertaken using diagnostic and interventional radiography equipment. The conversion factors produced can be used to convert a dose metric displayed on the equipment into E and covers the main body parts where CBCT imaging occurs. The conversion factors have been produced using a Monte Carlo simulation program (PCXMC) which was validated for both head and abdomen (liver) scans using an anthropomorphic phantom and TLDs. A comparison was also made with results found in the literature review.

The IR(ME)R2017 regulations require exposures to ionising radiation to be justified and optimised. They also require DRLs to be established and the radiation risks to be communicated to patients. The results from this work can be used to allow compliance with these regulations by providing the clinicians with E from the examination. E can be used to provide a radiation risk (based on the population) which will allow the IR(ME)R practitioner to justify the exposure, ensuring that the benefits from the exposure are greater than the risks. This includes comparison with alternative techniques that have the same objective but with lower radiation doses.

The results from this work can be used to assess the impact of different exposure factors on E allowing optimisation to be undertaken. Optimisation is undertaken to ensure that the radiation exposure is kept as low as reasonably practicable consistent with the intended purpose. The results from this work can be used to provide one aspect of the optimisation process by allowing the radiation doses for different scanning parameters to be assessed, however the diagnostic quality of the images produced for the different parameters will also need assessing to optimise the system.

IR(ME)R2017 also requires that an individual is provided with information about the benefits and risks from the exposure to ionising radiation. The conversion factors produced in this

work can be used to provide that information to the patients and allow the organisation to comply with this aspect of the IR(ME)R2017.

14. Future Work

The work has been undertaken using a standard adult hermaphrodite phantom representing a patient with a height of 178.6cm with a mass of 73.2kg. Future work could include investigating the impact of different adult patient demographics on the conversion factors. PCXMC also has paediatric phantoms available representing different age groups (0, 1, 5, 10 years) which would also be useful to assess.

Not all CBCT systems display the dose metrics of AK_{ref} or DAP for CBCT, instead CTDI or DLP are used. Further work using a different Monte Carlo simulation program could be undertaken to produce conversion factors for these systems.

The scope of this work was looking at CBCT scanning performed for interventional radiology applications using C-arm systems. There are extremity CBCT systems currently available which have different scanning geometries which this work could be expanded to investigate.

15. References

Abul-Kasim, K. et al., 2012. Optimization of radiation expsoure and image quality of the cone-beam O-arm intraoperative imaging system in spinal surgery. *Journal of Spinal Disorders and Techniques,* 25(1), pp. 52-58.

Aoyama, T., Kyoama, S. & Kawaura, C., 2002. An in-phantom dosimetry system using pin silicon photodiode radiation sensors for measuring organ doses in x-ray CT and other diagnostic radiology. *Medical Physics,* 29(7), pp. 1504-1510.

Ashland Inc., 2021. *Gafchromic EBT Films.* [Online] Available at: http://gafchromic.com/gafchromic-film/radiotherapy-films/EBT/index.asp [Accessed 19 March 2021].

Aveyard, E. & Katsidzira, N. M., 2016. *An investigation into the energy response of thermo-luminescent LiF:Mg,Ti material (TLD-100) for irradiation on a finger phantom.,* Birmingham: RRPPS, University Hospitals Birmingham NHS Foundation Trust.

Bai, M., Liu, X. & Liu, B., 2013. Effective patient dose during neuroradiological C-arm CT procedures. *Diagnostic and Interventional Radiology,* Volume 19, pp. 29-32.

Birch, R. & Marshall, M., 1979. Computation of bremsstrahlung X-ray spectra and comparison with spectra measured with a Ge(Li) detector. *Phys Med Biol.,* 24(3), pp. 505-517.

Bliznakova, K., Buliev, I. & Bliznakov, Z., 2018. *Anthropomorphic Phantoms in Image Quality and Patient Dose Optimization.* Bristol: IOP Publishing.

Bongartz, G. et al., 2004. *European guidelines on quality criteria for computed tomography.* [Online]
Available at: http://www.drs.dk/guidelines/ct/quality/htmlindex.htm [Accessed 26 February 2019].

Braak, S. J. et al., 2011. Effective dose during needle interventions: cone beam CT guidance compared with conventional CT guidance. *Journal of Vascular Interventional Radiology,* Volume 22, pp. 455-461.

Canon Medical Systems, 2020. *infinix_i_skyplus.* [Online] Available at: https://global.medical.canon/products/angiography/infinix_i_skyplus [Accessed 31 July 2020].

Castellano, I. A. et al., 1995. Assessment of organ radiation doses and associated risk for digital bifemoral arteiography. *Br J Radiol,* 68(809), pp. 502-507.

Choo, J. Y. et al., 2013. Percutaneous transthoracic needle biopsy of small (≤1 cm) lung nodules under C-arm cone-beam CT virtual navigation guidance. *Eur Radiol,* Volume 23, pp. 712-719.

Chu, W. F. et al., 2014. Radiation doses of cerebral blood volume measurements using c-arm CT: a phantom study. *American Journal of Neuroradiology,* Volume 35, pp. 1073-1077.

CIRS, n.d. *Atom Dosimetry Phantoms Models 701-706.* [Online] Available at: http://www.cirsinc.com/file/Products/701_706/701%20706%20ATOM%20PB%20110615.pdf [Accessed 24 January 2019].

Compagnone, G. et al., 2012. Calculation of conversion factors for effective dose for various interventional radiology procedures. *Medical Physics,* 39(5), pp. 2491-2498.

Costa, F. et al., 2016. Radiation exposure in spine surgery using an image-guided system based in intraoperative cone-beam computed tomography: analysis of 107 consecutive cases. *Journal of Neurosurgical: Spine,* Volume 25, pp. 654-659.

Cristy, M. & Eckerman, K. F., 1987. *Specific absorbed fractions of energy at various ages from internal photon sources. I Methods,* Tennessee: Oak Ridge National Laboratory.

Dance, D. R. & Castellano, I., 2014. Chapter 22 Patient Dosimetry. In: D. R. Dance, et al. eds. *Diagnostic Radiology Physics A handbook for teachers and students.* Vienna: IAEA, pp. 551-588.

Deak, P., Smal, Y. & Kalender, W., 2010. Multi selection CT protocols: sex and age specific conversion factors used to determine effective dose from dose length product. *Radiology,* Volume 257, pp. 158-166.

Department of Health, 2011. *Innovation Health and Wealth, Accelerating Adoption and Diffusion in the NHS,* London: Department of Health.

Farah, K. et al., 2018. Prospective comparative study in spine surgery between O-arm and Airo systems: efficacy and radiation exposure. *World Neurosurgery,* Volume 118, pp. E175-E184.

Fior, D. et al., 2019. Virtual guidance of percutaneous transthoracic needle biopsy with C-arm cone-beam CT: diagnostic accuracy, risk factors and effective radiation dose. *Cardiovasc Intervent Radiol.*

GE Healthcare, 2020. *IGS for hybrid OR.* [Online] Available at: https://www.gehealthcare.co.uk/products/interventional-image-guided-systems/igs-for-hybrid-or
[Accessed 31 July 2020].

Hart, D., Jones, D. G. & Wall, B. F., 1994. *NRPB-R262 Estimation of Effective Dose in Diagnostic Radiology from Entrance Surface Dose and Dose-Area Product Measurements,* London: HMSO.

Hart, D., Wall, B. F., Hillier, M. C. & Shrimpton, P. C., 2010. *Frequency and Collective Dose for Medical and Dental X-Ray Examinations in the UK, 2008,* Didcot: Health Protection Agency.

Health Protection Agency, 2009. *Application of the 2007 Recommendations of the ICRP to the UK. Advice from the Health Protection Agency,* Didcot: Health Protection Agency.

Hourdakis, J. C. & Nowotny, R., 2014. Instrumentation for Dosimetry. In: D. R. Dance, et al. eds. *Diagnostic Radiology Physics. A Handbook for Teachers and Students.* Vienna: IAEA, pp. 525-550.

Hwang, Y.-S., Tsai, H.-Y., Lin, Y.-Y. & Lui, K.-W., 2018. Investigations of organ and effective doses of abdominal cone-beam computed tomography during transarterial chemoembolization using Monte Carlo simulation. *BMC Medical Imaging,* 18(2).

IBM, 2013. *SPSS Statistics.* Armonk: IBM Corporation.

ICRP, 2007. The 2007 Recommendations of the International Commission on Radiological Protection. ICRP Publication 103.. *Ann. ICRP,* 37(2-4).

ImPACT, 2011. *ImPACT CT Patient Dosimetry Calculator Version 1.0.4,* London: ImPACT.

Institute of Physical Sciences in Medicine, 1992. *National Protocol for Patient Dose Measurements in Diagnostic Radiology,* Didcot: National Radiological Protection Board.

International Commission on Radiological Protection, 1991. 1990 Recommendations of the International Commission on Radiological Protection. ICRP Publication 60. *Ann. ICRP,* 21(1-3).

International Commission on Radiological Protection, 2007. ICRP Publication 103. The 2007 Recommendations of the International Commission on Radiological Protection.. *Annals of the ICRP,* 27(2-4).

International Commission on Radiological Protection, 2015. Publication 129 Radiological Protection in Cone Beam Computed Tomography. *Annals of the ICRP,* 44(1).

IR(ME)R, 2017. *Ionising Radiation (Medical Exposure) Regulations SI2017/1322,* London: The Stationery Office.

IRR, 2017. *The Ionising Radiations Regulations 2017 SI2017/1075,* London: The STationery Office.

ISO 4037-3, 1999. *X and gamma reference radiation for calibrating dosemeters and doserate meters and for determining their response as a function of photon energy - Part 3,* London: BSI.

ISO 60580, 2000. *Dose area product meters,* London: BSI.

ISO 60601-2-43, 2020. *Medical electrical equipment Part 2-43: Particular requirements for the safety of x-ray equipment for interventional procedures,* London: BSI.

Koivisto, J. H., Wolff, J. E., Kiljunen, T. & Schulze, D., 2015. Characterization of MOSFET dosimeters for low-dose measurements in maxillofacial anthropomorphic phantoms. *Applied Clinical Medical Physics,* 16(4), pp. 266-277.

Koyama, S., Aoyama, T., Oda, N. & Yamauchi-Kawaura, C., 2010. Radiation dose evaluation in tomosynthesis and C-arm cone-beam CT examinations with an anthropomorphic phantom. *Med. Phys.,* 37(8), pp. 4298-4306.

Kyoto Kagaku Co. LTD, n.d. *THRA1 Instruction Manual.* [Online] Available at: https://www.kyotokagaku.com/lineup/pdf/ph37_manual.pdf [Accessed 24 February 2019].

Lange, J. et al., 2013. Estimating the effective radiation dose imparted to patients by intraoperative cone beam computed tomography in thoracolumbar spinal surgery. *Spine,* 38(5), pp. 306-312.

Lockheed Martin, 2002. *Nuclides and Isotopes. Chart of the nuclides.* 16 ed. Niskayuna: KAPL, Inc..

Lui, J.-F.et al., 2019. Percutaneous bone biopsy using a flat-panel cone beam computed tomography virtual navigation system. *Saudi Med J,* Volume 39, pp. 519-523.

McKay, T. et al., 2016. Cone-beam CT with fluoroscopic overlay versus conventional CT guidance for percutaneous abdominopelvic abscess drain placement. *Journal of Vascular Interventional Radiology,* Volume 27, pp. 52-57.

McParland, B. J., 1998. A study of patient radiation doses in interventional radiological procedures. *Br J Radiol,* 71(842), pp. 175-185.

Moody, A., 2014. *Health Survey for England, Chapter 10: Adult anthropometric measures, overweight and obesity,* Leeds: The Health and Social Care Information Centre.

Nardi, C. et al., 2018. Radiation dose in non-dental cone beam CT applications: a systematic review. *La Radiologia Medica,* Volume 123, pp. 765-777.

Nardi, C. et al., 2017. Head and neck effective dose and quantitative assessment of image quality: a study to compare cone beam CT and multislice spiral CT. *Dentomaxillofacial Radiology,* Volume 46.

O'Donnell, C. et al., 2014. Comparative radiation exposure using standard fluoroscopy versus cone-beam computed tomography for posterior instrumented fusion in adolescent idiopathic scoliosis. *Spine,* 39(14), pp. 850-855.

Perry, B. C. et al., 2017. Pediatric percutaneous osteoid osteoma ablation: cone-beam CT with fluoroscopic overlay versus conventional CT guidance. *Cardiovasc Intervent Radiol,* Volume 40, pp. 1593-1599.

Petersen, A. G., Eiskjaer, S. & Kaspersen, J., 2012. Dose optimisation for intraoperative cone beam flat-detector CT in paediatric spinal surgery. *Pediatric Radiology,* Volume 42, pp. 965-973.

Petersen, T.-O.et al., 2018. Analysis of patient's x-ray exposure in 146 percutaneous radiologic gastrostomies. *Fortschr Röntgenstr,* Volume 189, pp. 820-827.

Philips Healthcare, 2020. *Azurion 7 C20 & Azurion 7 F20.* [Online] Available at: https://www.philips.co.uk/healthcare/product/HCNCVD005/azurion-7-c20-azurion-7-f20-image-guided-therapy-system#galleryTab=PI
[Accessed 31 July 2020].

Piergallini, L. et al., 2018. Flat-panel CT versus 128-slice CT in tomporal bone imaging: assessment of image quality and radiation dose. *European Journal of Radiology,* Volume 106, pp. 106-113.

Podnieks, E. C. & Negus, I. S., 2012. Practical patient dosimetry for partial rotation cone beam CT. *The British Journal of Radiology,* Volume 85, pp. 161-167.

Rogers, D. W. O. et al., 1994. BEAM: A Monte Carlo code to simulate radiotherapy treatment units. *Med. Phys.,* 22(5), pp. 503-524.

Rotolo, N. et al., 2016. Comparison of cone-beam CT-guided and CT flurorscopy-guided transthoracic needle biopsy of lung nodules. *Eur Radiol,* Volume 26, pp. 381-389.

Sailer, A. M. et al., 2015. Radiation exposure of abdominal cone beam computed tomography. *Cardiovasc Intervent Radiol,* Volume 38, pp. 112-120.

Scalzetti, E. M., Huda, W., Bhatt, S. & Ogden, K. M., 2008. A Method to Obtain Mean Organ Doses in a Rando Phantom. *Health Phys.,* 95(2), pp. 241-244.

Schegerer, A. A. et al., 2014. Dose and image quality of cone beam computed tomography as compared with conventional multislice computed tomography in abdominal imaging. *Investigative Radiology,* 49(10), pp. 675-684.

Shrimpton, P. C., Jansen, J. T. M. & Harrison, J. D., 2016. Updated estimates of the typical effective doses for common CT examinations in the UK following the 2011 national review. *Br J Radiol,* 89(1057).

Siemens Healthineers, 2020. *ARTIS icono.* [Online] Available at: https://www.siemens-healthineers.com/en-uk/angio/artis-interventional-angiography-systems/artis-icono
[Accessed 31 July 2020].

Siemens Healthineers, 2020. *Medical Accessories, OEM & Electronics - Siemens Healthcare Deutschland.* [Online] Available at: https://health.siemens.com/booneweb/index.html
[Accessed 5 May 2020].

Smith, I., Fleming, S. & Cernaianu, A., 1990. Mishaps during transport from the intensive care unit. *Critical Care Medicine,* 18(3), pp. 278-281.

Stanzi, A. et al., 2018. Tailored intraoperative localization of non-palpable pulmonary lesions for thoracoscopic wedge resection using hybrid room technology. *Clin Respir J.,* Volume 12, pp. 1661-1667.

Steuwe, A. et al., 2016. Comparison of radiation exposure associated with intraoperative cone-beam computed tomography and follow-up multidetector computed tomography angiography for evaluating endovascular aneurysm repairs. *Journal of Endovascular Therapy,* 23(4), pp. 583-592.

Strocchi, S., Colli, V. & Conte, L., 2012. Multidetector CT fluoroscopy and cone-beam CT-guided percutaneous transthoracic biopsy:comparison based on patient doses. *Radiation Protection Dosimetry,* 151(1), pp. 162-165.

STUK, 2011. *PCXMC Dose Calculations Version 2.0.1.4.* Helsinki: STUK.

STUK, 2012. *PCXMC Rotation Dose Calculations Version 2.0.1.5 Rotation.* Helsinki: STUK.

Supply Chain Coordination Limited, 2019. *Diagnostic, Pathology and Therapy Technologies and Services.* [Online] Available at: https://www.supplychain.nhs.uk/categories/diagnostic-equipment/ [Accessed 1 November 2019].

Suzuki, S. et al., 2009. Effective dose during abdominal three dimensional imaging with a flat panel detector angiography system. *Radiology,* Volume 250, pp. 545-550.

Tapiovaara, M. & Siiskonen, T., 2008. *PCXMC 2.0 User's Guide,* Helsinki: STUK.

Tapiovaara, M. & Siiskonen, T., 2008. *PCXMC A Monte Carlo program for calculating patient doses in medical x-ray examinations (2nd Edition),* Helsinki: STUK.

The Phantom Laboratory, n.d. *Rando Data Sheet.* [Online] Available at: http://phantomlab.client-proof.com/library/pdf/rando_datasheet.pdf [Accessed 24 February 2019].

ThermoFisher, 2016. *Harshaw TLD materials and dosimeters.* [Online] Available at: https://www.thermofisher.com/document-connect/document-

connect.html?url=https%3A%2F%2Fassets.thermofisher.com%2FTFS-Assets%2FLSG%2FCatalogs%2FDosimetry-Materials-Brochure.pdf&title=Q2F0YWxvZzogSGFyc2hhdyBUTEQgTWF0ZXJpYWxzIGFuZCBEb3NpbWV0ZXJz

[Accessed 19 March 2021].

University Hospitals Birmingham NHS Foundation Trust, 2020. *Personal radiation monitoring service.* [Online] Available at: https://www.uhb.nhs.uk/rrpps-personal-radiation-monitoring.htm [Accessed 31 May 2020].

Wall, B. F. et al., 2011. *Radiation Risks from Medical X-Ray Examinations as a Function of the Age and Sex of the Patient,* Didcot: Health Protection Agency.

Wang, C. et al., 2014. Evaluation of patient effective dose of neurovascular imaging protocols for C-arm cone-beam CT. *Maerican Journal of Roentgenology,* Volume 202, pp. 1072-1077.

Xiong, Z. et al., 2018. Investigation of organ dose variation with adult head size and pediatric age for neuro-interventional projections. *Proc SPIE 10573, Medical Imaging 2018, Physics of Medical Imaging,* Volume 105734D, pp. 1-14.

Yoshimura, E. M., 2014. Chapter 3: Fundamentals of Dosimetry. In: D. R. Dance, et al. eds. *Diagnostic Radiology Physics A Handbook for Teachers and Students.* Vienna: IAEA, pp. 35-53.

Ziehm Imaging, 2019. *Ziehm Vision RFD 3D. The revolution in 3D imaging. Brochure,* Nuremberg: Ziehm Imaging.

Ziehm Imaging, 2020. *Ziehm Vision RFD 3D.* [Online] Available at: https://www.ziehm.com/en/products/3d-c-arms/ziehm-vision-rfd-3d.html [Accessed 31 July 2020].

16. Appendix 1 - List of Alliance Manchester Business School A Units and Medical Physics B Units Together with Assignments

Alliance Manchester Business School – A Units		
Unit Title	**Credits**	**Assignment Word Count**
A1: Professionalism and professional development in the healthcare environment	30	A1 – assignment 1 – 1500 words A1 – assignment 2 – 4000 words
A2: Theoretical foundations of leadership	20	Practice paper – 2000 words A2 – assignment 1 – 3000 words A2 – assignment 2 – 3000 words
A3: Personal and professional development to enhance performance	30	A3 – assignment 1 – 1500 words A3 – assignment 2 – 4000 words
A4: Leadership and quality improvement in the clinical and scientific environment	20	A4 – assignment 1 – 3000 words A4 – assignment 2 – 3000 words
A5: Research and innovation in health and social care	20	A5 – assignment 1 – 3000 words A5 – assignment 2 – 3000 words
Medical Physics – B Units		
B1: Medical Equipment Management	10	2000 word assignment
B2: Clinical and Scientific Computing	10	2000 word assignment
B3: Dosimetry	10	Group presentation 1500 word assignment
B4: Optimisation in Radiotherapy and Imaging	10	Group presentation 1500 word assignment
B6: Medical statistics in medical physics	10	3000 word assignment

B8: Health technology assessment	10	3000 word assignment
Unit Title	**Credits**	**Assignment Word Count**
B9: Clinical applications of medical imaging technologies in radiotherapy physics	20	Group presentation 2000 word assignment
B10b: Assessment of Image Quality	10	Group presentation 1500 word report
B10e: Novel Imaging Techniques	10	Group presentation 1500 word report
B10f: Radiation Protection Advice	10	1500 word report/piece of evidence for portfolio
Generic - B Units		
B5: Contemporary issues in healthcare science	20	1500 word assignment + creative project
B7: Teaching Learning Assessment	20	20 minute group presentation
Section C		
C1: Innovation Project	70	4000-5000 word Literature Review Lay Presentation

17. Appendix 2 – Summary of Papers Included in the Literature Review

Reference	Scope	CBCT Equipment	Effective Dose Calculation Method	Summary of findings
(Fior, et al., 2019)	CBCT guided lung biopsy	Philips Xper FD20	DAP to effective dose conversion factor	Mean 7.12 ± 8.78mSv
(Farah, et al., 2018)	Spinal surgery – thoracic or lumbosacral pedical screw placement	Medtronic O-Arm	DAP and DLP to effective dose conversion factor	3.52mSv (2.1-9.4mSv)
(Xiong, et al., 2018)	Fluoroscopy and CBCT guided head procedures	Toshiba Infinix C-arm	Monte Carlo modelling (BEAMnrc & Zubal phantom)	Organ doses: 54.2mGy to lens of eye
(Piergallini, et al., 2018)	Temporal bone imaging	Philips Allura Xper FD20	Rando phantom with TLDs	0.584mSv

Reference	Scope	CBCT Equipment	Effective Dose Calculation Method	Summary of findings
(Nardi, et al., 2018)	Systematic review of effective dose for non-dental CBCT	Various including dental systems used for non-dental applications and extremity systems: Planmed Verity Newtom 5G PedCAT 3D Accuitomo i-CAT Maxiscan Carestream 9300	Literature review of previous dose calculations. Methods discussed: • Rando Phantom with TLD, MOSFET or OSL • Dose Metric (DAP/CTDI) with conversion factor • Monte Carlo simulations	Knee: 5.6-12.6µSv Ankle: 0.9-14.3µSv Wrist: 7-10µSv C-Spine: 248µSv Ear: 80-400µSv Paranasal Sinuses: 90-130µSv
(Hwang, et al., 2018)	Abdominal TACE procedures	BRANSIST Safire VC17	Monte Carlo modelling (PCXMC)	3.5±0.5mSv (2.1-4.5mSv)
(Stanzi, et al., 2018)	Lung wedge resections with CBCT guidance	No details – Siemens guidance used	Monte Carlo Modelling (PCXMC)	11.6mSv (1.9-24.7mSv)

Reference	Scope	CBCT Equipment	Effective Dose Calculation Method	Summary of findings
(Lui, et al., 2019)	Percutaneous bone biopsies (80 patients): Vertebral, L-Spine, T-Spine, C-Spine, Leg, Pelvis, Sternum, Rib, Arm	No Details	No Details	Quoted: mean 11.3 ± 5.1mSv (No mention of biopsy site)
(Nardi, et al., 2017)	Head and neck CBCT scans (compared to MDCT)	Newtom 5G	Rando Phantom with TLDs	C-spine: 0.3mSv Head: 0.3mSv Ear: 0.3mSv
(Perry, et al., 2017)	Paediatric CBCT for radiowave or microwave ablations with tumours of: Femur, tibia, foot and pelvis	Philips Angiography system	DAP to effective dose conversion factor	0.01 – 0.38mSv
(Petersen, et al., 2018)	Percutaneous gastrostomies	GE Innova 4100	DAP to effective dose conversion factor	Mean 7.6mSv Median 7.9mSv
(Costa, et al., 2016)	Spinal surgery	Medtronic O-arm	DLP to effective dose conversion factor	2.52mSv per scan

Reference	Scope	CBCT Equipment	Effective Dose Calculation Method	Summary of findings
(McKay, et al., 2016)	Abdomen and Pelvis	Philips XperGuide	DAP to effective dose conversion factor	Median: 9.6mSv (2.6-37.4mSv)
(Rotolo, et al., 2016)	Thoracic CBCT for needle biopsy	Phillips Allura Xper FD20	DAP to effective dose conversion	11.1mSv (8.9-16mSv)
(Steuwe, et al., 2016)	EVAR procedures	Siemens Artis Zeego	Rando Phantom with TLDs	4.9 ± 1.1 mSv
(Sailer, et al., 2015)	Abdominal CBCT for endovascular interventions	Philips Xper FD20	Monte Carlo (PCXMC)	4.3mSv (1.1 – 7.4mSv)
(Chu, et al., 2014)	Head CBCT	Siemens Axiom Artis	Rando Phantom with TLDs	Slab 0.87mSv Whole brain 3.91mSv
(Schegerer, et al., 2014)	Abdomen	Siemens Artis Zee	Rando Phantom and TLDs	0.35 – 17.1mSv
(Wang, et al., 2014)	Head	Philips XPerCT/Allura FD20	CIRS Phantom and MOSFET Monte Carlo Simulation (PCXMC)	MOFFET 0.8 – 1.6 mSv PCXMC 0.9 – 1.9 mSv

Reference	Scope	CBCT Equipment	Effective Dose Calculation Method	Summary of findings
(O'Donnell, et al., 2014)	Spinal Surgery	Medtronic O-arm	Literature review	7-9mSv navigation 14-18mSv Navigation and confirmation
(Choo, et al., 2013)	CBCT lung scans for needle biopsy	Philips Xper FD20	DAP to effective dose conversion factor – established using a Rando Phantom with EBT2 GafChromic film	Mean 5.72 ± 4.19mSv
(Bai, et al., 2013)	Head	Siemens Axiom Artis dTA	Rando phantom with TLD Monte Carlo simulation (PCXMC)	0.3mSv (0.12 – 0.43mSv)
(Lange, et al., 2013)	Spinal Surgery	Medtronic O-arm	ESD to DLP to effective dose Conversion factors	3.24mSv (small) 8.09mSv (large)
(Podnieks & Negus, 2012)	Upper, Middle and Lower Abdomen	Siemens Artis Zee	Monte Carlo simulation (PCXMC)	13mSv (Upper) 10mSv (Middle) 12mSv (Lower)

Reference	Scope	CBCT Equipment	Effective Dose Calculation Method	Summary of findings
(Strocchi, et al., 2012)	Thorax	Philips XPerCT/Allura FD20	Monte Carlo simulation (PCXMC)	7.88mSv (3.24 – 14.89mSv)
(Abul-Kasim, et al., 2012)	Spinal Surgery	Medtronic O-Arm	Monte Carlo simulation (PCXMC)	0.3 – 11mSv (T-Spine) 0.2 – 8.6mSv (L-Spine) 0.1 – 20mSv (Whole Spine)
(Petersen, et al., 2012)	Spinal Surgery for paediatric patients	Medtronic O-Arm	Monte Carlo simulation (PCXMC)	0.5mSv (low dose) 8.3mSv (medium dose)
(Braak, et al., 2011)	Thorax and Abdomen	Philips XPerCT/Allura FD20	Monte Carlo simulation (PCXMC)	Upper Thorax: 4.3 (2.7-5.8) mSv Lower Thorax: 7.8 (4.5-11.2) mSv Upper Abdomen: 5.7 (4.6-6.8) mSv Lower Abdomen: 5.8 (2.9-8.8) mSv

Reference	Scope	CBCT Equipment	Effective Dose Calculation Method	Summary of findings
(Koyama, et al., 2010)	Comparison of tomosynthesis and CBCT with MDCT for Head, Chest, Abdomen and Hip Joint	Shimadzu BRANSIST Safire	Koyoto Kagaku phantom with Hamamatsu S8385-04/S2506-04 photodiodes	Head 1.2mSv Abdomen (17in) 4.0mSv Abdomen (9in) 5.2mSv
(Suzuki, et al., 2009)	Abdominal CBCT	GE Innova 4100	Rando Phantom with TLDs Monte Carlo Simulation (PCXMC)	2.1mSv (155cm phantom) 3.2mSv (163cm phantom) 4.2mSv (174cm phantom)

18. Appendix 3 – PCXMC Set-up

Parameter	Description	PCXMC values used
Projection	Parameter to define the incident angle of the x-ray beam around the patient.	**For AP Scans (Patient Supine):** 150° – 360°/0° - 30° in 0.6° intervals **For PA Scans (Patient Supine):** 350° - 360°/0° - 190° in 0.667° intervals 0° - 90° - 180° in 0.285° intervals 0° - 90° - 180° in 0.575° intervals
Oblique Angle	Parameter to define the cranio-caudal angle of the incident x-ray beam.	0° for all projections
Patient Height	Parameter to define the individual patient height.	Standard: 178.6cm
Patient Weight	Parameter to define the individual patient mass.	Standard: 73.2kg
Patient Age	Parameter to define the individual patient age.	Standard: 30
X-ray tube voltage	Parameter to define the x-ray kVp used in the simulation.	60kV – 120kV in 10kV steps
Filtration (mm Al)	Parameter to define the inherent filtration for the x-ray beam.	2.5mm Al 3.3mm Al These were adjusted as necessary if the table was included in the primary beam.
Additional Filter (mm Cu)	Parameter to define the additional copper filtration for the x-ray beam.	0mm Cu 0.1mmCu 0.3mmCu 0.5mmCu 0.6mmCu 0.9mmCu 1.0mmCu
FRD	Parameter to define the focus to rotation distance.	75cm 81cm 82cm
X-ray beam width	Parameter to define the x-ray beam width (perpendicular to z-axis) at the FRD.	A) 27.33cm B) 26.66cm C) 23.25cm D) 21.6cm E) 14.38cm F) 12.89cm G) 10.13cm H) 8.12cm I) 7.78cm
X-ray beam height	Parameter to define the x-ray beam height (parallel to z-axis) at the FRD.	A) 27.33cm B) 19.91cm C) 18.44cm D) 21.6cm E) 14.38cm F) 12.89cm G) 10.13cm H) 8.12cm I) 7.78cm
Xref	Parameter to define the x coordinate of the centre of the x-ray beam.	Xref = 0 for all projections (This is how the equipment is set up clinically to allow space for detector rotation)

Parameter	Description	PCXMC values used
Yref	Parameter to define the y coordinate of the centre of the x-ray beam.	Yref = 0 for all projections This is how the equipment is set up clinically to allow space for detector rotation
Zref	Parameter to define the z coordinate of the centre of the x-ray beam.	Head: 87.5cm Heart: 50.0cm Kidney: 31cm Liver: 35cm Prostate: 0cm
Arms in Phantom	Parameter to define if arms are included in the scan.	Set to 0 (arms out) for all projections.
Input Dose quantity	Parameter to define the dose metric used as an input.	For AK_{ref}: EAK For DAP: DAP
Input Dose Value	Parameter to define the quantity of the dose metric.	Set so total dose over all projections was either 1Gy or 1000mGycm² then adjusted depending on if the table was in the view table.
Number of photons	Defines the number of photons used in the simulation for each projection. Is varied by changing Macro.	20,000 used for all projections.
Tube Target Angle	Defines the angle of the target in the x-ray tube. Is varied by changing Macro.	Default value (16°) used for all projections.

19. Appendix 4 – TLD Positions

For the head examinations the number and positions of the TLDs are given in Table 41. The coordinates relate to the hole into which the TLD was positioned. For each slice this is based on Cartesian coordinates with the point 0, 0 being the patient's left posterior. The x-coordinate increases from left to right and the y-coordinate increases from posterior to anterior. The Rando slices are numbered from 1 to 35 with 1 being the top of the head.

Table 41 Positioning of TLDs in various organs for Head Scans

Organ	Number of TLDs	Rando Slice	TLD Coordinate
Brain	14	1	(0,1), (1,0), (1,2),(2,1)
		2	(0,0), (0,4), (2,0), (2,4)
		3	(1,0), (1,3), (3,0), (3,3)
		4	(1,0)
		5	(1,0)
Breast	2	16	On phantom surface
Eyes	2	3	(0,4), (3,4)
Heart	6	16	(4,4)
		17	(4,4), (4,5)
		18	(3,3), (3,4), (3,5)
Liver	4	19	(5,4), (5,5)
		20	(5,4), (5,5)
Lung	23	10	(0,3), 3,1), (5,1)
		11	(1,2), (5,2)
		12	(3,1),(4,2), (8,2), (9,1)
		13	(4.2), (8,2)
		14	(3,1), (4,3), (8,3), (9,1)
		15	(1,2), (6,2)
		16	(3,2), (7,2)
		17	(3,2), (7,2)
		18	(2,2), (6,2)
Oral Mucosa	1	7	(1,4)
Salivary Glands	2	6	(0,2), (2,2)
Stomach	2	20	(3,4), (3,5)
Thymus	3	12	(4,3), (6,2)
		13	(6,4)
Thyroid	2	9	(1,3), (3,3)

For the liver examinations the number and positions of the LDs are given in table 42. For these scans the point 0, 0 is the patient's right anterior. The x-coordinate increases from right to left and the y-coordinate increases from anterior to posterior.

Table 42 Positioning of TLDs in various organs for Liver Scans

Organ	Number of TLDs	Rando Slice	TLD Coordinate
Adrenals	2	21	(4,6)
		22	(6,5)
Bladder	6	31	(6,2), (6,3)
		32	(6,2), (6,3)
		33	(6,2), (6,3)
Breast	2	16	Phantom surface
Colon	12	24	(7,3), (7,4)
		25	(7,3), (7,4)
		26	(7,3), (7,4)
		27	(7,3), (7,4)
		28	(7,3), (7,4)
		29	(7,3), (7,4)
Gall Bladder	2	22	(3,3), (4,3)
Heart	6	16	(7,2)
		17	(6,1), (6,2)
		18	(7,1), (7,2)
Kidney	8	22	(3,6), (7,6)
		23	(3,6), (7,6)
		24	(3,6), (7,6)
		25	(3,6), (7,6)
Liver	12	19	(2,3), (4,3)
		20	(3,2), (4,3)
		21	(3,2), (4,4)
		22	(3,2), (4,4)
		23	(2,2), (4,4)
		24	(3,3), (4,2)
Lung	22	10	(5,4), (6,3), (1,3)
		11	(1,2), (5,2)
		12	(4,3), (5,4), (9,3), (10,4)
		13	(5,4), (9,4)
		14	(5,3), (6,5), (10,4)
		15	(4,4), (8,4)
		16	(4,4), (8,4)
		17	(3,4), (7,4)
		18	(3,4), (7,4)
Oesophagus	2	12	(7,3)
		13	(7,2)
Ovaries	2	31	(4,3), (7,3)
Pancreas	2	23	(2,4), (3,3)
Prostate	2	34	(6,2), (6,3)

Organ	Number of TLDs	Rando Slice	TLD Coordinate
Small Intestine	10	24	(4,3), (6,3)
		25	(4,3), (6,3)
		26	(4,3), (6,3)
		27	(4,3), (6,5)
		28	(4,2), (6,2)
Spleen	6	21	(8,1), (8,2)
		22	(7,1), (8,1)
		23	(8,1), (8,2)
Stomach	10	20	(7,2), (7,3)
		21	(7,2), (7,3)
		22	(6,3), (7,2)
		23	(6,2), (6,3)
		24	(6,2), (7,2)
Testes	1	35	Phantom surface
Thymus	1	12	(6,1)
Uterus	2	31	(6,4)
		32	(6,4)